CHARACTERIZATION OF ATM KINASE-DEPENDENT SIGNAL TRANSDUCTION IN HUMAN MAMMARY TISSUE CELLS

By

WILLIAM SCOTT STREITFELD

A THESIS PRESENTED TO THE GRADUATE SCHOOL
OF THE UNIVERSITY OF FLORIDA IN PARTIAL FULFILLMENT
OF THE REQUIREMENTS FOR THE DEGREE OF
MASTER OF SCIENCE

UNIVERSITY OF FLORIDA

2017

To the people that helped me to see that the most fruitful learning starts with the acceptance of one's initial and limited understanding and ability.

ACKNOWLEDGMENTS

I would like to thank my thesis mentor, Dr. Kevin Brown, and my committee members, Dr. Brian Cain and Dr. Michelle Gumz. I would like to thank the faculty members at the University of Florida, the University of North Florida, Florida State College at Jacksonville, the California University of Pennsylvania, Ashford University, and Los Angeles Harbor College for providing excellent instruction and academic guidance. I would like to thank the staff at the Mayo Clinic Jacksonville, Florida, for their support and guidance during my time spent there. Finally, I would like to thank my friends, family, peers, and professional accomplices for their undying and limitless patience.

TABLE OF CONTENTS

page

LIST OF TABLES

LIST OF FIGURES

Abstract of Thesis Presented to the Graduate School
of the University of Florida in Partial Fulfillment of the
Requirements for the Degree of Master of Science

CHARACTERIZATION OF ATM KINASE-DEPENDENT SIGNAL TRANSDUCTION IN HUMAN MAMMARY TISSUE CELLS

By

William Scott Streitfeld

August 2017

Chair: Kevin D. Brown
Major: Biochemistry and Molecular Biology

The events that cause malignant transformation of normal breast tissue include intracellular signals that respond to insufficient delivery of oxygen to cells (hypoxia). Hypoxia-induced oxidative stress further exacerbates tumor dissemination and disease status in breast cancer. Previous work has elucidated the role of the ataxia telangiectasia-mutated kinase (ATM) and hypoxia-inducible factors (HIFs) during hypoxia-induced cellular oxidative stress response. It has also characterized the production of intracellular reactive oxygen species (ROS), and the nature of intracellular signaling cascades involving ATM and HIFs. In the current work, antioxidants were used to treat human mammary epithelial cells to further characterize the ROS-dependency of intracellular ATM signaling in response to hypoxia-induced oxidative stress. Additionally, recombinant DNA vectors were constructed for the development of human mammary epithelial cells devoid of mitochondrial DNA (termed “rho-zero” (ρ^0) cells), to further identify the source of intracellular ROS during hypoxia. It was observed that the antioxidant n-acetylcysteine (NAC) decreased the transcript abundance of genes activated by HIFs in response to hypoxia. HIF protein levels after treatment with NAC also showed decreased accumulation, which correlated with transcript abundance of

HIF target genes. It was also observed that the antioxidant TEMPOL increased transcript abundance of the HIF target gene carbonic anhydrase IX (CA9). The antioxidant molecules that were used possessed differing mechanisms, and further characterized ATM-dependent HIF signaling during hypoxia. Quantitative PCR and immunoblotting were used to further support previous work characterizing the nature of ATM oxidative stress-induced activation.

CHAPTER 1
INTRODUCTION

Cancer-related deaths account for 22.5% of deaths in the United States as of 2014, second only to heart disease as the leading cause of death, with the cancer-related death count reaching a total of nearly 600,000 persons annually (1). When comparing the cancer-related death rate statistics with those obtained in 1950, adjusting for the fact that people are living longer and therefore experiencing a higher overall lifetime cancer risk, the cancer death rate has decreased; this suggests that cancer-related deaths are becoming less frequent (1).

Breast cancer represents one of the most frequently occurring cancerous diseases in women in the United States as of 2017, and breast cancer is estimated to represent approximately 30% of new cancer cases in American females (2). Based upon age-adjusted estimates, breast cancer-related death among females in the United States is on the decline when observing statistics gathered since 1930; however, carcinoma of the mammary gland remains the third leading cause of death among American females, surpassed only by lung cancer and heart disease (2). This poses a serious public health concern and continues to deserve scientific attention.

Low Oxygen Tension Within Neoplastic Tissue

Neoplastic lesions that develop in breast tissue as a consequence of exposure to carcinogens, presence of germline DNA mutations, and other endogenous physiological insults carry an inherent risk of becoming malignant (3). As neoplastic lesions increase in size, they can potentially grow beyond the range of the vasculature shared with neighboring normal tissue, due to high rates of cellular proliferation and aberrant tissue morphology characteristic of neoplasms. Due to the limited diffusion range of molecular

oxygen in human tissue (200 μm), cells within neoplastic lesions can experience variable oxygen tensions, including hypoxia (defined as a cellular pO_2 less than 4%, but greater than 0%) (4). Cells exposed to hypoxia have been shown to exhibit changes in their gene expression, fuel metabolism, cell cycle behavior, phenotype, and viability, with potential changes including the chain of events necessary to cause malignant transformation (3,5-8). Malignant tumor cells further exposed to hypoxia adapt by regulating changes in metabolic programming, neovascularization, cellular motility, and metastatic potential, demonstrating a specific effect of hypoxia during the proliferative expansion phase of cancer progression (7,9,10). Consequently, clinical data shows a correlation between tumor hypoxia and poor prognosis (11).

The cellular adaptations within tumors that result from the presence of hypoxia increase resistance to multiple cancer treatment methods through a variety of mechanisms. Firstly, hypoxia-driven reactive oxygen species (ROS) cause upregulation of genes including nuclear respiratory factor 2 (NRF2), a transcription factor which upregulates genes that combat accumulation of ROS (12-14). Constitutive activation of this gene can cause an increase in the cell's antioxidant defenses (12-14). The oxidation-augmenting mechanism of radiotherapy becomes less effective in cells with high NRF2 activity (13).

Secondly, hypoxia directly causes an anti-proliferative effect, which can cause cellular quiescence when pO_2 drops below 0.5% (8). Regions of quiescent cells that form in perinecrotic tumor tissue due to inadequate vascularization can demonstrate resistance to chemotherapies, especially those that depend upon rapid proliferation for efficient cell killing (15).

Thirdly, hypoxia can cause upregulation of genes that encode ATP-binding cassette family proteins, increasing the activity of active transporters such as the multidrug resistance 1 protein (MDR1), which acts as a cellular efflux pump and prevents efficient delivery of a variety of cancer drugs (16). Two major factors are believed to initiate these and other drug resistance scenarios during malignant transformation and cancer progression: the decrease in the availability of molecular oxygen and the increase in the cellular production of ROS (17-23).

Reactive Oxygen Species and Signal Transduction

Although there are many intracellular ROS molecule types, four major molecule types accumulate that influence the activity of signaling pathways: hydroxyl radical (•OH), superoxide anion radical ($\bullet O_2^-$), hydrogen peroxide (H_2O_2), and oxygen-containing reactive nitrogen species (RNS) (24). Molecular oxygen is reduced through a variety of mechanisms to produce $\bullet O_2^-$, which can be converted to H_2O_2 by a family of compartmentalized enzymes known as superoxide dismutases (SODs). H_2O_2 can be further reduced enzymatically to form H_2O, resulting in its elimination from the cell. Multiple inducible cytosolic enzymes including inducible nitric oxide synthase (iNOS) produce RNS such as nitric oxide (NO (25)). Classes of ROS vary in their reactivity and in their half-lives, with the most reactive (and therefore most toxic) and shortest-lived (nanosecond range) class being •OH (24). H_2O_2 represents the most abundant and longest-lived (hours to days) intracellular ROS, and is the predominant mediator of redox-dependent modulation of intracellular signaling (24,26). Additionally, H_2O_2 acts as a substrate for cellular detoxification via vesicular elimination of intracellular waste products and phagocytosed xenobiotic debris (e.g., within peroxisomes and

redoxosomes) (24). Although H_2O_2 is much less reactive than •OH, the mechanism by which H_2O_2 may participate in redox-mediated intracellular signaling pathways lies within its spontaneous conversion to •OH via iron-dependent Fenton chemistry (12,27). At high concentrations, H_2O_2 damages cellular components including proteins, lipids, and nucleic acids, and can cause genomic instability through formation of DNA adducts (28). Events that change cellular control of H_2O_2 concentration, due to their potential for modulation of intracellular activity, collectively construct a fulcrum that delicately governs intracellular redox balance, and provides a mechanism of induction for the intracellular oxidative stress response.

Accumulation of $\bullet O_2^-$ produced from multiple cellular sources can tip the balance of redox status due to SOD-dependent change in H_2O_2 concentration. Redox imbalance results in an intracellular status of "oxidative stress," which can be defined generally as an increase in the accumulation of H_2O_2 and other ROS beyond the capacity of intracellular ROS-eliminating antioxidant systems (29). H_2O_2-induced lipid peroxidation within the plasma membrane can result in cell lysis and subsequent initiation of extracellular inflammatory response through receptor-activated upregulation of NF-κB and AP-1 target genes in adjacent cells (12,26,30,31). The target genes of NF-κB include nicotinamide-adenine dinucleotide phosphate (NADPH) oxidase and iNOS enzymes, which produce cytosolic $\bullet O_2^-$ and RNS respectively, propagating the effect of oxidative stress in neighboring cells (24-26,32). NF-κB can also downregulate ROS production by upregulating genes including SOD1 (cytosolic SOD), SOD2 (mitochondrial SOD), and ferritin heavy-chain (FHC) (33). Although upregulation of SODs would potentially increase cellular damage through increased conversion of $\bullet O_2^-$

to H_2O_2, FHC expression would sequester iron and prevent subsequent conversion of H_2O_2 to •OH; however, inflammatory response-induced oxidative stress signals acting upon hypoxic tissue could further exacerbate hypoxia-induced cellular adaptations in that tissue, further complicating the landscape of malignant and/or pre-malignant lesions (26,34,35). The presence of this feed-forward “ROS cycle” provokes the question: “where is all of the ROS coming from?”

Sources of Cellular Reactive Oxygen Species and Their Induction During Hypoxia

The generation of intracellular ROS occurs as the result of four major cellular processes. In the first process, plasma membrane receptors for cytokines and growth factors including epithelial growth factor (EGF) and platelet-derived growth factor (PDGF) produce ROS as a by-product of the activation of receptor tyrosine kinase motifs (26,36). A second group of metabolic processes involves ROS production as a by-product of lipid oxidation reactions catalyzed by enzymes including cyclooxygenase (COX) and lipoxygenase (LOX), and the production of RNS by enzymes including iNOS (26,37). A third process of more substantial ROS production, specifically that of $\bullet O_2^-$, involves both protein folding in the endoplasmic reticulum and vesicular waste elimination, each catalyzed by specific isoforms of the NADPH oxidase family of enzymes (e.g., NOX1, NOX4, and DUOX) (38-41). The fourth and perhaps most paradoxical source of ROS is the mitochondrial electron transport chain (ETC). The production of $\bullet O_2^-$ primarily occurs at NADH:ubiquinone oxidoreductase (complex 1) and at the cytochrome bc_1 complex (complex 3), through two major mechanisms: the proximity-dependent transfer of a single electron to molecular O_2 at the active sites of heme protein-bound electron acceptors, and the transfer of a single electron to

molecular O_2 from the unstable semiquinone radical ion ($\bullet Q^-$) at the Q_i binding site of complex 3 (42,43).

Although the transfer of a single electron to O_2 is thermodynamically favored, it is limited kinetically by the structures of complex 1 and complex 3, which offer limited exposure of their enzymatic active sites to the aqueous environments of the mitochondrial intermembrane space and matrix (42,43). Mitochondrial $\bullet O_2^-$ concentration is difficult to measure in vivo due to its rapid dismutation to H_2O_2 by SOD2, and experimental evidence does not unequivocally confirm which reaction(s) within the mitochondrion is responsible for ROS production (42,43). Although experimental evidence has been provided demonstrating that highly reduced states of electron carriers and substantial proton-motive force are required to cause production of ROS from the ETC, it has also been shown that the ETC can be decoupled from oxidative phosphorylation without an effect on the downstream transduction of ROS-dependent signaling (20,42,43). Experimentation has specifically implicated the ETC in the activation of ROS dependent signaling, independent of oxidative phosphorylation, using a variety of inhibitor-based and ETC depletion experiments (18-20,44); however, conflicting results from similar experimentation has created a debate regarding the requirement of a functional ETC for hypoxia-induced ROS-dependent signal transduction (45-48).

The hypoxic induction of ROS is somewhat paradoxical in that the concentration of specific forms of oxygen-based molecules increases in a manner that appears to be dependent upon a decrease in molecular O_2. The paradox suggests that it is unlikely that a decrease in O_2 concentration is directly responsible for any increase in ROS,

prompting the search for hypoxia-induced signaling pathways that might be responsible for changes in intracellular ROS-producing processes. For example, glutathione (GSH) is present in the mitochondria in concentrations that are high relative to the cytosol, and the high concentration is maintained by specific mitochondrial transporters (43). GSH scavenges $\bullet O_2^-$ and is thus oxidized in a process that is dependent upon glutathione-S-transferase (GST) and glutathione reductase (GR) enzymes for co-enzymatic scavenging and GSH replenishment, respectively (43). It was shown experimentally that GSH depletion from the mitochondrial matrix to a concentration less than 50% of basal levels resulted in an increase in intracellular H_2O_2 concentration, suggesting that modulation of GSH through regulation of enzymatic activity could increase the efflux of ROS from the mitochondrion through an oxygen-independent hypoxia-driven mechanism (49); however, experimental evidence in support of this suggestion has not been provided. The paradox notwithstanding, a hypoxia-induced ROS increase from the ETC could shift redox balance and cause oxidative stress in pre-malignant and malignant mammary lesions. Taken together, the hypoxic induction of increased ROS concentration and the implication of the ETC as its source provide targets for further experimental investigation that would identify the most upstream point in the cascade of events leading to this cause of cancer progression.

Hypoxia-Inducible Factors: Master Regulators of Hypoxia Response

The hypoxia-inducible factor (HIF) protein family is composed of three members (HIF-1, HIF-2, and HIF-3), and all function as heterodimers, with unique alpha and beta subunits (50). HIF-1 and HIF-2 act as positive regulators of intracellular response to hypoxia by binding DNA and upregulating transcription of specific sets of genes. HIF-1

and HIF-2 play non-redundant roles as observed by the phenotypic changes caused by expression of their target genes (50). HIF-3 acts as a negative regulator of hypoxia response, and is itself a target gene of both HIF-1 and HIF-2 (51). HIF-3 transcript depletion was shown to cause physical endurance enhancements in rats, including increased efficiency of cellular respiratory activity, demonstrating its effects as a regulator of HIF-1 and HIF-2 activity (51).

HIF family protein heterodimers are composed of a constitutively expressed beta subunit and an alpha subunit that is degraded by the proteasome as a means of regulating the transcription-activating function of the HIF dimer (52). Inhibition of alpha subunit degradation in the cytosol allows stable accumulation of HIF-1α and HIF-2α. This allows alpha subunits to bind to their beta counterparts, forming the HIF-1 and HIF-2 dimers. The HIF-1β protein is also known as aryl hydrocarbon receptor nuclear translocator (ARNT) and HIF-2β is also known as ARNT2 (53). Dimer formation is followed by nuclear translocation and a subsequent increase in target gene transcript abundance (16,52,54). HIF-1α and HIF-2α accumulation in cancer cell samples taken from patients with various cancer types is associated with increased mortality, and loss of function of either protein has been shown to correlate with decrease in tumor size (52). Of the two positive regulatory HIFs, HIF-1α is the more studied family member, and has been extensively characterized in terms of its role in cancer biology and therapeutics (21,22,52,55,56). Hundreds of genes are transactivated by HIF-1 (57). A short list of examples that have been identified and their functions are listed in Table 1-1.

Hypoxia induces stabilization of HIF-1α protein accumulation by indirectly causing inhibition of its proteasomal degradation, and inhibition may occur temporally as multiple regulatory pathways converge. The predominant hypoxia-driven inhibitory mechanism of HIF-1α degradation is prevention of hydroxylation of two specific HIF-1α proline residues by prolyl hydroxylase (PHD) enzymes (56). Proline hydroxylation of HIF-1α protein creates a motif necessary for recognition by the von Hippel-Landau protein (VHL) (50,56). VHL binding to HIF-1α recruits a ligase that ubiquitinates HIF-1α and targets it for proteasomal degradation (56). HIF-1α protein stability can also be increased by the direct upregulation of its transcript, which can occur through mitogen-activated protein kinase (MAPK) and NF-κB signaling pathways (52).

The mechanism of hypoxia-driven PHD inhibition is not fully understood, and this fact underscores the need for clarification when attempting to unravel regulation of the HIF-mediated hypoxia response. There are several plausible explanations for decreases in PHD activity during hypoxia, the simplest one being that one of the major substrates for the hydroxylation reaction, O_2, is much less available in the cell. This explanation has been complicated by evidence from experiments using cells devoid of their mitochondrial DNA, termed rho-zero (ρ^0) cells. Because ρ^0 cells lack a functioning ETC, and exhibit lower concentrations of ROS than normal cells when exposed to hypoxia, they are widely viewed as an effective model for testing whether HIF-1α stabilization in response to hypoxia requires mitochondrial ROS. Multiple experiments have demonstrated that HIF-1α stabilization is lost or severely blunted in ρ^0 cells, which suggests not only that PHDs are still active when oxygen concentrations are extremely low (~1-2%), but also that mitochondrial ROS are required to stabilize HIF-1α in

response to hypoxia (18,19,58,59). It is important to note that many additional experiments have produced equally compelling results that demonstrate exactly the opposite conclusion in similar ρ^0 cells. In these experiments, HIF-1α stabilization was not affected by loss of ETC function (45,46,48,60). These data obscure any clear definition of the mitochondrial role upstream of hypoxic adaptation.

Although there are several additional plausible explanations for the decrease in PHD activity during hypoxia, evidence clearly identifying one mechanism as solely responsible is lacking. It is possible that cellular ROS accumulation, particularly that of H_2O_2, could cause oxidation of ferrous iron (Fe^{2+}) to ferric iron (Fe^{3+}), inhibiting the ferrous iron-dependent catalytic action of PHDs (61). It is also possible that increased expression of FHC could sequester Fe^{2+} sufficiently to prevent its incorporation into the PHD active site (33,62). Additionally, decreased availability of α-ketoglutarate (α-KG), a substrate necessary for the PHD reaction, or decreased availability of ascorbate, an antioxidant necessary to reduce Fe^{3+} to Fe^{2+}, could blunt PHD activity sufficiently to establish HIF-1α stabilization (61). Finally, increased accumulation of the Krebs cycle metabolite succinate, which becomes the by-product of the α-KG-dependent PHD reaction, acts as a negative feedback inhibitor of PHDs, and could play a role in regulating PHD activity during hypoxia (61). It is important to note that the preceding suggestions for regulation of PHD activity involve processes that would not be instantaneous, and the amount of time required to cause these modes of change in activity therefore becomes a consideration when attempting to identify a plausible mechanism. HIF-1α stabilization in response to hypoxia can occur within minutes, whereas protein turnover requiring transcription, protein synthesis, and post-

translational modifications can take hours (63). Additional experiments are required that would identify a clear pathway upstream of PHD activity, and that would determine whether the mechanism differs and/or involves cross-regulatory features in a cell-type specific manner.

Ataxia-Telangiectasia Mutated Kinase-Dependent Signaling in Response to Hypoxia

Regulation of HIF-1α stabilization during hypoxia has also been shown to be mediated by phosphorylation at a specific serine residue (S696) by ataxia-telangiectasia mutated kinase (ATM). Ataxia-telangiectasia is an autosomal recessive disorder caused by a mutation-driven loss of function in the ATM gene (64). Those that suffer from the disorder display progressive cerebellar ataxia, telangiectasia (a vascular abnormality resembling spider veins), immunodeficiency, and predisposition to cancers, especially those originating in lymphoid cells (64,65). ATM belongs to the phosphatidylinositol 3-kinase like kinase (PIKK) family of serine/threonine protein kinases (64), and has been well characterized as a mediator of DNA double-strand break (DSB) repair and as an integral part of the DNA damage response (DDR) (64,66). Recent experimental evidence revealed that in addition to the nuclear distribution and DDR function of ATM, a non-canonical function of ATM in response to oxidative stress exists (65). Isolated ATM treated with H_2O_2 was shown to become activated through a mechanism independent of the canonical DDR activation mechanism, and was shown to be capable of phosphorylating target proteins in the absence of DSBs (65). Additionally, ATM activation in response to oxidative stress was shown to take place through disulfide-bridge mediated homodimerization of two ATM molecules, and this covalent dimerization was shown to be the result of oxidation at a key cysteine residue (C2991)

(65). The configuration of activated ATM in response to oxidative stress differs from ATM activated by DDR. ATM activated in response to DNA DSBs can phosphorylate its targets as a monomer (67,68). ATM phosphorylates mediators of cell cycle arrest in response to both DNA DSBs and hypoxia (45,67). ATM-dependent cell cycle arrest allows stalling of cell proliferation in cells that have sustained damage (including DSBs) caused by dynamic hypoxia/re-oxygenation-induced ROS that accumulate as blood flow is reestablished in tissue (45).

Recent experimental evidence has demonstrated that not only does ATM phosphorylate HIF-1α at S696 when it is activated in response to hypoxia but also that HIF-1α stabilization in response to hypoxia is ATM-dependent in immortalized human mammary epithelial cell lines (5,6). Although experimental evidence has not been provided that would explain how phosphorylation of HIF-1α might prevent its proteasomal degradation, it is suspected that the addition of a phosphoryl group at this position would either sterically hinder the binding of HIF-1α to the active site of PHDs, or prevent VHL binding (69).

Experimental approaches that would seek to identify the mechanism by which hypoxia drives phenotypic changes in breast cancer cells would have to consider that ATM participates in the stabilization of HIF-1α through an incompletely characterized mechanism, and that the nature of ROS-mediated effects upon this mechanism are unknown.

Hypothesis and Experimental Approach

Hypothesis

A clear consensus is lacking, but experimental evidence strongly suggests that the mitochondria are the predominant source of cellular ROS production, and that the increase in ROS observed during hypoxia is the result of the action of the ETC (18-20,34,58,62,63,70,71). Experimental evidence also provides a clear demonstration of the upregulation of HIF-1 activity in response to hypoxia, by showing an increase in the stabilization of the HIF-1α protein and an increase in the transcript abundance of HIF-1 target genes; however, this is without clear demonstration of the complete mechanism of this effect (5,6,10,72,73). Since it has been shown that the stabilization of HIF-1α is ATM-dependent in response to hypoxia, the following hypothesis was proposed: In response to hypoxia, ROS generated by the mitochondria activate ATM, and cause ATM-dependent upregulation of HIF-1α.

Experimental Approach: Administration of Antioxidant Drugs

Exogenous introduction of antioxidant drugs to mammary epithelial cell lines was selected as a method for characterizing the ROS-dependency of ATM activation and/or the ROS-dependency of HIF-1α stabilization in response to hypoxia. Antioxidants are ROS scavengers that work through a variety of mechanisms to modulate the concentrations of various intracellular ROS (27,74-81). N-acetylcysteine (NAC) was selected based on its mechanism of action that allows it to participate in thiol-disulfide exchange reactions, and because it acts intracellularly as a precursor to GSH, which scavenges $\bullet O_2^-$ (76). It is predicted that the activity of NAC would ablate ATM dimer formation in response to hypoxia, destabilizing HIF-1α, and/or it would decrease H_2O_2

concentration, potentially further destabilizing HIF-1α by allowing the activation of PHDs. The thiol-disulfide exchange mechanism of NAC is shown in Figure 1-1. This experiment was designed to demonstrate the ROS-dependency of ATM-dependent stabilization of HIF-1α in response to hypoxia in support of the current hypothesis.

4-hydroxy-TEMPO (TEMPOL) was selected as second antioxidant drug, due to its SOD-mimetic action that causes increased concentration of H_2O_2 by directly converting $\bullet O_2^-$ to H_2O_2 (27). The activity of TEMPOL would bolster the H_2O_2 produced by hypoxia, and potentially show a downstream effect on HIF-1α stabilization. The mechanism of TEMPOL activity is shown in Figure 1-2.

Experimental Approach: Development of ρ^0 Mammary Epithelial Cell Lines

Prior experimentation in various cell lines has shown that destruction or alteration of the human mitochondrial genome results in cells that display defects in respiratory function, mimicking specific human genetic diseases and providing a platform for experiments aimed at characterizing ETC activity (20,82-84). Cells devoid of mitochondrial DNA (ρ^0 cells) have been developed previously, through a variety of techniques, and can be maintained indefinitely if their growth media are adequately supplemented with uridine and pyruvate (85,86). Uridine supplementation is required due to the pyrimidine auxotrophy in ρ^0 cells that ensues following dysfunction of dihydoorate dehydrogenase (DOD), which is part of the pyrimidine biosynthesis pathway (85). DOD is anchored to the mitochondrial inner membrane and its catalytic activity requires normal electron transport (87). Pyruvate is required to supplement growth due to a depletion that is suspected to occur following the increase in lactate

dehydrogenase activity driven by excess NADH that accumulates in cells deficient in ETC function (85).

Recombinant DNA vectors aimed at depleting cells of their mitochondrial DNA were designed, using two separate approaches, in preparation for further experimentation that might demonstrate the mitochondrial ROS dependency of ATM-dependent HIF-1α stabilization in support of the current hypothesis.

Table 1-1. Examples of HIF-1 target genes and their functions (57).

Gene Name	Abbreviation	Function
Erythropoietin	EPO	Increases erythropoiesis
Vascular endothelial growth factor	VEGF	Promotes angiogenesis.
Carbonic anhydrase 9	CAIX	Increases carbon dioxide metabolism.
Glucose transporter family-member 1	GLUT	Increases cellular glucose uptake.
Pyruvate dehydrogenase-kinase isozyme 1	PDK1	Inhibits carbon entry to the Krebs cycle.
Platelet-derived growth factor subunit A	PDGFA	Mesenchymal cell mitogen.
Phosphoglycerate kinase 1	PGK1	Glycolytic enzyme.
Inducible nitric oxide synthase	iNOS	Catalyzes nitric oxide production.
Protein C-ets-1	ETS1	Transcription factor: inhibits lymphocyte development – oncogenic.
Alpha-enolase	ENO1	Glycolytic enzyme.

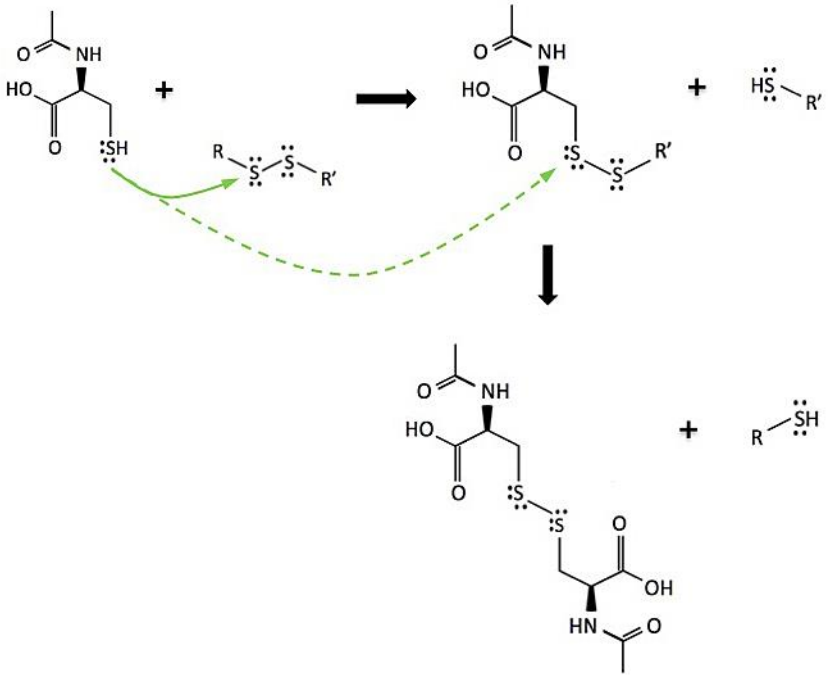

Figure 1-1. Thiol-disulfide exchange reaction mechanism. NAC is shown reacting with a target molecule. When ATM reacts with NAC, R and R' represent two identical ATM monomers. Dashed line indicates stoichiometric excess of NAC.

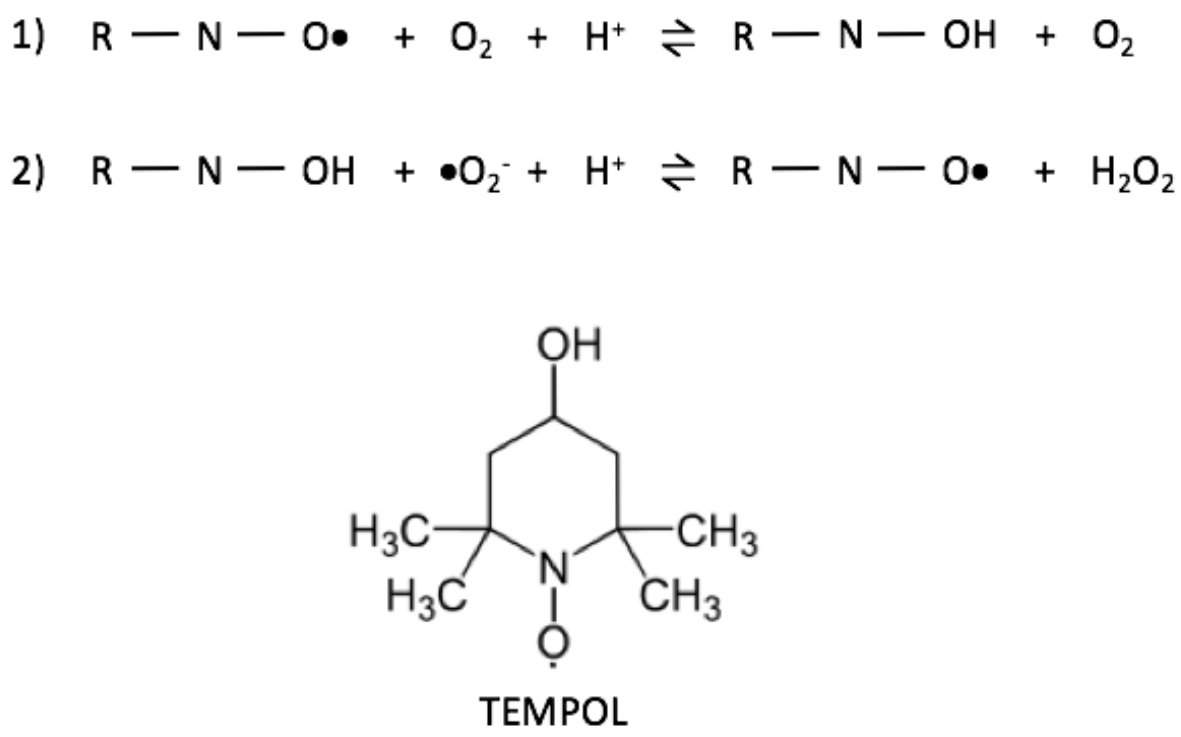

Figure 1-2. Structural diagram and mechanism of superoxide scavenging of TEMPOL. The variable “R” in in the chemical equation represents the rest of the TEMPOL molecule.

CHAPTER 2
MATERIALS AND METHODS

Quantitative PCR and Reverse Transcriptase PCR Analysis

Polymerase-γ Knockout Cells

Genomic DNA (gDNA) was isolated by incubating harvested cell pellets with lysis buffer (10 mM Tris pH 8.0, 100 mM NaCl, 10 mM EDTA, 0.5% SDS) at 55 °C for 3 hours, followed by phenol-chloroform extraction and precipitation with 100% ethanol. Relative mitochondrial DNA (mtDNA) abundance was quantified by interpolation of standard curves. Standard curves were constructed for both mtDNA and nuclear DNA (nDNA) using an arbitrary cell line (SKBr3 cells), that was not involved in the experiment. Standard curves were constructed by logarithmic serial dilution of 25 or 50 ng gDNA over six orders of magnitude. mtDNA and nDNA abundances were interpolated and mtDNA was normalized to nDNA. Relative mtDNA abundance in the POLG knockout candidate cells was then normalized to that of untreated cells.

DNA for mtDNA and for nDNA abundance was measured using real-time quantitative PCR (qPCR) with a MJ Research Opticon 2 DNA Engine (Bio-Rad) and Opticon Monitor 3 Software (Bio-Rad), using 10 µL reaction volumes containing iTaq Universal SYBR Green Supermix (BioRad), 500 nM concentration of both forward and reverse oligonucleotide primers (IDT, Coralville, IA) (Table 3-2), and approximately 5, 0.5, 0.005, or 0.0005 ng/µL of gDNA.

Cells Exposed to Hypoxia

Total RNA was isolated from harvested cells using TRI Reagent (Sigma-Aldrich) according to the manufacturers specifications. RNA was then used to synthesize complementary DNA (cDNA) using the Verso cDNA Synthesis Kit (Thermo Fisher,

Waltham, MA) by adding 500 ng RNA to a 20 µL reaction volume. Relative mRNA transcript abundance was measured using the MJ Research Opticon 2 DNA Engine (Bio-Rad, Hercules, CA) and Opticon Monitor 3 Software (Bio-Rad), using 10 µL reaction volumes containing iTaq Universal SYBR Green Supermix (BioRad), 350 nM concentration of both forward and reverse oligonucleotide primers (IDT), and 1 ng/µL concentration of cDNA. Relative transcript abundance was calculated using the $2^{-\Delta\Delta CT}$ method (88). The glyceraldehyde 3-phosphate dehydrogenase (GAPDH) gene was used as an endogenous standard (primers #9 and #10, Table 3-1). All experiments were performed in triplicate (three biological replicates), with each biological replicate representing an independent population of cells. Each biological replicate was also performed in triplicate (three technical replicates per biological replicate).

Cells transduced with pMSP-6 plasmid Vector

Total RNA was isolated from harvested cells using TRI Reagent (Sigma-Aldrich) according to the manufacturers specifications. RNA was then used to synthesize complementary DNA (cDNA) using the Verso cDNA Synthesis Kit (Thermo Fisher, Waltham, MA) by adding 500 ng RNA to a 20 µL reaction volume. Relative mRNA transcript abundance was measured by visualizing band intensity of electrophoresed PCR products using agarose gel electrophoresis and ethidium bromide. PCR was carried out using cDNA or plasmid template samples, oligonucleotide primer sets (IDT), and GoTaq DNA Polymerase (Promega).

Genome Editing Using CRISPR-Cas9

Exon 2 of the gene encoding the catalytic subunit of POLG was selected as a target for CRISPR-Cas9 genome editing. Single-guide RNA (sgRNA) oligonucleotide sequences were selected and queried against the NCBI gene database for specificity

ranking using an online sequence analysis tool (http://crispr.mit.edu). Two sgRNA oligonucleotides were synthesized (IDT) (Table 3-2), using a pLentiCRISPR v.1 (pLC) protocol (http://genome-engineering.org/gecko/) as a guide for design of the necessary ligation overhang nucleotides. Digestion of pLC plasmid with BsmB1 endonuclease, annealing and phosphorylation of the oligonucleotides, and ligation of the sgRNAs into pLC (Addgene, Cambridge, MA) were carried out according to the pLC protocol. Ligations were chemically transformed into KRX cells (Promega, Madison, WI) followed by plasmid DNA isolation using the GeneJet Plasmid Miniprep Kit (Thermo Fisher). Sequences were confirmed by Sanger chain termination sequencing (GeneWiz, South Plainfield, NJ) using a universal hU6 primer (Table 3-2). Lenti-X human embryonic kidney (HEK) 293T cells (Takara Bio, Mountain View, CA) were co-transfected with psPAX2 (Addgene #12260), pMD2.G (Addgene #12259), and sgRNA-containing pLC plasmid vectors, using Lipofectamine 2000 Reagent (Thermo Fisher) as the transfection medium, according to the manufacturer's instructions. As an experimental control, Lenti-X cells were also co-transfected with psPAX2, pMD2.G, and empty pLC plasmid. Lenti-X supernatant virus-containing medium was collected after approximately 72 hours post-transfection, and used to transduce HMEC cells. Transduced cells were selected using puromycin (2 μg/mL) (Sigma-Aldrich) for approximately 2 weeks, followed by harvesting of cells for immunoblot analysis.

Immunoblot Analysis

Determination of protein concentration of cellular lysates was performed by Smith assay (Thermo Fisher), using either the test-tube or microplate method, with Pierce bicinchoninic acid (BCA) reagent (Thermo Fisher). 96-well plates were scanned on a BioTek Cytation5 plate reader using BioTek Gen5 software (BioTek, Winooski, VT).

SDS-PAGE and nitrocellulose membrane electrotransfer were performed using protocols established previously by the Brown laboratory. Nitrocellulose membranes were probed either with α-POLG rabbit monoclonal IgG (#13609 Cell Signaling, Danvers, MA) or α-Hif1α polyclonal rabbit IgG (#NB100-134 Novus Biologicals, Littleton, CO) primary antibodies, followed by horseradish peroxidase-conjugated (HRP) goat anti-rabbit secondary antibody incubation. Blot images were recorded by developing x-ray film exposed to chemiluminescence using luminol substrate (Thermo Fisher). Equal loading of samples was confirmed by probing nitrocellulose with an HRP-conjugated α-β-Actin mouse IgG (#sc47778, Santa Cruz Biotechnology, Dallas, TX), or by Coomassie Brilliant Blue staining of duplicate acrylamide gels.

Cell Culture and Exposure to Hypoxia

Immortalized human mammary epithelial cells (HMECs) were the generous gift of Dr. Jianrong Lu (University of Florida). The SKBr3 and HEK 293T (Lenti-X) cell lines were obtained from ATCC (Manassas, VA). Cells were cultured in Dulbecco's Modification of Eagle's Medium (DMEM) (Mediatech, Manassas, VA), containing 4.5 g/L glucose, supplemented with penicillin (50 U/mL), (GE Healthcare, Pittsburgh, PA) streptomycin (50 µg/mL) (GE Healthcare), 10% heat-inactivated fetal bovine serum (FBS), and ciprofloxacin (10 µg/mL). POLG knockout candidate cells were further supplemented with sodium pyruvate (100 µg/mL) (GE Healthcare) and uridine (50 µg/mL) (GE Healthcare). Lenti-X transfections were incubated in serum-free RPMI medium (Thermo Fisher) for the first 24 hours. Cells were incubated at 37 °C in a water-jacketed CO_2 incubator (Thermo Fisher), at 5% CO_2 concentration.

To expose cells to hypoxia, 60-80% confluent 60 or 100 mm diameter Petri dishes were placed in a sealed chamber (Billups-Rothenberg, Inc. MIC-101, San Diego,

CA) and purged with a gas mixture containing 1% O_2, 5% CO_2, and 94% N_2. Cells were exposed to hypoxia for 18 hours, at which time the chamber was opened to allow for trypsinization and harvesting of cells.

Antoxidant Drugs

Cells were exposed to N-acetylcysteine (NAC) (Sigma-Aldrich, St. Louis, MO) at 1.0, 5.0, 10.0, 12.5, or 15.0 mM concentrations, or 4-hydroxy-TEMPO (TEMPOL) (Sigma-Aldrich) at 100, 200, 500, 1000, or 1500 μM concentrations. Cells in 60-80% confluent 60 or 100 mm Petri dishes were treated with antioxidants, immediately placed into a hypoxia chamber as described above, and harvested after 18 hours.

Recombinant DNA Vector Construction: Eco-R1 Endonuclease

The pMB3 plasmid containing the EcoR1 endonuclease nucleotide sequence was the generous gift of New England Biolabs (NEB, Ipswitch, MA). The pLV-mitoGFP and pLenti-Puro plasmids were obtained from Addgene (#44385, #39481), the pBluescript plasmid was obtained from Stratagene (#212207 Agilent Technologies, Santa Clara, CA), and the pGIPZ plasmid was obtained from GE Healthcare/Dharmacon (#RHS4348). Oligonucleotide primer synthesis for sequencing primers and for PCR amplification primers was carried out by IDT. PCR amplification of plasmid DNA templates was carried out using GoTaq DNA Polymerase (Promega). Precipitation of PCR amplified DNA and of endonuclease-digested DNA was accomplished with 4 M ammonium acetate and 100% ethanol. TA cloning of the EcoR1 sequence from the pMB3 plasmid was carried out using the pCR4-TOPO TA Cloning Kit (Thermo Fisher). EcoR1-HF, Kpn1-HF, EcoRV, and Xho1 endonucleases were obtained from NEB. Sanger chain termination sequencing verification was carried out by GeneWiz. Chemical transformation of ligated DNA plasmids was carried out using KRX

cells (Promega). Transfection into Lenti-X cells was accomplished using Lipofectamine 2000 Reagent (Thermo Fisher). Selection of target cells was accomplished using puromycin at 2 μg/mL concentration (Sigma Aldrich). Fluorescence microscopy images were generated using a Nikon Diaphot microscope (Nikon, Melville, NY) attached to a Q-Imaging Retiga EXi camera, operated by Q-Capture Pro v. 600412 software (Q-Imaging, Surrey, BC, Canada).

Statistical Methods

Unpaired one-tailed *t*-test calculations were performed to compare the qPCR-generated mean relative expression values from independent treatment conditions, to establish any statistical difference between the means. For the hypoxia-treated cell experiments, the inter-quartile range of each set of ΔCT values from each treatment condition with n>3 was calculated, to identify statistical outliers, and to establish equal variance between treatment groups. Statistical significance was established by comparing the *t*-test value returned with the p value from the t-table. Values returned by the *t*-test that were found to be less than the p value were found to be statistically significant.

CHAPTER 3
RESULTS

Characterization of Reactive Oxygen Species-Dependent Gene Expression in HIF1 Target Genes

Based on the hypothesis that ROS generated in cells during exposure to hypoxia would activate ATM kinase and cause ATM-dependent upregulation of HIF-1α, it was proposed that treatment of cells with antioxidant drugs during hypoxic exposure would alter hypoxia-induced upregulation of HIF-1 target genes. Based on experimental data, the carbonic anhydrase IX (CA9), glucose transporter family-member 1 (GLUT1), pyruvate dehydrogenase kinase isozyme 1 (PDK1), and vascular endothelial growth factor (VEGF) genes were selected as surrogate markers for hypoxic HIF-1-dependent response, and for measurement of any change in response caused by treatment with antioxidant drugs (5,21,60,89,90).

HMEC and SKBr3 cells were treated either with 20% (untreated cells incubated at normal atmosphere) or 1% oxygen for 18 hours, as previously outlined (5). Following this, total cellular RNA was isolated from cells, cDNA was synthesized using random hexamers as primers, and qPCR was used (Figures 3-1, 3-2) to measure relative transcript abundance of the selected genes using gene-specific primer sets (Table 3-1). Based on the results from these initial experiments, the CA9 and VEGF genes were selected as hypoxia response markers for additional experiments in HMEC and SKBr3 cells, respectively.

NAC was selected as an antioxidant to be used in the current experiment, based upon its mechanism of action and upon recent experimentation in an immortalized breast cancer cell line that demonstrated reduction of cellular ROS and downregulation of ATM activity following NAC exposure (91). To determine the concentration of NAC

that would demonstrate a decrease in the hypoxia-induced response in the CA9 and VEGF genes, gradually increasing concentrations ranging from 1 to 15 mM were administered to HMEC and SKBr3 cells during hypoxia, and qPCR was used to measure the relative transcript abundance (Figures 3-3A, 3-4A). The $2^{-\Delta\Delta CT}$ method of calculation of the mean relative transcript abundance was used to quantify the comparative abundance levels of each condition, and all resulting values were normalized to the abundance value for untreated cells (20% oxygen without addition of NAC). The results from the gradually increasing concentrations allowed selection of 1 and 5 mM concentrations of NAC for administration in a larger number of experiments in both cell types.

TEMPOL was selected as a second antioxidant to be used, based upon its mechanism of action and recent experimentation in immortalized mammary epithelial cell lines that demonstrated downregulation of ATM activity during normoxic (20%) oxygen tension (92). To determine the concentration of TEMPOL that would cause a decrease in ATM activity in response to hypoxia, gradually increasing concentrations ranging from 100 to 1500 μM were administered to HMEC and SKBr3 cells during hypoxia (Figures 3-3B, 3-4B). qPCR was conducted as described above, and the results from the gradually increasing concentrations allowed selection of 200 and 500 μM concentrations of TEMPOL for administration in a larger number of experiments in both cell types.

Figures 3-5 and 3-6 show the results of qPCR assays measuring relative transcript abundance of the CA9 and VEGF genes in HMEC and SKBr3 cells, respectively, after exposure to either 20% or 1% oxygen, with or without the addition of

NAC at 1 or 5 mM concentrations. Quantification of the qPCR results was conducted as described above, with the aggregate mean values from three experiments (biological replicates) normalized to the aggregate mean values for three experiments using untreated (20% oxygen) cells. Unpaired one-tailed *t*-tests were conducted to establish any statistical difference between the mean relative expression values for various conditions, and equal variance was assumed in all conditions compared. In HMEC cells, the results of the experiment showed that 5 mM NAC significantly ($p<0.05$) reduced the hypoxia-induced upregulation of the CA9 gene. In SKBr3 cells, the results of the experiment showed a similar degree of reduction in the hypoxia-induced upregulation of the VEGF gene, which was shown to be significant ($p<0.05$).

To characterize any change in HIF-1α protein accumulation that would have resulted from the treatment of cells with hypoxia and/or NAC at 5 mM concentration, total cellular protein extracts were collected after conditions identical to those used for the qPCR quantification described above. Immunoblotting was conducted using a polyclonal rabbit anti-HIF-1α antibody to compare three of the experimental conditions in SKBr3 cells (Figure 3-7). The results of the immunoblot showed a clear upregulation of HIF-1α upon treatment with hypoxia, with basal levels in untreated cells that fell below detectable limits. Treatment with 5 mM NAC resulted in undetectable hypoxia-induced accumulation of HIF-1α. The results of the experiments that introduced hypoxia at 1% O_2 for 18 hours, with or without administration of 5 mM NAC therefore showed that NAC blunts the hypoxia-induced upregulation of HIF-1 target genes by prevention of HIF-1α protein accumulation.

Figures 3-8 and 3-9 show the results of qPCR assays measuring relative transcript abundance of the CA9 and VEGF genes in HMEC and SKBr3 cells, respectively, after exposure to either 20% or 1% oxygen, with or without the addition of TEMPOL at 200 or 500 μM concentrations. Measurement of relative transcript abundance and statistical comparison of resulting values was conducted in the same manner described above for NAC administration. In HMEC cells the results showed that the 500 μM concentration of TEMPOL during hypoxic exposure significantly ($p<0.05$) increased CA9 transcript abundance relative to cells exposed to hypoxia without TEMPOL. In SKBr3 cells this result was not shown, as neither concentration of TEMPOL resulted in a significant change in the transcript abundance of VEGF relative to cells exposed to hypoxia without TEMPOL.

To characterize any change in HIF-1α protein accumulation that would have resulted from the treatment of HMEC cells with hypoxia and/or TEMPOL at 500 μM concentration, total HMEC cellular protein extracts were collected after conditions identical to those used for the qPCR quantification described above. Immunoblotting was conducted using a polyclonal rabbit anti-HIF-1α antibody to compare three of the experimental conditions in HMEC cells (Figure 3-10). The results of the immunoblot showed a clear upregulation of HIF-1α upon treatment with hypoxia, with basal levels in untreated cells that fell below detectable limits. Treatment with 500 μM TEMPOL resulted in undetectable hypoxia-induced accumulation of HIF-1α. The results of the experiments that introduced hypoxia at 1% O_2 for 18 hours, with or without administration of 500 μM TEMPOL showed that upregulation of the CA9 gene in TEMPOL-treated HMEC cells was not caused by HIF-1α protein accumulation.

Disruption of Electron Transport Via Digestion of the Mitrochondrial Genome with EcoR1 Endonuclease

It has been shown previously that digestion of the human mitochondrial chromosome with exogenously introduced EcoR1 endonuclease (EcoR1) results in loss of protein expression from mitochondrial genes and depletion of mitochondrial DNA and mitochondrial copy number in daughter cells (82,85). Successful introduction of a recombinant DNA vector encoding EcoR1 and a mitochondrial targeting sequence (MTS) has been shown to result in the generation of cells displaying the rho-zero (ρ^0) phenotype, which is characterized by absence of mitochondrial DNA and loss of associated mitochondrial functions (82,85). To develop ρ^0 cells for further characterization of cellular signaling in human mammary epithelial cell lines, a recombinant DNA expression vector was constructed.

New England Biolabs provided the generous gift of the pMB3 plasmid, that contained the EcoR1 nucleotide sequence (Figure 3-11). The sequence was confirmed by Sanger chain termination sequencing using primers that were designed using a reference nucleotide sequence (Table 3-2, primers #9 and #10 (93)). Sequencing data provided confirmation of the EcoR1 sequence and revealed that a suitable restriction site was absent from the 3' end of sequence (Figure 3-11 (92)). A set of primers was designed that would amplify only the portion of the pMB3 plasmid that contained the EcoR1 coding sequence, for TOPO TA cloning of the EcoR1 sequence into the pCR4-TOPO linear backbone (Table 3-2, primers #16 and #17). The PCR amplicon from primers #16 and #17 was precipitated using 4 M ammonium acetate and 100% ethanol, and was ligated into pCR4-TOPO. The ligation was transformed into chemically competent KRX cells, and colonies from bacterial culture were selected and enriched

for plasmid DNA isolation, which was carried out using the GeneJet Plasmid Miniprep Kit. To confirm the presence of recombinants, plasmids were subjected to restriction digest with EcoR1. A flanking set of EcoR1 restriction sites resident within pCR4-TOPO identified a band approximately the size of the EcoR1 insert (0.85 kb) following electrophoresis of the digested plasmids. The sequence of the EcoR1/pCR4-TOPO plasmid was confirmed by Sanger chain termination sequencing using primers #28 and #29 (Table 3-2). Ligation of the EcoR1 fragment into pCR4-TOPO and subsequent ligations conducted during construction of the final pMSP-6 vector are outlined in a schematic diagram (Figure 3-12).

A set of primers was then constructed that would re-amplify the EcoR1 sequence, using the pCR4-TOPO plasmid as a template, while integrating new unique restriction sites at both the 5' and 3' ends of the sequence (Table 3-2, primers #20 and #21). The forward primer integrated a unique Kpn1 site at the 5' end, and the reverse primer integrated a unique Xho1 site at the 3' end. These specifically designed primers also removed the existing EcoR1 sites resident in the pCR4-TOPO vector. The PCR amplicon made from this primer set was precipitated as described above, then digested with Kpn1-HF and Xho1 endonucleases (Figure 3-12). The digested amplicon was re-precipitated with ethanol and re-suspended in nuclease-free water. This insert was then ligated into the pBluescript (pBS) plasmid after digestion of pBS Kpn1-HF and Xho1. The ligation was transformed and plasmid DNA was isolated as described above, and plasmid extracts were subjected to Sanger chain termination sequencing to confirm that PCR had not introduced errors in the sequence during amplification. The sequence was confirmed as previously, using primers #9 and #10 (Table 3-2). The position of the

EcoR1 insert within the pBS plasmid was designed deliberately to allow a second insert to be placed 5' of the EcoR1 insert, with conservation of the reading frame, using a digestion scheme of EcoR1-HF and Kpn1-HF. The pBS plasmid was selected for this sub-cloning scheme due to the flexibility of its multiple cloning site, and the ability to use blue-white color selection.

A second insert containing the MTS sequence upstream of the green fluorescent protein (GFP) gene was selected for ligation into the position upstream of the EcoR1 insert in pBS. GFP was selected as a visual marker for recombinant protein expression and as a marker for mitochondrial targeting as previously outlined (82,85). The DNA fragment for MTS-GFP was obtained from the pLV-mitoGFP plasmid, and expression of GFP by this plasmid was confirmed by transfecting Lenti-X cells and observing fluorescence by microscopy after 24-48 hours (Figure 3-13A). For comparison of GFP signal, the pGIPZ plasmid, which had been tested previously by the Brown lab, was used as a positive control for GFP expression (Figure 3-13B). It was observed that the GFP signal from pLV-mito-GFP was considerably weaker than that from pGIPZ, and it was hypothesized that the mitochondrial localization of the GFP protein encoded by pLV-mitoGFP may have prevented accumulation levels identical to that of pGIPZ. Co-localization of GFP rendered by pLV-mito-GFP with mitochondria was not tested, but a test was planned as part of characterization of the final vector construct.

Primers were constructed, using the pLV-mitoGFP reference sequence as a guide (Table 3-2, primers #18 and #19), that would amplify only the portion of pLV-mitoGFP that contained the MTS-GFP open reading frame (Figure 3-14). The PCR amplicon from this primer set was then blunt cloned into pBS after digest of pBS with

EcoRV endonuclease. Plasmid DNA was isolated as previously and the sequence was confirmed by Sanger chain termination using primers #11 and #12 (Table 3-2). This intermediate blunt cloning step was performed to insure the recovery of the proper sequence from pLV-mitoGFP, using the flexibility of the pBS plasmid.

Primers were then constructed, using the pBS/MTS-GFP plasmid as a guide, that would re-amplify the MTS-GFP sequence. Using primer-encoded restriction sites, unique restriction sites were introduced at both the 5' and 3' ends of the amplicon. The forward primer placed an EcoR1 site at the 5' end, and the reverse primer placed a Kpn1 site at the 3' end (primers #22 and #23, Table 3-2). The PCR amplicon was precipitated as described previously and digested with EcoR1-HF and Kpn1-HF. After re-precipitation, the insert was ligated into the pBS plasmid containing the EcoR1 insert, via digestion of that plasmid with EcoR1-HF and Kpn1-HF (Figure 3-12). Identification of recombinant plasmids was accomplished using restriction mapping and Sanger chain termination sequencing using primers #9-12 (Table 3-2). Sequencing data confirmed that the two inserts were intact and that the reading frame was conserved throughout the length of the tandem insert.

To construct the transduction vector pMSP-6, a lentiviral destination vector for the tandem insert housed in pBS was selected that contained a puromycin resistance gene for selection of transduced cells. The pLenti-Puro plasmid was selected due to its featuring of the puromycin resistance gene and a multiple cloning site that would allow directional cloning of the tandem insert downstream of the cytomegalovirus (CMV) promoter, using a digestion scheme of EcoR1 and Xho1 (Figures 3-12, 3-15). After ligation of the tandem insert into pLenti-Puro, KRX cells were again transformed, and

plasmid DNA was isolated from colonies as previously described. The sequence of the vector was confirmed a final time by Sanger chain termination sequencing, using primers #10, #11, #13, and #14 (Table 3-2). Figure 3-16 shows the plasmid map of the final construct of the plasmid vector pMSP-6.

Following sequence verification (Figures 3-17, 3-18, 3-19), pMSP-6 was co-transfected, along with the lentiviral packaging plasmids psPAX2 and pMD2.G into Lenti-X cells, and incubated for approximately 72 hours. After incubation, supernatant culture medium was used to transduce SKBr3 target cells. Target cell media were supplemented with pyruvate (100 µg/mL) and uridine (50 µg/mL), followed by selection of cells using puromycin (2 µg/mL). After approximately 48 hours, Petri dishes containing selected cells were observed by fluorescence microscopy, and the GFP expression level appeared to be the same as that of control cells that had not been transduced (Figure 3-13C). It was suspected that the target cells did not express the transcript encoded by pMSP-6. Total RNA extract from puromycin-selected SKBr3 cells was collected, and cDNA was synthesized using the Verso cDNA Synthesis Kit as described previously. PCR was carried out using primers #10 and #11 (Table 3-2), using either cDNA from pMSP-6 transduced cells, empty vector (EV) pLenti-Puro transduced cells, or pMSP-6 plasmid DNA as positive control. A GAPDH primer set was used as an indicator of successful cDNA synthesis (primers #9 and #10, Table 3-1), and as a readout for successful PCR reactions from transduced cell cDNA samples. Figure 3-20 shows the results of this PCR assay, with a clear indication that the transcript from the pMSP-6 transduction into SKBr3 cells was not produced. Plans were made to transfect the pMSP-6 plasmid into Lenti-X cells again, without viral packaging plasmids,

and to harvest the RNA extract directly from Lenti-X cells. This plan would seek to determine by PCR if the pMSP-6 transcript would be produced by cells at an earlier stage of the transduction process.

Disruption of Electron Transport Via CRISPR-Cas9-mediated Gene Knockout of the Polymerase-γ Catalytic Subunit

It was hypothesized that CRISPR-Cas9-mediated gene knockout of the polymerase-γ catalytic subunit (POLG) gene would result in inhibition of mtDNA replication, and would therefore prevent the expression of proteins encoded by the mitochondrial genome during cell division. Based on this hypothesis, it was suspected that knockout of the POLG gene would result in daughter cells that displayed the ρ^0 phenotype. The sequence encoding the start codon of the POLG protein was identified by examining the first and second exons of the genomic DNA locus, using a reference amino acid sequence as a guide. The translational start codon was identified within exon two, which provided identification of the region of interest for selection of single guide RNA (sgRNA) target sequences within the exon, downstream of the start codon. Oligonucleotides containing the target sequences and the necessary ligation overhangs were synthesized, then phosphorylated, annealed, and ligated into the pLC plasmid according to the pLC protocol (Figures 3-21, 3-22).

The sgRNA destination site within the pLC plasmid was prepared by digestion with BsmB1 endonuclease, followed by DNA purification via gel electrophoresis. Ligation was carried out according to the pLC protocol, followed by chemical transformation into KRX cells and enrichment of plasmid DNA candidate clones. Plasmid DNA candidates were identified by gel electrophoresis after linearization with EcoR1 endonuclease. Clones that showed gel migrations greater than 10k base pairs

were suspected of being successful, and were subjected to Sanger chain termination sequencing using the hU6 primer (Table 3-2, primer #15). Analysis of sequencing results using Sequencher version 4.5 software provided identification of successful integration of sgRNA #1 and sgRNA #2 into the pLC plasmid (Figures 3-23, 3-24).

Plasmid DNA containing either the sgRNA #1 or the sgRNA #2 sequence (sg1 or sg2) was co-transfected along with the lentiviral packaging plasmids psPAX2 and pMD2.G, into HEK 293T (Lenti-X) cells. Supernatant cell culture medium from transfected Lenti-X cells was used to transduce HMEC target cells, either singularly or in tandem, creating three versions of the CRISPR-Cas9-mediated gene knockout attempt (sg1, sg2, and sg1/sg2). Target cell media were supplemented with uridine and sodium pyruvate, followed by selection of cells using puromycin (2 µg/mL). Protein extracts from polyclonal HMEC populations were subjected to immunoblotting to examine POLG protein levels. Out of the three pools of cells created, only the sg1/sg2 population demonstrated a partial decrease in POLG accumulation (Figure 3-25). Equal loading of immunoblotted protein extracts from untreated, sg1, sg2, sg1/sg2, and pLC empty vector cells was confirmed by Coomassie Brilliant Blue staining of a duplicate protein gel (Figure 3-26).

Genomic DNA from sg1/sg2 cells was isolated, and qPCR was used to measure the relative abundance of mtDNA in sg1/sg2 cells versus untreated cells. The standard curve method of quantification was used to determine the relative abundance of mtDNA in cells, and the HIF-1α gene was used as an arbitrary nDNA locus for endogenous reference control. (94). Individual standard curves were constructed for both mtDNA and for nDNA, using SKBr3 cells (Figures 3-27, 3-28). Primer sets #24-27 (Table 3-2)

were used to detect HIF-1α and mtDNA for both the standard curve construction and for the relative quantification in HMEC cells.

The abundance values of mtDNA in cells, based on the interpolated values from the standard curve, were normalized to the interpolated values of the abundance of nDNA, and the mean relative abundance was determined (Figures 3-27, 3-28). This procedure was carried out in sg1/sg2 cells and in untreated cells, creating two ratios for mean relative mtDNA abundance. The ratio generated by sg1/sg2 cells was then normalized to the ratio generated by untreated cells. The resulting fraction demonstrated a 32% reduction in mtDNA accumulation in sg1/sg2 cells versus untreated cells (Figure 3-29). This difference was not found to be significant when comparing the data points that generated the mean relative abundance figures for mtDNA normalized to nDNA. An unpaired *t*-test assuming equal variance was used to determine statistical significance ($p > 0.05$).

After observing a decrease in protein accumulation and a decrease in mtDNA abundance in sg1/sg2 cells, it was suspected that the cell population contained a subpopulation of POLG heterozygous and/or homozygous knockout cells. To isolate homozygous knockout cells from the potential subpopulation of cells expressing decreased levels of POLG and mtDNA, the polyclonal sg1/sg2 cell population was cloned by serial dilution, so that monoclonal populations could be cultured and tested for homozygous knockout of POLG expression. Clonal populations (clones A-O) were subjected to immunoblotting. This analysis did not demonstrate any decrease in POLG protein accumulation within any of the clones assayed (Figure 3-30). Additional clones (clones P-X) were gathered but not tested in favor of the development and transduction

of additional sgRNA plasmids that would target alternate sequences in exon 2 or exon 3 of the POLG locus.

Table 3-1. List of primer sequences used for qPCR detection of relative expression of selected genes.

No.	Name	Sequence	Purpose
1	CA9-FOR	GTCTCGCTTGGAAGAAATCG	qPCR detection of relative CA9 transcript abundance in response to hypoxia.
2	CA9-REV	AGAGGGTGTGGAGCTGCTTA	qPCR detection of relative CA9 transcript abundance in response to hypoxia.
3	GLUT1-FOR	TCACTGTCGTGTCGCTGTTT	qPCR detection of relative GLUT1 transcript abundance in response to hypoxia.
4	GLUT1-REV	TGAAGAGTTCAGCCACGATG	qPCR detection of relative GLUT1 transcript abundance in response to hypoxia.
5	PDK1-FOR	GGACTTCGGATCAGTGAATGC	qPCR detection of relative PDK1 transcript abundance in response to hypoxia.
6	PDK1-REV	TAGCTTTAGCATCCTCAGCAC	qPCR detection of relative PDK1 transcript abundance in response to hypoxia.
7	VEGF-FOR	TGAAGGAAGAGGAGACTCTGC	qPCR detection of relative VEGF transcript abundance in response to hypoxia.
8	VEGF-FOR	TCTCTAATCTTCCGGGCTCG	qPCR detection of relative VEGF transcript abundance in response to hypoxia.
9	GAPDH-FOR	ACCCAGAAGACTGTGGATGG	qPCR/RT-PCR detection of GAPDH endogenous control.
10	GAPDH-REV	TTCAGCTCAGGGATGACCTT	qPCR/RT-PCR detection of GAPDH endogenous control.

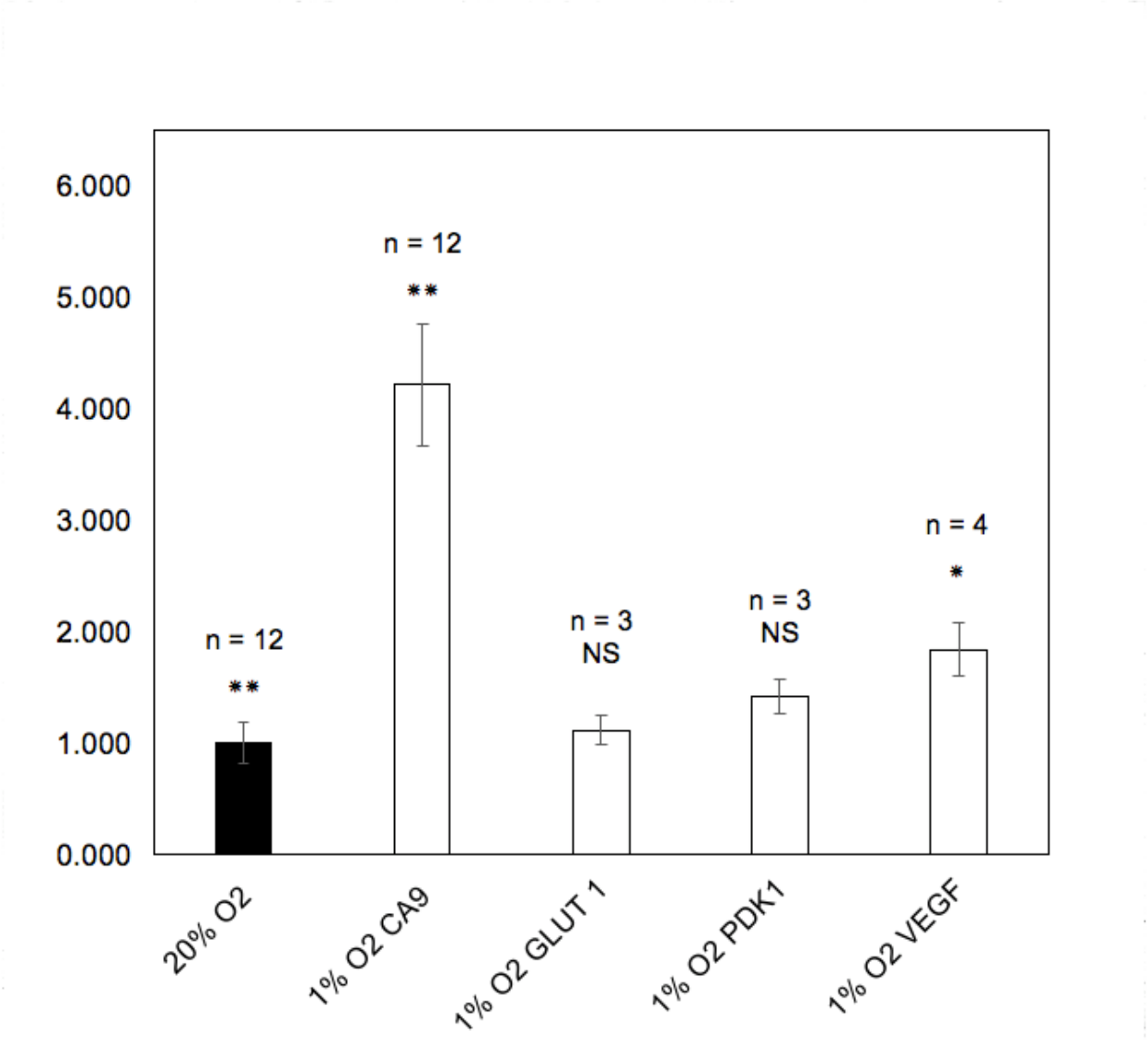

Figure 3-1. Mean relative transcript abundance levels of HIF1 target genes in HMEC cells, following 18-hour exposure to 20% or 1% oxygen. Relative transcript abundance was quantified by qPCR, using the $2^{-\Delta\Delta CT}$ method, and transcript abundance was normalized to untreated HMEC cells. Error bars represent standard error of the mean for the number of experiments equal to n. Unpaired *t*-tests were performed to determine the difference between untreated and treated mean values for each gene. Equal variance was assumed in all conditions. *, $p<0.05$; **, $p<0.01$; NS, not significant.

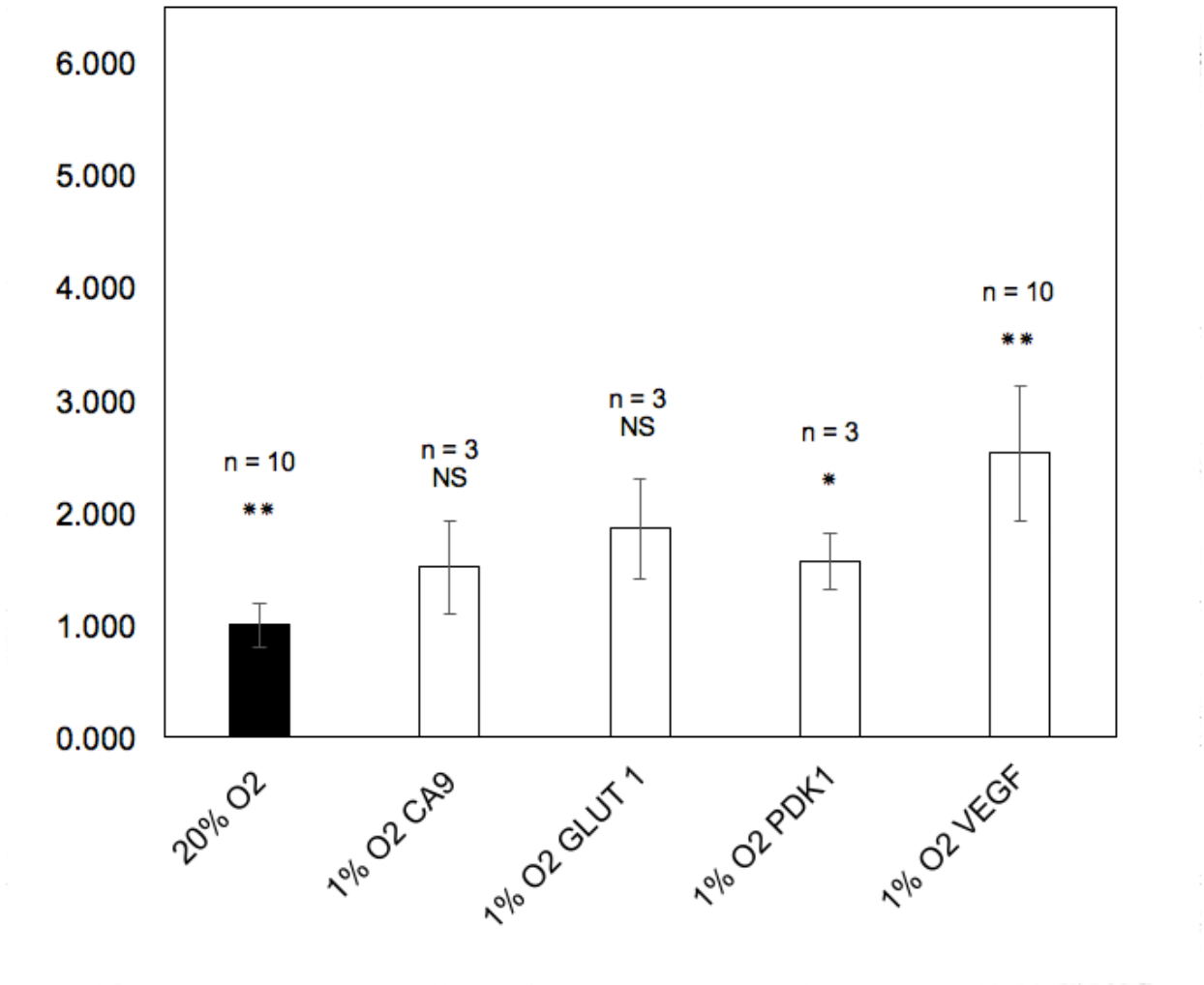

Figure 3-2. Mean relative transcript abundance levels of HIF1 target genes in SKBr3 cells, following 18-hour exposure to 20% or 1% oxygen. Relative transcript abundance was quantified by qPCR, using the $2^{-\Delta\Delta CT}$ method, and transcript abundance was normalized to untreated SKBr3 cells. Error bars represent standard error of the mean for the number of experiments equal to n. Unpaired *t*-tests were performed to determine the difference between untreated and treated mean values for each gene. Equal variance was assumed in all conditions. *, $p<0.05$; **, $p<0.01$; NS, not significant.

A.

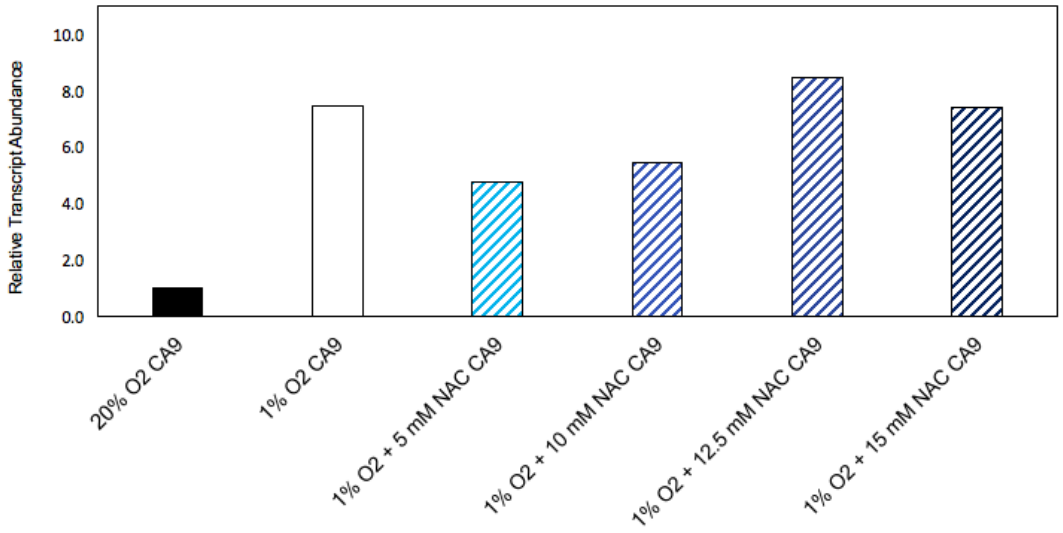

B.

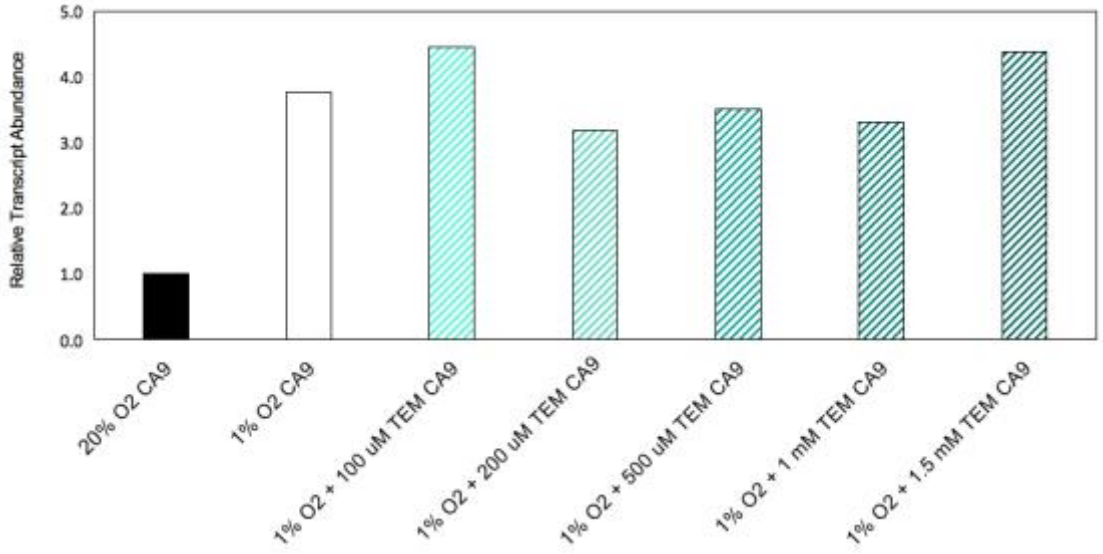

Figure 3-3. Mean relative transcript abundance of the CA9 gene in HMEC cells following treatment with either 20% or 1% oxygen, with or without the addition of A) NAC or B) TEMPOL at the indicated concentrations. Relative transcript abundance was measured by qPCR using the $2^{-\Delta\Delta CT}$ method and normalized to untreated HMEC cells (20% O_2) for n = 1 experiment. TEM, TEMPOL.

A.

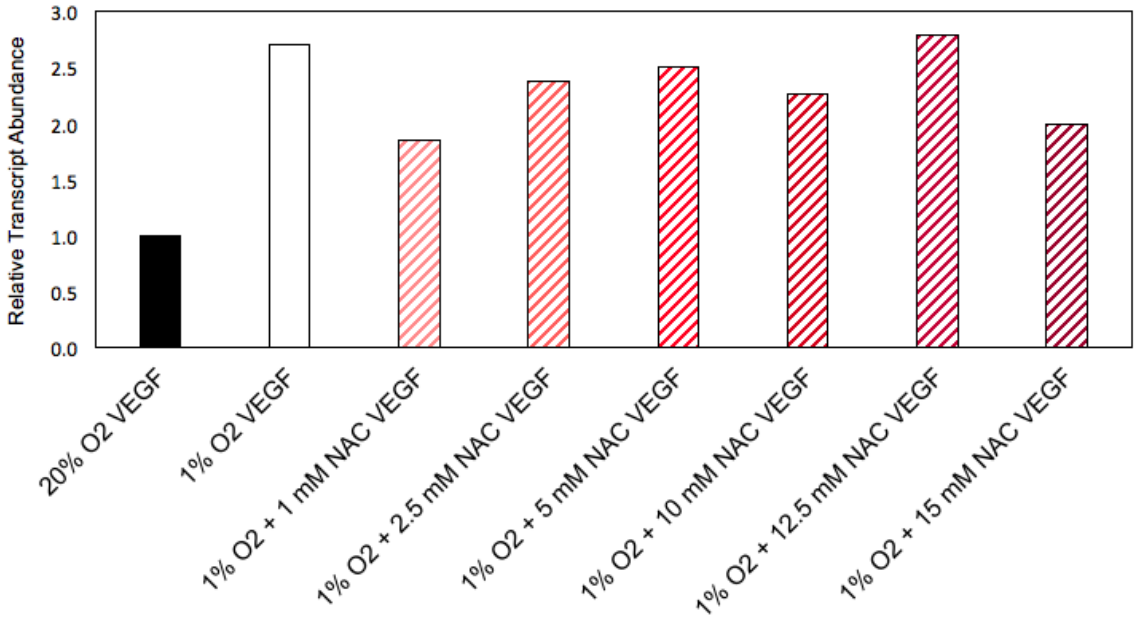

B.

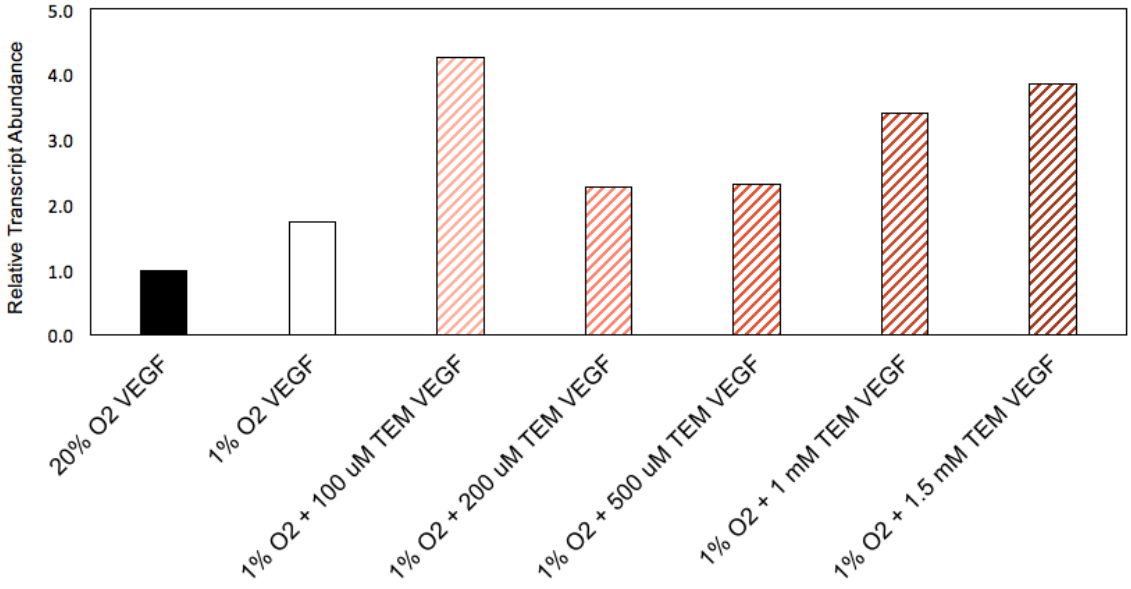

Figure 3-4. Mean relative transcript abundance of the VEGF gene in SKBr3 cells following treatment with either 20% or 1% oxygen, with or without the addition of A) NAC or B) TEMPOL at the indicated concentrations. Relative transcript abundance was measured by qPCR using the $2^{-\Delta\Delta CT}$ method and normalized to untreated SKBr3 cells (20% O_2) for n = 1 experiment. TEM, TEMPOL.

A.

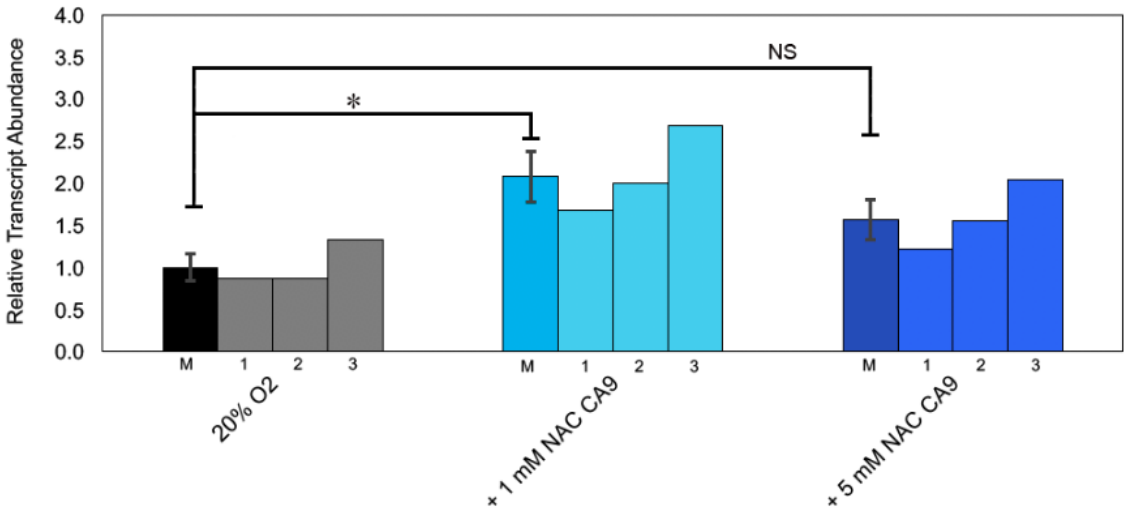

B.

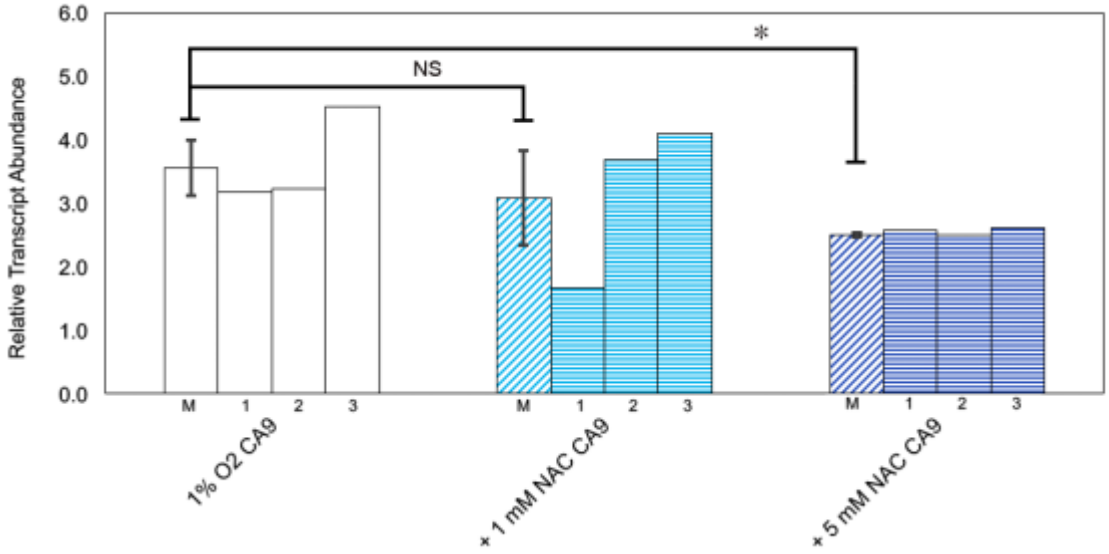

Figure 3-5. Mean relative transcript abundance of the CA9 gene in HMEC cells, following treatment with either A) 20% or B) 1% oxygen for 18 hours, with or without the addition of NAC at the indicated concentrations. Relative transcript abundance was measured by qPCR using the $2^{-\Delta\Delta CT}$ method and normalized to the mean transcript abundance value for untreated HMEC cells (20% O_2) for n = 3 experiments. Unpaired *t*-tests were performed to determine the differences between the means, and equal variance was assumed in all conditions. *, $p<0.05$; NS, not significant; M, mean.

A.

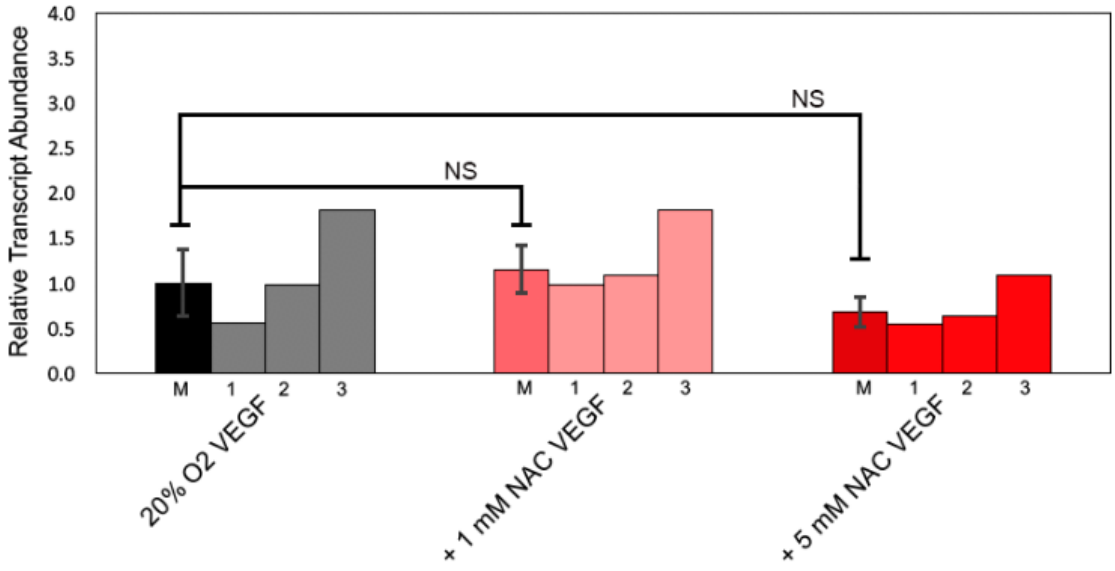

B.

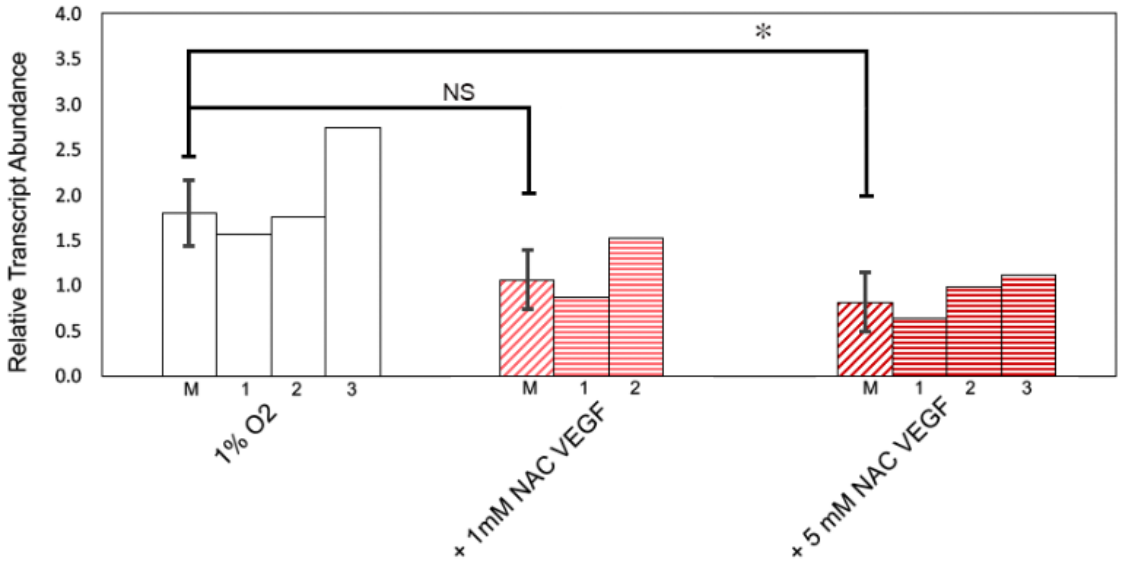

Figure 3-6. Mean relative transcript abundance of the VEGF gene in SKBr3 cells, following treatment with either A) 20% or B) 1% oxygen for 18 hours, with or without the addition of NAC at the indicated concentrations. Relative transcript abundance was measured by qPCR using the $2^{-\Delta\Delta CT}$ method and normalized to the mean transcript abundance value for untreated SKBr3 cells (20% O_2) for n = 3 experiments. Unpaired *t*-tests were performed to determine the differences between the means, and equal variance was assumed in all conditions. *, $p<0.05$; NS, not significant; M, mean.

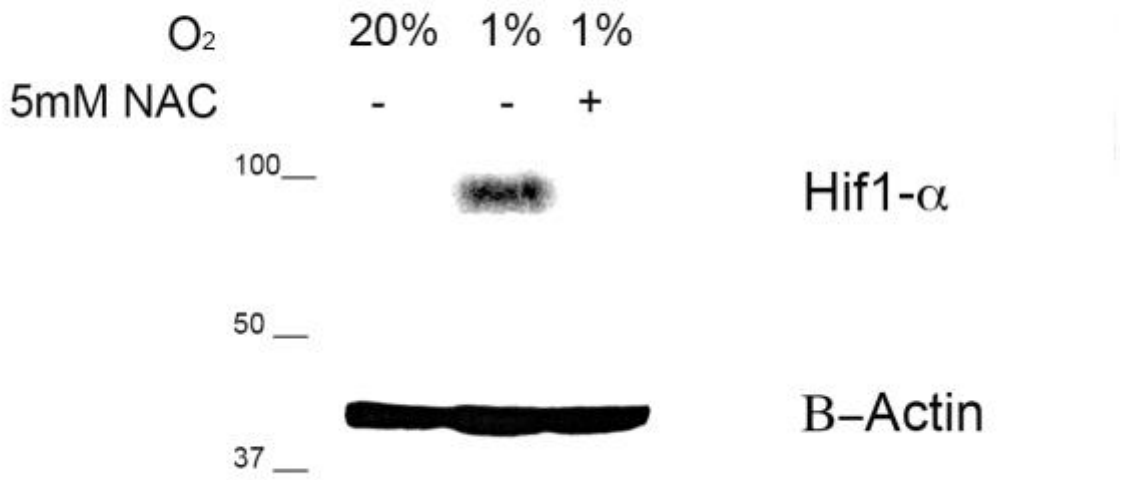

Figure 3-7. Immunoblot of SKBr3 cell protein extracts following treatment with either 20% or 1% oxygen for 18 hours, with or without the addition of 5 mM NAC. A nitrocellulose membrane containing the indicated samples was incubated with unconjugated rabbit anti-HIF-1α IgG, followed by incubation with HRP-conjugated goat anti-rabbit IgG. HRP-conjugated anti-β-Actin IgG was used to establish equal loading of protein samples. Images were captured by exposure to x-ray film after incubation with luminol.

A.

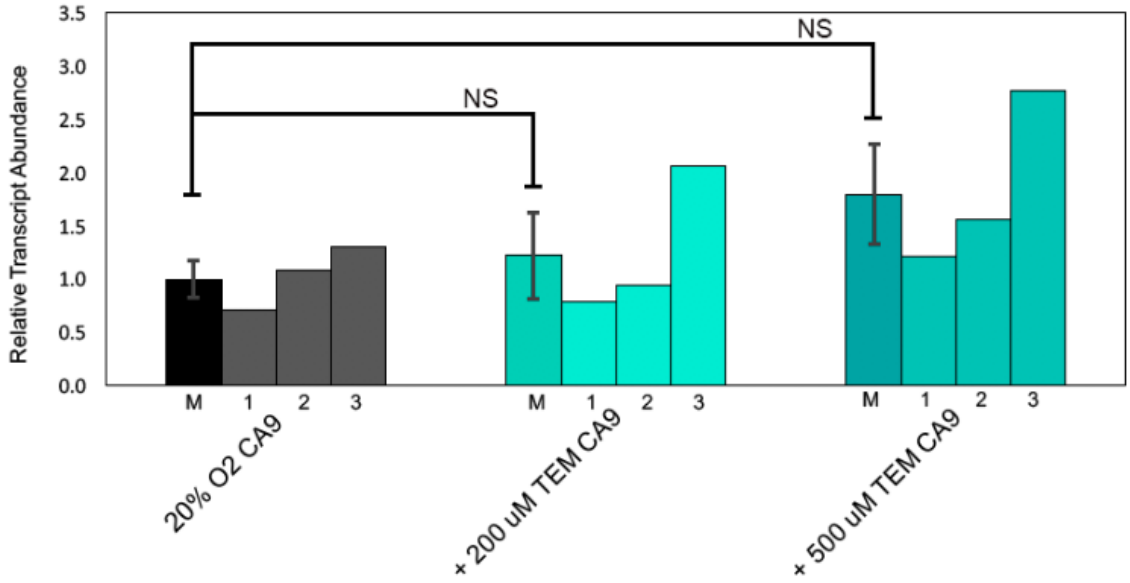

B.

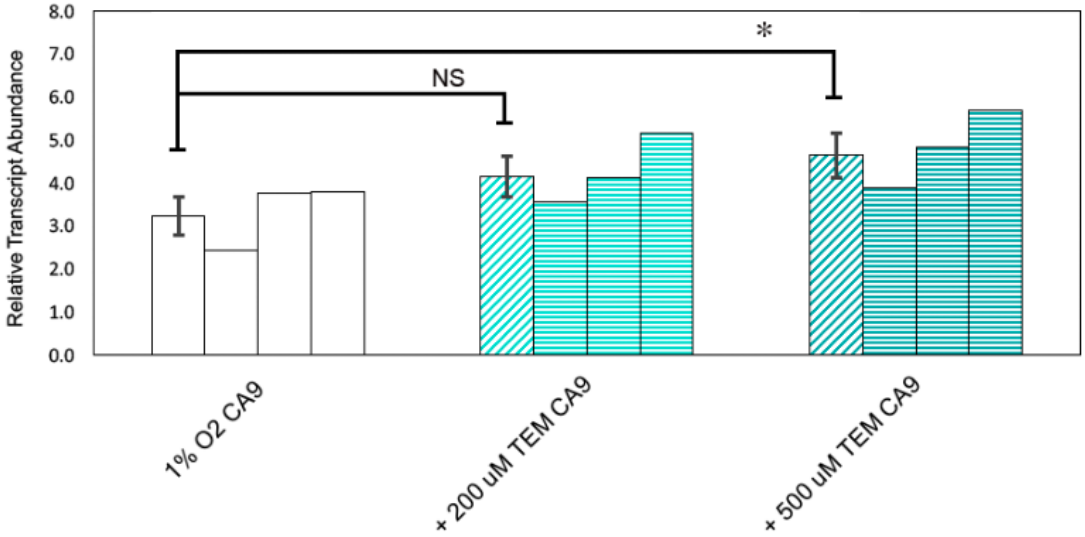

Figure 3-8. Mean relative transcript abundance of the CA9 gene in HMEC cells, following treatment with either A) 20% or B) 1% oxygen for 18 hours, with or without the addition of TEMPOL at the indicated concentrations. Relative transcript abundance was measured by qPCR using the $2^{-\Delta\Delta CT}$ method and normalized to the mean transcript abundance value for untreated HMEC cells (20% O_2) for n = 3 experiments. Unpaired *t*-tests were performed to determine the differences between the means, and equal variance was assumed in all conditions. *, $p<0.05$; NS, not significant; TEM, TEMPOL; M, mean.

A.

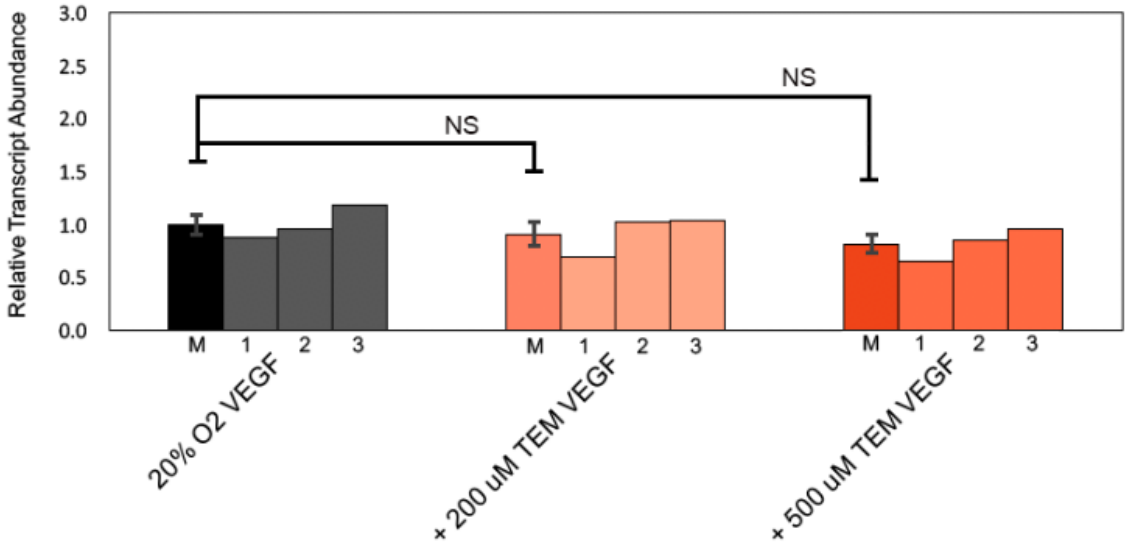

B.

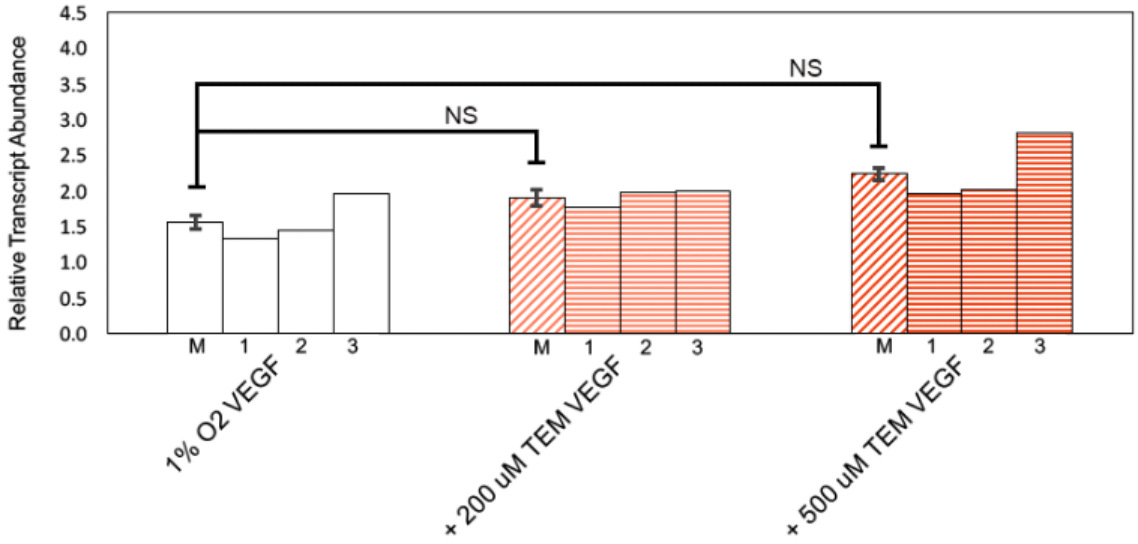

Figure 3-9. Mean relative transcript abundance of the VEGF gene in SKBr3 cells, following treatment with either A) 20% or B) 1% oxygen for 18 hours, with or without the addition of TEMPOL at the indicated concentrations. Relative transcript abundance was measured by qPCR using the $2^{-\Delta\Delta CT}$ method and normalized to the mean transcript abundance value for untreated SKBr3 cells (20% O_2) for n = 3 experiments. Unpaired *t*-tests were performed to determine the differences between the means, and equal variance was assumed in all conditions. NS, not significant; TEM, TEMPOL; M, mean.

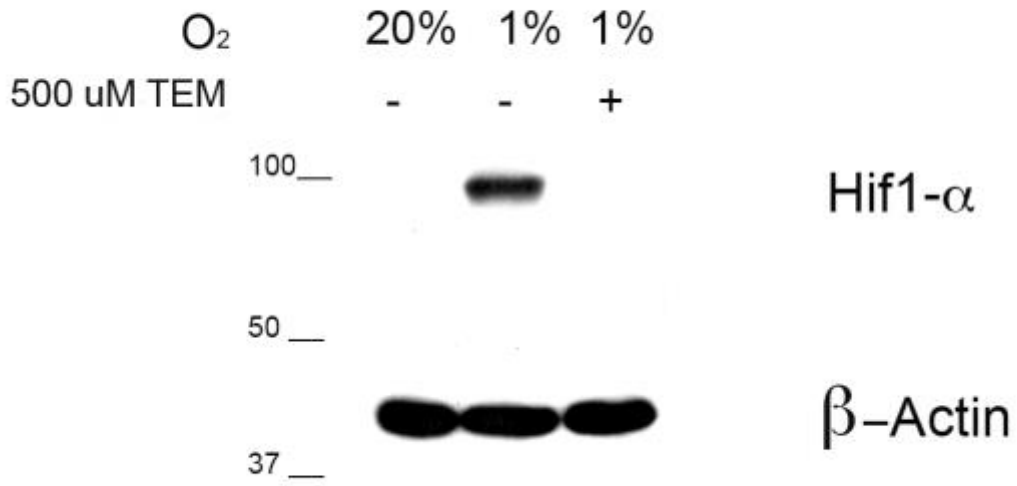

Figure 3-10. Immunoblot of HMEC cell protein extracts following treatment with either 20% or 1% oxygen for 18 hours, with or without the addition of 500 μM TEMPOL. A nitrocellulose membrane containing the indicated samples was incubated with unconjugated rabbit anti-HIF-1α IgG, followed by incubation with HRP-conjugated goat anti-rabbit IgG. HRP-conjugated anti-β-Actin IgG was used to establish equal loading of protein samples. Images were captured by exposure to x-ray film after incubation with luminol. TEM, TEMPOL.

Table 3-2. List of additional primer sequences used. All sequences are listed starting with the 5' end of the oligonucleotide.

No.	Name	Sequence	Purpose
9	R1-seq-FOR	ATTGACCCTGATCTTGGCGG	Sequencing: pMB3 and pBS/pMSP-6.
10	R1-seq-REV	GGTTAGATCGACTAACTGCAG	Sequencing: pMB3, and pBS/pMSP-6.
11	GFP-FOR	GAGGGTGAAGGTGATGCAA	Sequencing: pBS/pMSP-6.
12	GFP-REV	TTTCAAGAGTGCCATGCCC	Sequencing: pBS/pMSP-6.
13	CMV-FOR	CGCAAATGGGCGGTAGGCGTG	Sequencing: pMSP-6.
14	pL-Puro-REV	CTGACACACATTCCACAG	Sequencing: pMSP-6.
15	hU6	GAGGGCCTATTTCCCATGATT	Sequencing: sgRNA candidate plasmids.
16	R1-FOR	GGATCCATGTCTAATAAAAAACAGTCAAATAGG	PCR extraction of EcoR1 sequence from pMB3.
17	R1-REV	TGCATCTCGAGCCATTAATTAAAACC	PCR extraction of EcoR1 sequence from pMB3.
18	mitoGFP-FOR	AACTTAAGATGTCCGTCCTGACGC	PCR extraction of MTS-GFP sequence from pLV-mitoGFP.
19	mitoGFP-REV	GGAGGTACCTTTGTATAGTTCATCCA	PCR extraction of MTS-GFP sequence from pLV-mitoGFP.
20	EcoR1-FAB-FOR	TCTGCAGATATCGCCCTTCATGGTACCATGTCTAATAAA	Integration of Kpn1 site into pCR4-TOPO/EcoR1.
21	ANN-FAB-REV	TGTGCTGGATATCGCCCTTCTCGAGATAAAAAATATCAC	Integration of Xho1 site into pCR4-TOPO/EcoR1.
22	ANN-FAB-FOR	ACGGTATGAATTCGCTTGATAACTTAAGATGTCCGTCCT	Integration of EcoR1 site into pBS/MTS-GFP.
23	GFP-FAB-REV	GGGCTGCAGGATATCGATGGAGGTACCTTTGTATAGTTC	Integration of Kpn1 site into pBS/MTS-GFP.
24	HIF-1α-FOR	ACAGTTACAGTATTCCAGCAGAC	qPCR: endogenous control (nDNA detection).
25	HIF-1α-REV	GTTGCCGTGAGCTGAGATG	qPCR: endogenous control (nDNA detection).
26	Mito-FOR	ACCCAGACAATTATACCCTAGC	qPCR: mtDNA detection.
27	Mito-REV	GAGCCCGTCTAAACATTTTCAATG	qPCR: mtDNA detection.
28	T3	ATTAACCCTCACTAAAG	Sequencing: pCR4-TOPO/EcoR1
29	T7	TAATACGACTCACTATAGGG	Sequencing: pCR4-TOPO/EcoR1

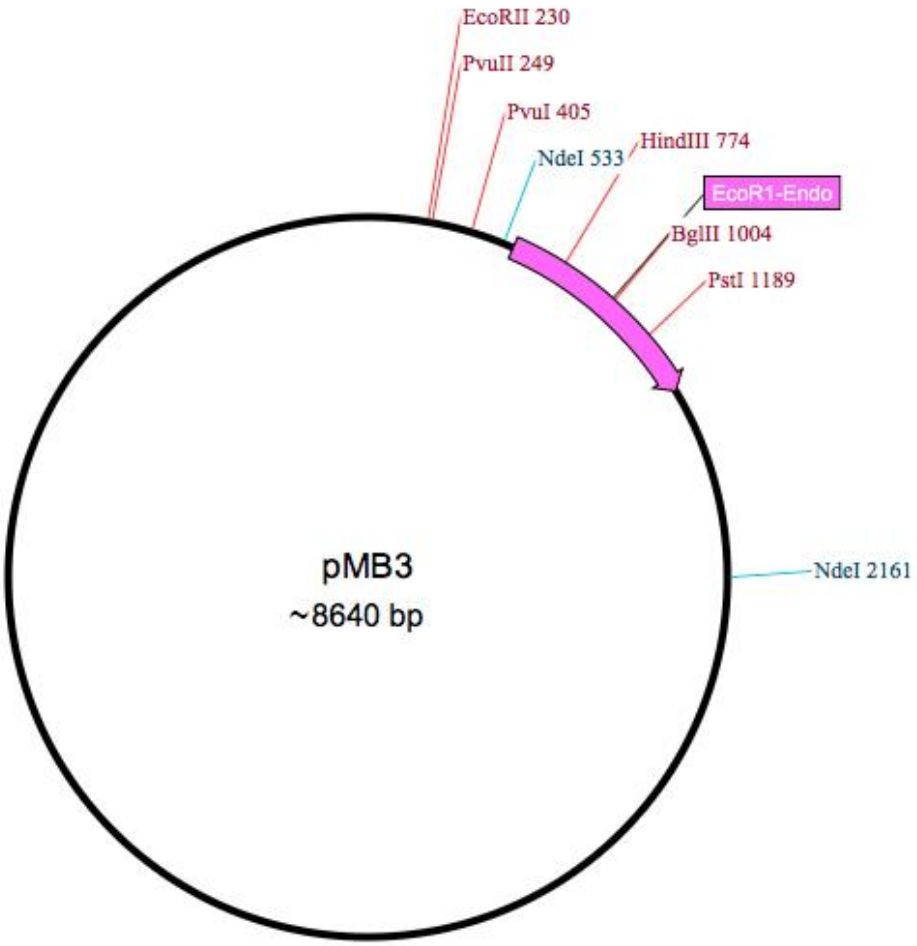

Figure 3-11. Approximate plasmid map of the pMB3 plasmid showing the position of the EcoR1 endonuclease coding sequence (EcoR1-Endo, pink) as provided by New England Biolabs. Restriction sites shown were confirmed by Sanger chain termination sequencing.

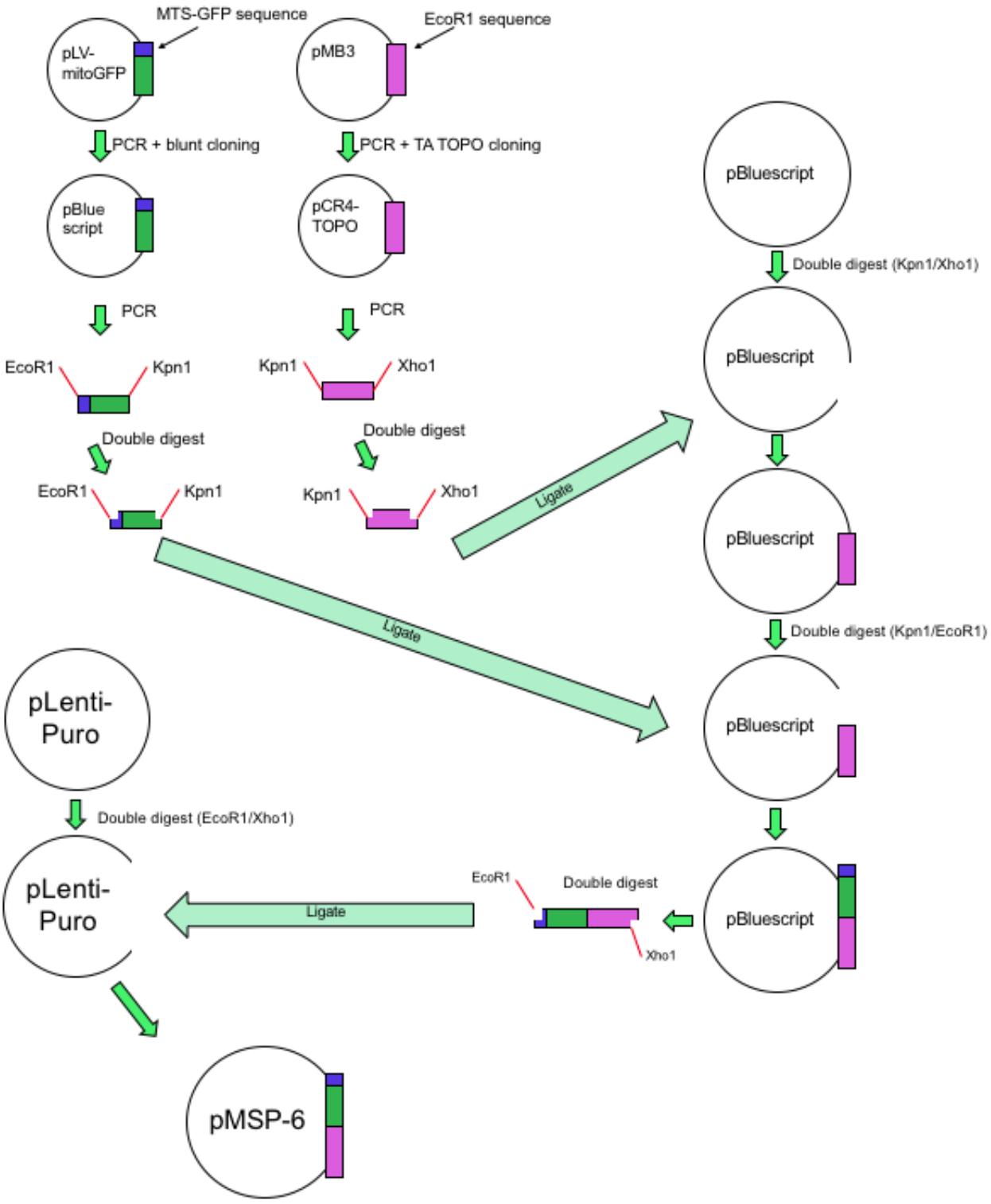

Figure 3-12. Flow chart depicting the steps taken to assemble pMSP-6.

A.

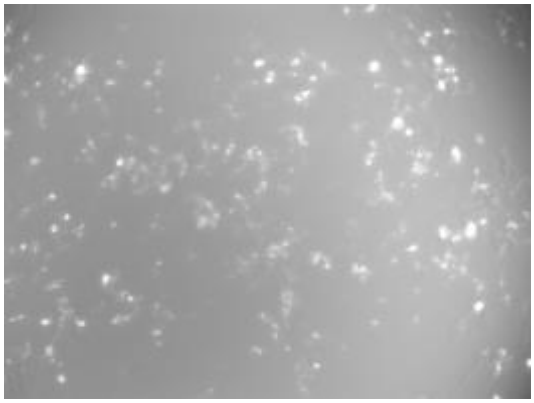

B.

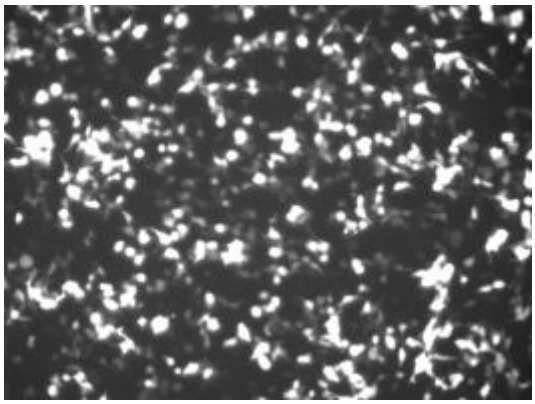

C.

Figure 3-13. Fluorescence microscopy images showing expression of GFP after transfection of GFP expression plasmids into Lenti-X cells. A) pLV-MitoGFP, B) pGIPZ plasmid (Addgene) used as a positive control for the expected expression level, C) no plasmid.

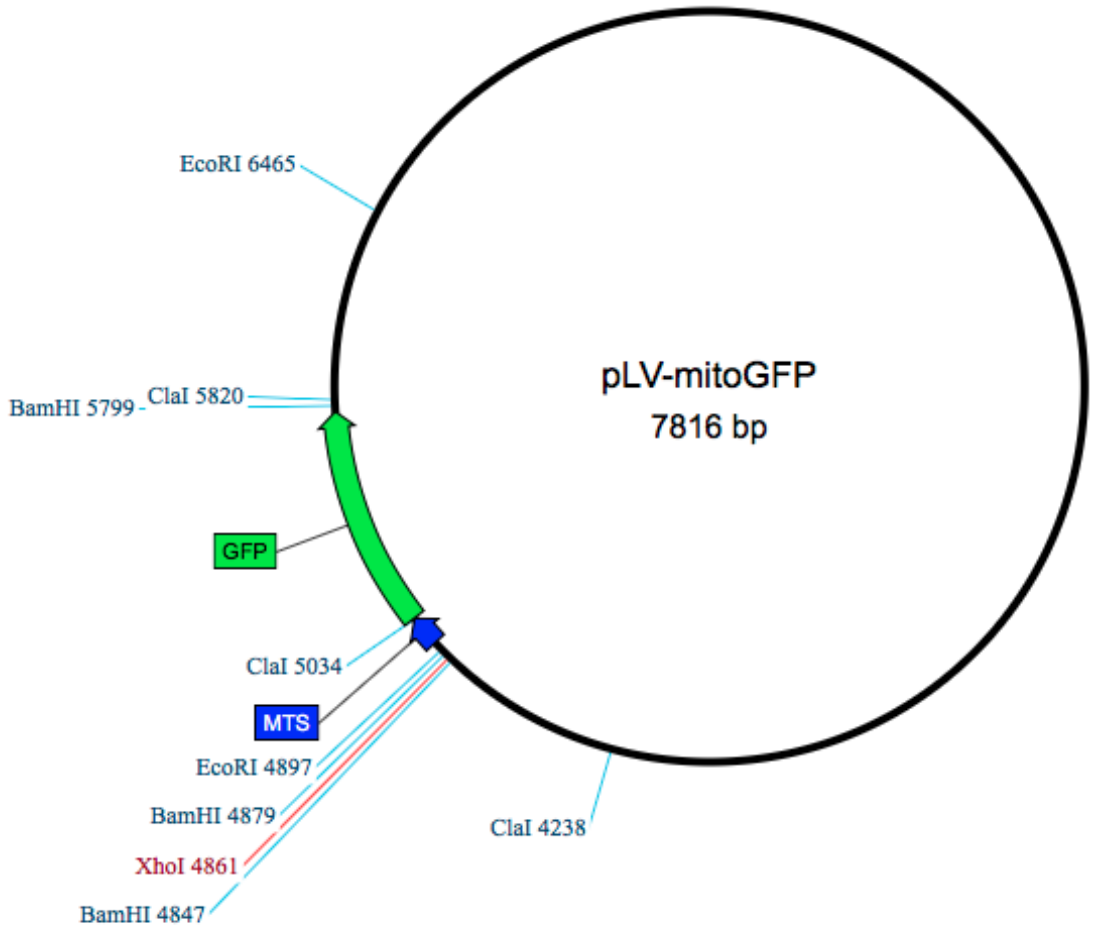

Figure 3-14. Plasmid map of the pLV-mito GFP plasmid (Addgene) showing the relative position of the open reading frame containing the MTS and GFP coding sequences.

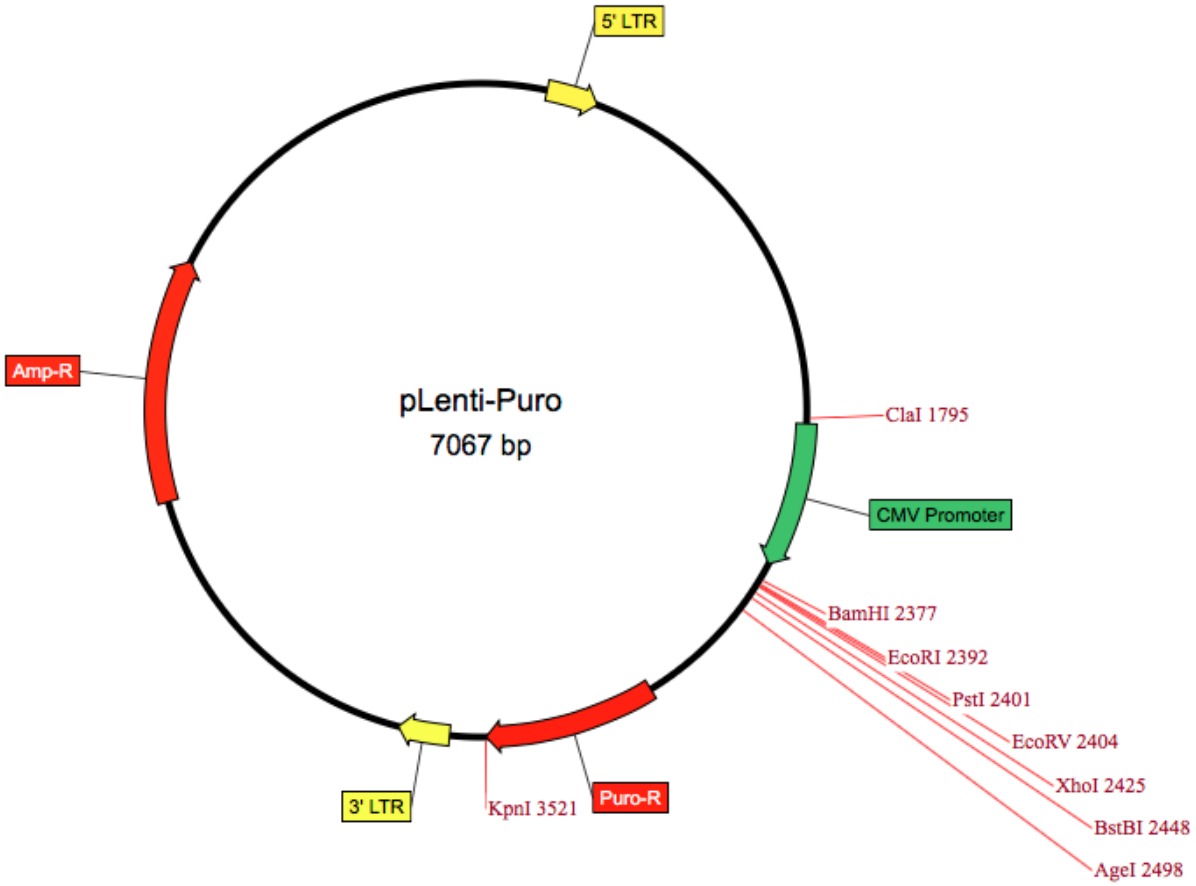

Figure 3-15. Plasmid map of the pLenti-Puro destination plasmid (Addgene) showing the positions of key elements.

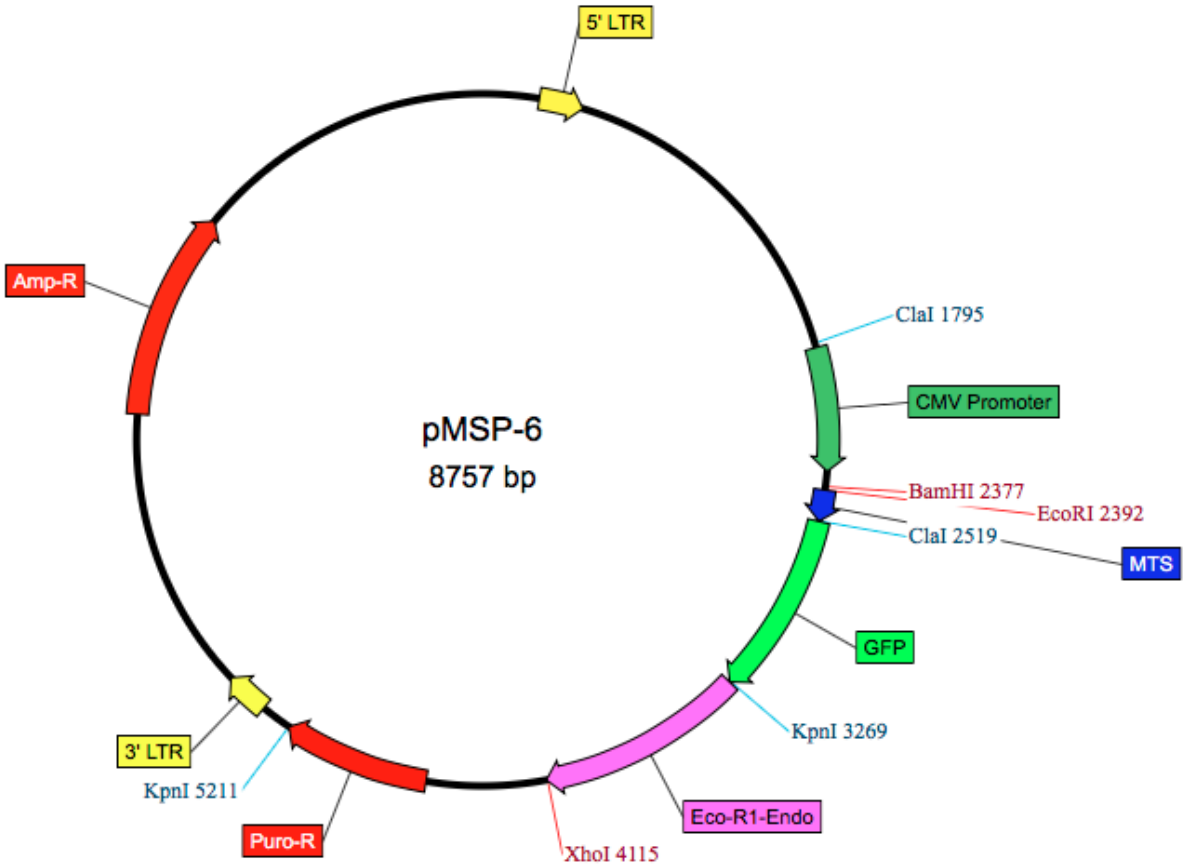

Figure 3-16. Plasmid map of the pLenti-Puro plasmid vector containing the coding sequences for the MTS/GFP/EcoR1-endonuclease fusion protein (renamed pMSP-6).

A.

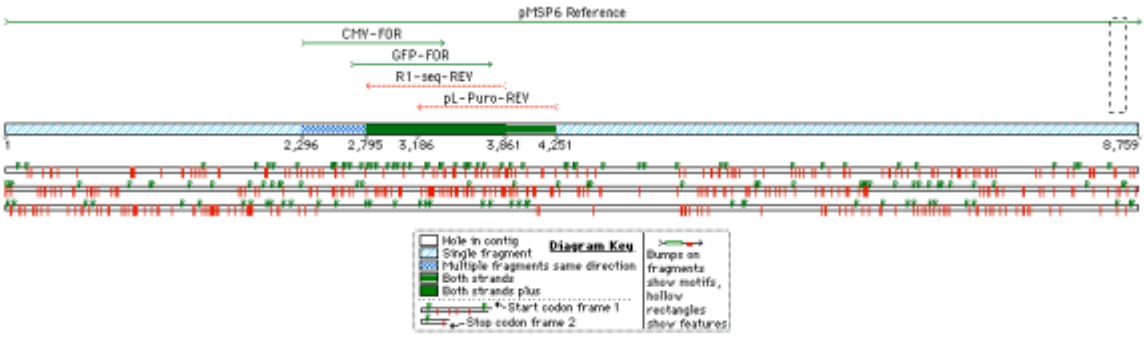

B.

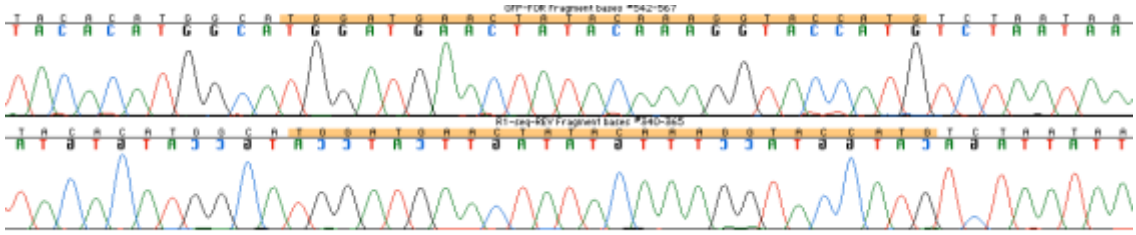

Figure 3-17. Sequencing verification of successful ligation of the MSP6 insert into the pLenti-Puro plasmid, as shown by Sequencher v. 4.5 software “contig” mapping. A) Contig overview showing the alignment of the four primers used (Table 3-2) relative to the reference sequence of pMSP-6, B) chromatogram showing the signal clarity gathered from Sanger chain termination fluorescence. Nucleotides are identified by separate colors and a selection from the GFP-FOR and R1-seq-REV sequences containing the Kpn1 restriction site within the insert (GGTACC) is highlighted in orange.

A.

B.

Figure 3-18. Sanger chain termination sequencing verification as shown by Sequencher v. 4.5 software “contig” alignment. A) Agreement between the base pairs of the pMSP-6 reference sequence and the CMV-FOR primer sequencing run, with the selection containing the EcoR1 restriction site (GAATTC) shown in orange highlight. B) Agreement between the base pairs of the pMSP-6 reference sequence and the pL-Puro-REV primer sequencing run, with the selection containing the Xho1 restriction site (CTCGAG) shown in orange highlight.

A.

B.

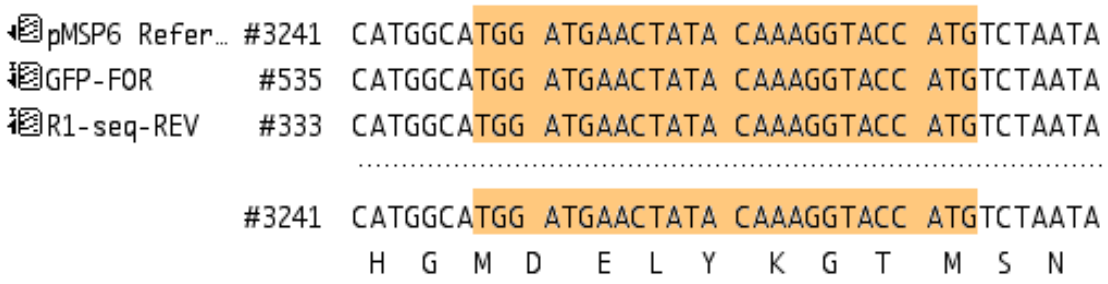

Figure 3-19. Sanger chain termination sequencing verification as shown by Sequencher v. 4.5 software “contig” alignment. A) Agreement between the base pairs of the pMSP-6 reference sequence and the GFP-FOR and R1-seq-REV primer sequencing runs. The selection containing the Kpn1 restriction site (GGTACC) is shown in orange highlight. B) A smaller selection of the same alignment (orange highlight) showing the start codon of the EcoR1-endonuclease segment of the MSP6 insert, downstream of the terminal tyrosine and lysine residues of the GFP segment of the insert, with conservation of the reading frame. Linker residues (glycine and threonine) are shown as resulting from the incorporation of the Kpn1 restriction site (GGTACC).

A.

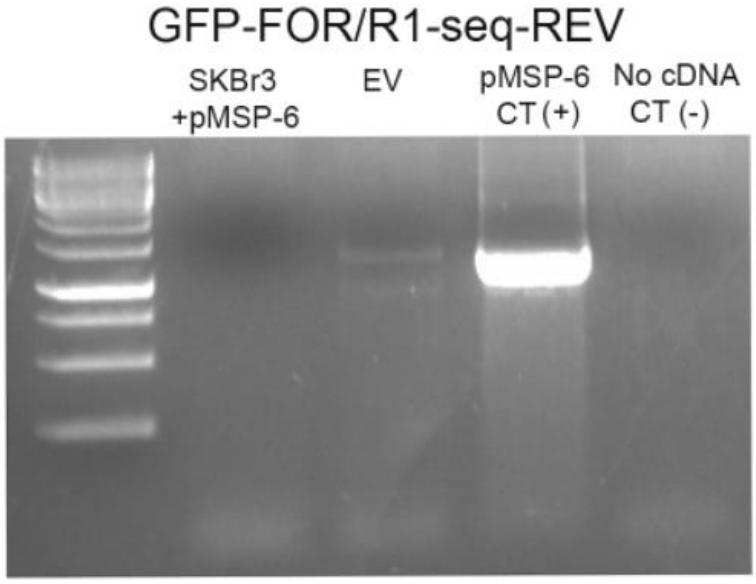

B.

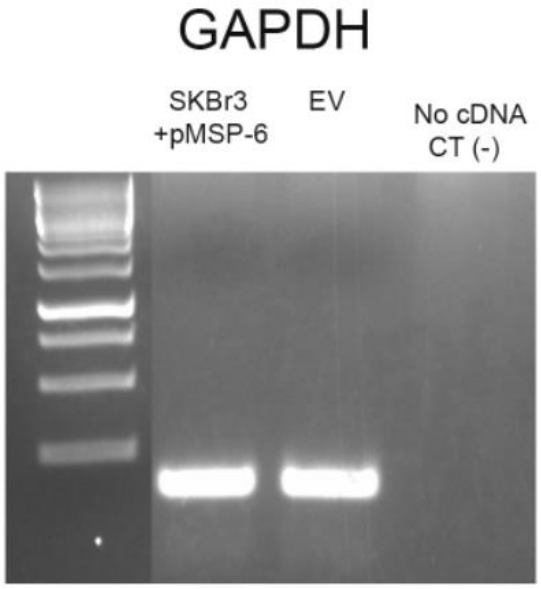

Figure 3-20. Agarose gel electrophoresis of PCR amplicons using either A) the GFP-FOR/R1-seq-REV primer set (Table 3-2) or B) the GAPDH primer set (Table 3-1), with either cDNA or plasmid (pMSP-6 (+)) template samples as indicated. cDNA template samples were synthesized from total RNA extracts from pMSP-6 transduced SKBr3 cells after puromycin selection. EV, Empty vector; CT, control.

A.

```
                                5′ –  GATTTGGGGTGGAAGGCAGGCATG
GTCAAACCCATTTCACTGACAGGAGAGCAGAGACAGGACGTGTCTCTCTCCAC
GTCTTCCAGCCAGTAAAAGAAGCCAAGCTGGAGCCCAAAGCCAGGTGTTCTGA
CTCCCAGCGTGGGGGTCCCTGCACCAACCATGAGCCGCCTGCTCTGGAGGAAG
GTGGCCGGCGCCACCGTCGGGCCAGGGCCGGTTCCAGCTCCGGGGCGCTGGGT
CTCCAGCTCCGTCCCCGCGTCCGACCCCAGCGACGGGCAGCGGCGGCGGCAGC
AGCAGCAGCAGCAGCAGCAGCAGCAGCAACAGCAGCCTCAGCAGCCGCAAGTG
CTATCCTCGGAGGGCGGGCAGCTGCGGCACAACCCATTGGACATCCAGATGCT
CTCGAGAGGGCTGCACGAGCAAATCTTCGGGCAAGGAGGGGAGATGCCTGGCG
AGGCCGCGGTGCGCCGCAGCGTCGAGCACCTGCAGAAGCACGGGCTCTGGGGG
CAGCCAGCCGTGCCCTTGCCCGACGTGGAGCTGCGCCTGCCGCCCCTCTACGG
GGACAACCTGGACCAGCACTTCCGCCTCCTGGCCCAGAAGCAGAGCCTGCCCT
ACCTGGAGGCGGCCAACTTGCTGTTGCAGGCCCAGCTGCCCCCGAAGCCCCCG
GCTTGGGCCTGGGCGGAGGGCTGGACCCGGTACGGCCCCGAGGGGGAGGCCGT
ACCCGTGGCCATCCCCGAGGAGCGGGCCCTGGTGTTCGACGTGGAGGTCTGCT
TGGCAGAGGGAACTTGCCCCACATTGGCGGTGGCCATATCCCCCTCGGCCTG
```

B.

```
sgRNA #1: 5′ – CACCGTGGACCCGGTACGGCCCCGA
                CACCTGGGCCATGCCGGGGCTCAAA – 5′

sgRNA #2: 5′ – CACCGAACTTGCCCCACATTGGCGG
                CTTGAACGGGGTGTAACCGCCCAAA – 5′
```

C.

```
5′ –  AAAGGACGAAACACCGGAGACGGTTGTAAATG.......CTTTTTTGTACGTCTCTGTTTTAGAGCTAGAA
      TTTCCTGCTTTGTGGCCTCTGCCAACATTTAC.......GAAAAAACATGCAGAGACAAAATCTCGATCTT – 5′
Position:  1944          1960                  3845
```

Figure 3-21. sgRNA oligonucleotides and destination pLC plasmid integration. A) The DNA nucleotide sequence of exon two of the POLG catalytic subunit gene. Target sequences for sgRNA vectors are shown in red (sgRNA #1) and blue (sgRNA #2). Proto-spacer adjacent motifs (PAMs) are shown in green. The sequence coding the start codon is shown underlined in bold. B) Synthesized sgRNA sequences, for ligation into the pLC plasmid. Complementary overhang sequences are shown in red. C) Ligation targeting within the pLC plasmid. BsmB1 recognition sites are shown in purple, discarded nucleotide sequence is shown in green, purple, and red. Overhangs used to synthesize complementary sgRNA oligonucleotides are shown in red. Abbreviated sequence is denoted by ellipses. Position number indicates nucleotide position relative to FASTA sequence provided by Addgene.

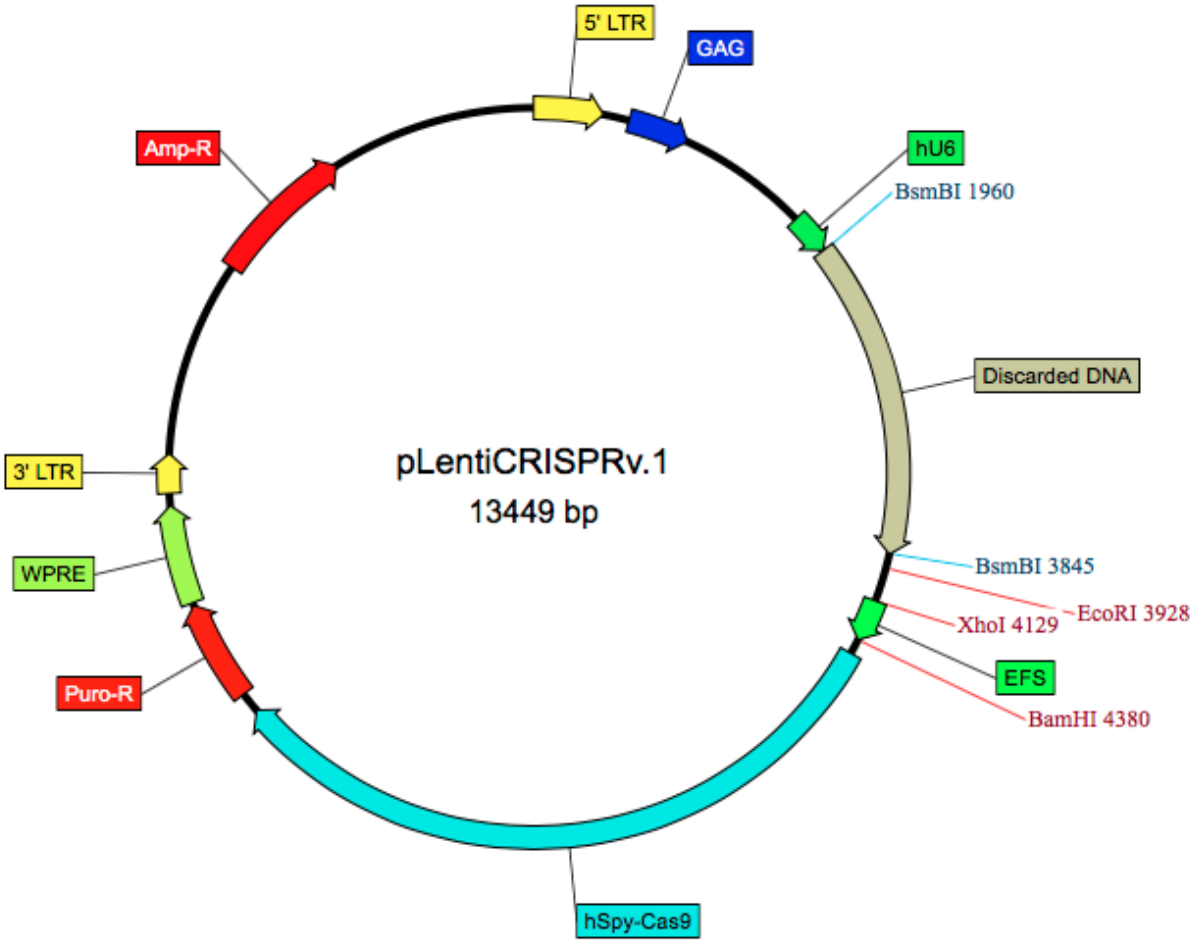

Figure 3-22. Map of pLC destination plasmid.

A.

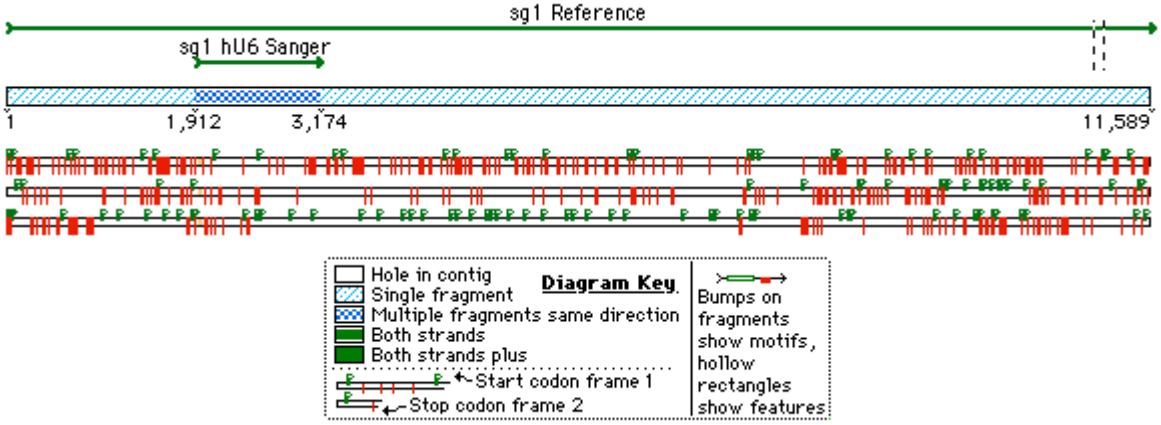

B.

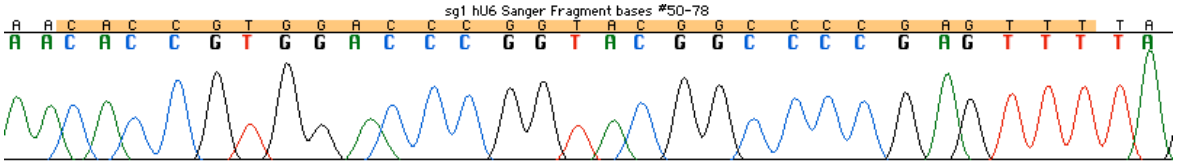

C.

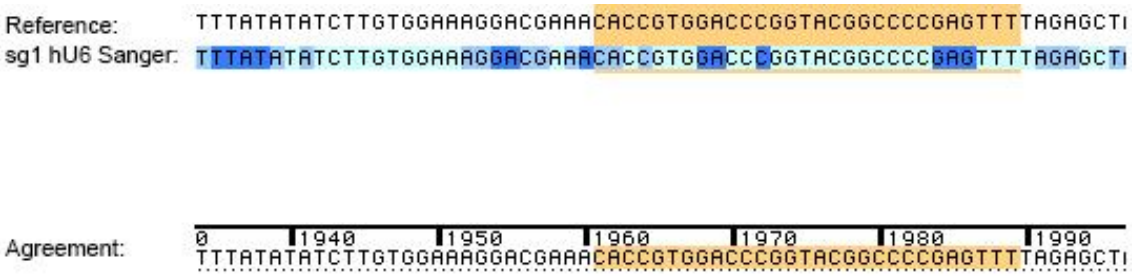

Figure 3-23. Sequencing verification of successful ligation of sgRNA #1 into the pLC plasmid, as shown by Sequencher v. 4.5 software “contig” mapping. A) Contig overview showing the alignment of the hU6 forward sequencing run relative to the reference sequence of sg1, B) chromatogram showing the signal clarity gathered from Sanger chain termination fluorescence. Nucleotides are identified by separate colors and the sgRNA #1 sequence is highlighted in orange, C) contig alignment showing the agreement between the base pairs of the reference and sg1 hU6 forward sequencing run, with sgRNA#1 sequence shown in orange highlight.

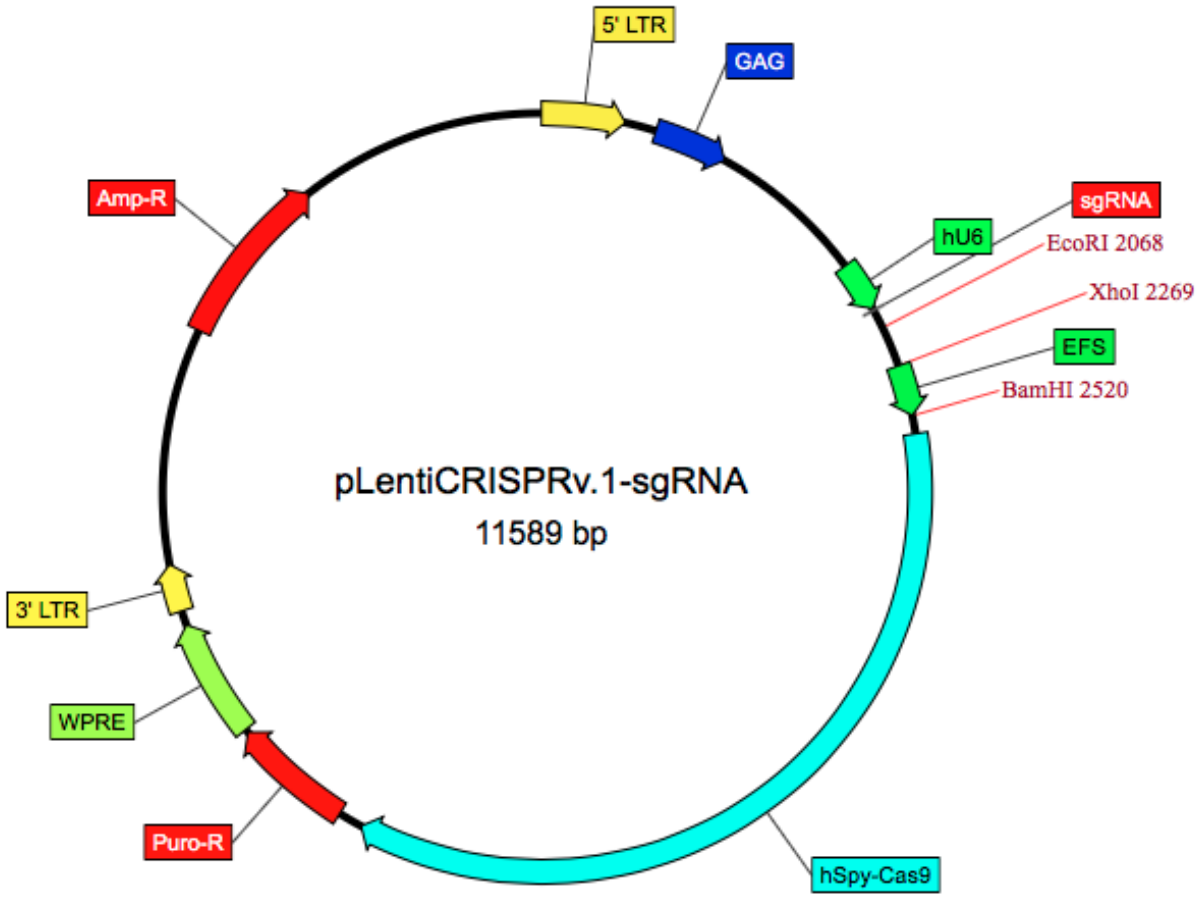

Figure 3-24. Map of the pLC plasmid with sgRNA sequence ligated.

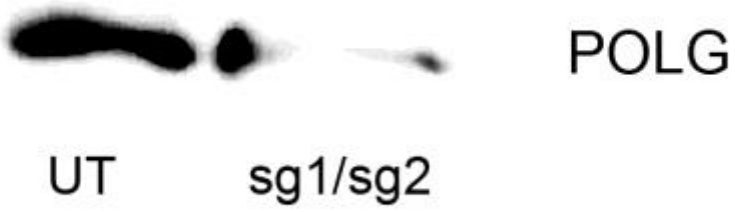

Figure 3-25. Immunoblot of HMEC cells co-transduced with lentiviruses containing the pLC_sg1 and pLC_sg2 (sg1/sg2) plasmids. Protein extracts of the puromycin-selected polyclonal cell population were analyzed by immunoblot using α-POLG monoclonal rabbit IgG, followed by incubation with HRP-conjugated goat anti-rabbit IgG. UT, untreated.

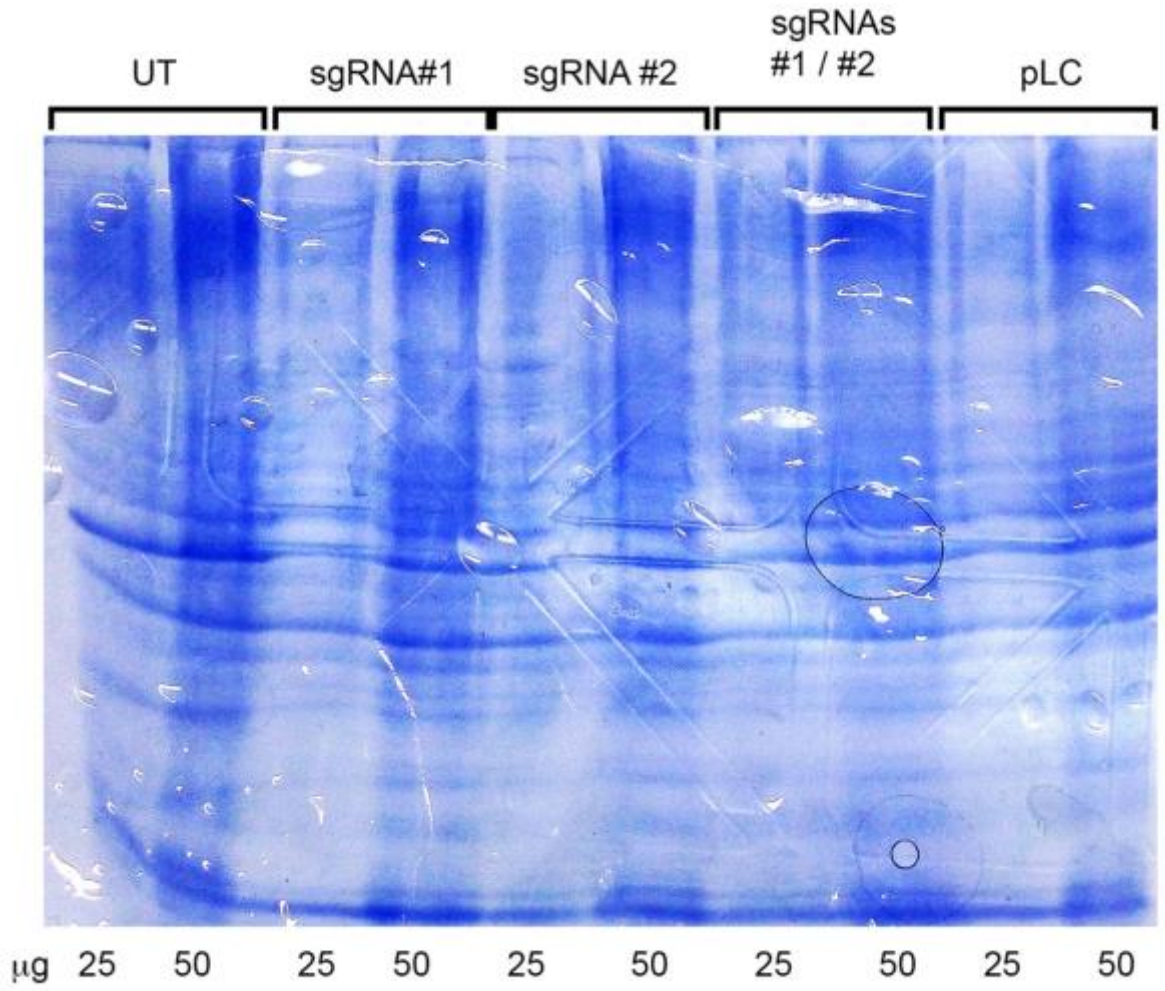

Figure 3-26. Polyacrylamide gel of three sgRNA-infected polyclonal cell population protein extracts, stained with Coomasie Brilliant Blue, for determination of equal sample loading.

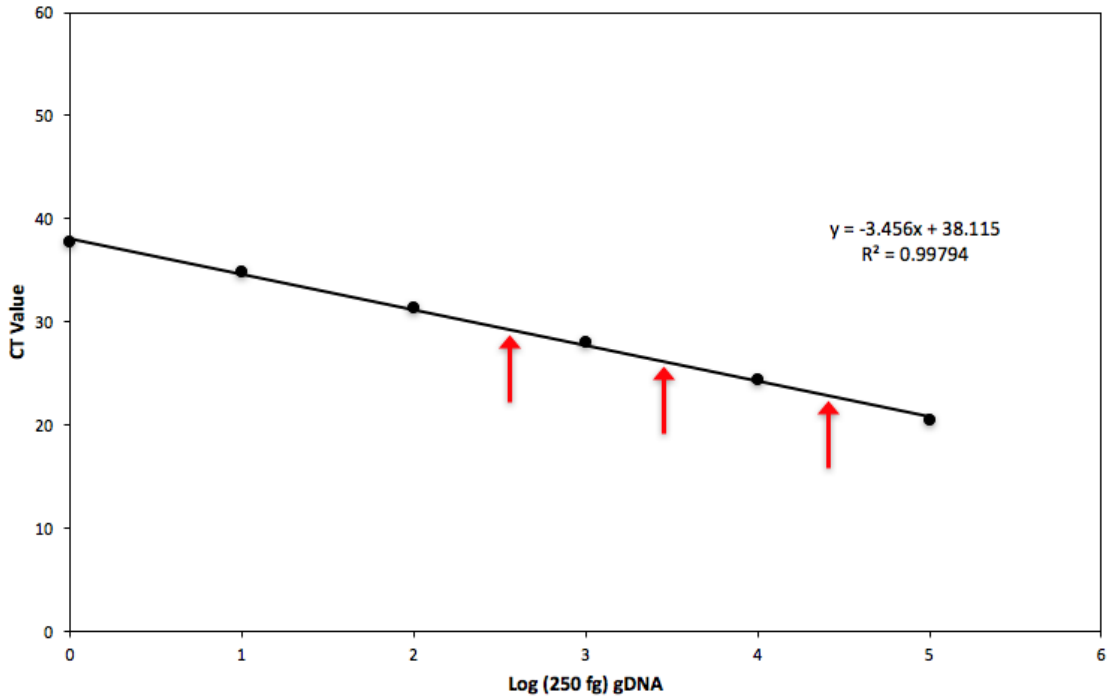

Figure 3-27. SKBr3 gDNA extract was used to generate a standard curve of nDNA abundance. Serial logarithmic dilutions of approximately 25 ng of genomic DNA were loaded, each in triplicate, into a qPCR thermocycler, with an oligonucleotide primer set specific to the HIF-1α nuclear locus. CT values were plotted versus the approximate mass of DNA extract, based on a 25 ng/μL full strength extract concentration. Red arrows indicate the approximate points of interpolation for the untreated and sg1/sg2 HMEC nDNA qPCR CT results (results were similar), using the same HIF-1α primer set. CT, cycle threshold.

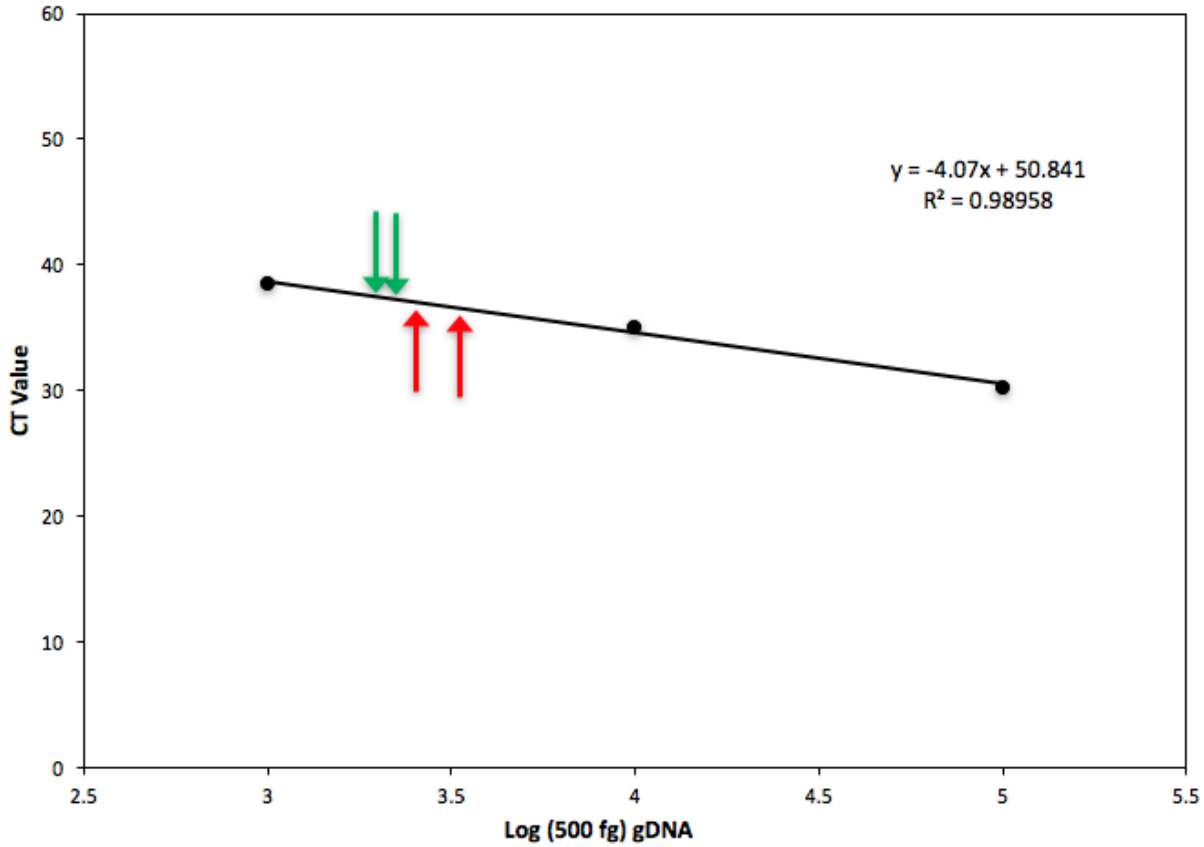

Figure 3-28. SKBr3 gDNA extract was used to generate a standard curve of mtDNA abundance. Serial logarithmic dilutions of approximately 50 ng of gDNA were loaded, each in triplicate, into a qPCR thermocycler, with an oligonucleotide primer set specific to the human mitochondrial chromosome. CT values were plotted versus the approximate mass of DNA extract, based on a 50 ng/μL full strength extract concentration. Red arrows indicate the untreated CT values interpolated, and green arrows indicate the sg1/sg2 CT values interpolated, for HMEC cells based upon their respective mtDNA qPCR results, using the same primer set.

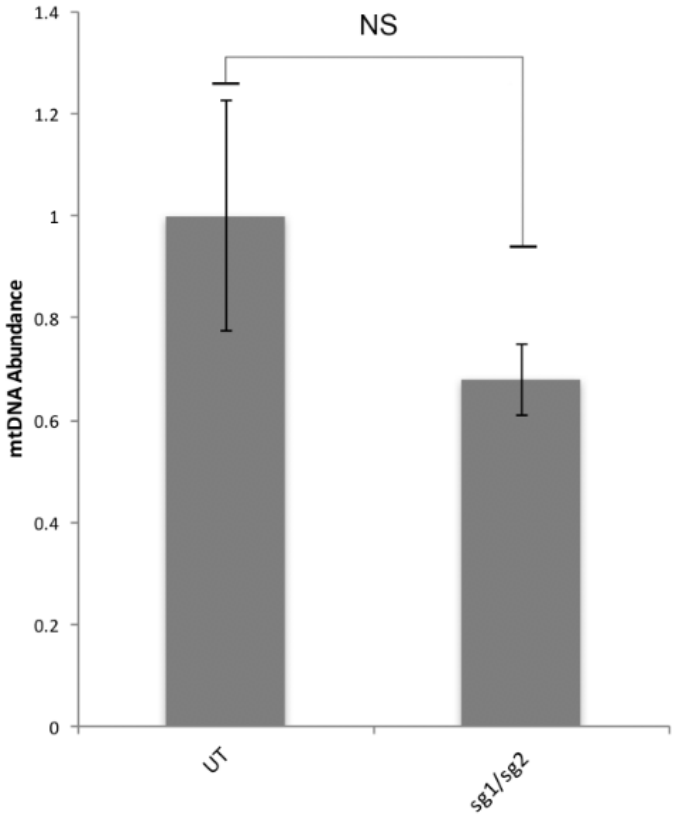

Figure 3-29. Relative accumulation of mtDNA in sg1/sg2 versus untreated HMEC cells. Statistical significance was determined via unpaired *t*-test assuming equal variance ($p > 0.05$). NS, not significant.

A.

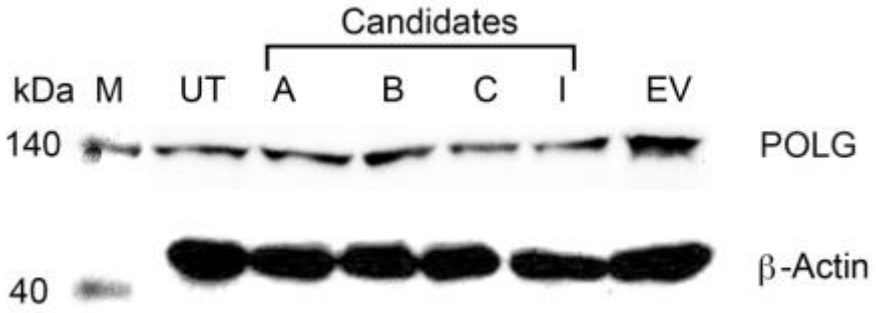

B.

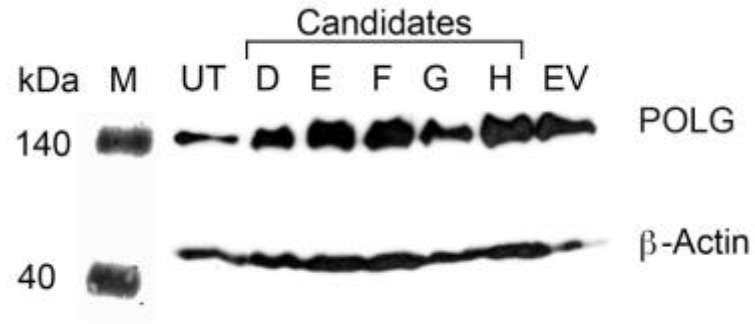

C.

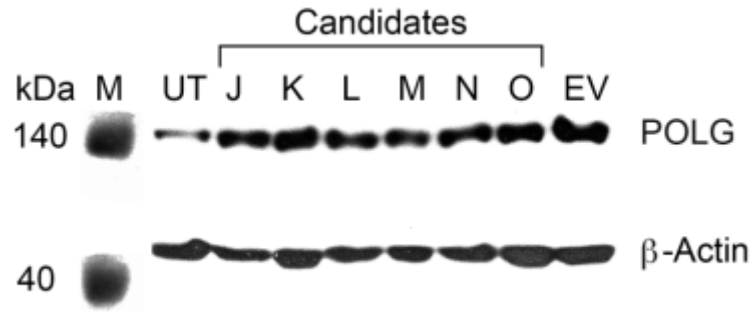

Figure 3-30. Immunoblots of monoclonal candidate sg1/sg2 HMEC cell populations using anti-polymerase-γ (α-POLG) monoclonal rabbit IgG, followed by incubation with HRP-conjugated goat anti-rabbit IgG. HRP-conjugated anti-β-Actin IgG was used to establish equal loading of protein samples. Images were captured by exposure to x-ray film after incubation with luminol. A) Candidates A-C, I, B) candidates D-H, C) candidates J-O. UT, untreated HMEC cells; EV, empty vector; M, molecular weight marker; kDa, kiloDaltons.

CHAPTER 4
DISCUSSION

Characterization of ATM signal transduction in human mammary epithelial cells is integral to understanding ways that cancer can evade chemotherapy and radiotherapy. Pharmacological inhibition of ATM has been shown to reduce cell viability in cisplatin-resistant head and neck cancers (95), and has been shown to induce apoptosis in human mammary carcinoma cells in preclinical studies (94,96). Understanding the modes of ATM activation and signaling may provide the basis for strategies that improve the efficacy of conventional cancer treatment methods.

The production of ROS in response to hypoxia has been well-characterized (18,19,70,97,98), and hypoxia has been shown to cause a measurable increase in intracellular H_2O_2 concentration (18). Paradoxically, in some cases, hypoxia can cause a decrease in ROS (99-101); of note, the studies revealing this behavior were conducted in isolated mitochondria or in human pulmonary arterial smooth muscle cells, which may be examples of experiments that utilize conditions that are difficult to examine in a side-by-side manner with studies in human mammary epithelial cell lines. It has been shown previously in human fibroblasts and in human mammary epithelial carcinoma cells that ATM becomes activated after cells are treated with H_2O_2, in the absence of DNA DSBs (65,67,102,103). Additionally, it has been shown that in leukemia cells, ATM activation is required to activate NF-κB after cells are treated with H_2O_2 (104). More recently it was demonstrated in the Brown lab that incubation of human mammary epithelial carcinoma cells with NAC resulted in downregulation of NF-κB and reduction of ROS levels, during normoxic O_2 exposure (91). The most recent experimental evidence from the Brown lab has demonstrated that HIF-1α protein stabilization in response to hypoxia is ATM-

dependent (5). The evidence produced in the Brown lab followed the elucidation of a phosphorylation event at S696 of HIF-1α in embryonic stem cells during hypoxia exposure that was shown to be the result of ATM activity (6). It was also shown that phosphorylation of S696 by ATM in HEK cells caused upregulation of the HIF-1 target gene REDD1 through stabilization of HIF-1α (6). The progression of evidence suggests therefore that it is reasonable to hypothesize that administration of NAC or TEMPOL would suppress ATM activity during hypoxia, and that suppression would be caused by antioxidant-driven decrease in the concentration of ROS. ATM suppression would result in destabilization of HIF-1α and decreased transcript abundance in HIF-1 target genes. In addition to causing a decrease in ROS accumulation, NAC would potentially participate in direct deactivation of ATM through thiol-disulfide exchange activity (105). Consistent with the findings of the current experiment, administration of NAC has previously been shown to decrease hypoxia-generated ROS in human microvascular endothelial cells that upregulate HIF-1 and VEGF in response to hypoxia (106).

Although ROS accumulation was not measured in this experiment, confirmation of an increase in ROS-mediated activity was shown as measured by the increase in HIF-1 activity pursuant to the stabilization of HIF-1α. Administration of NAC showed a downregulation of HIF-1 target genes in both HMEC and SKBr3 cell lines in support of the current hypothesis. Additionally, loss of hypoxia-induced HIF-1α stabilization was shown by immunoblot of SKBr3 cell extracts after administration of NAC, further supporting that ROS are required to induce the response to hypoxia in mammary epithelial carcinoma cell lines. It is important to note that although ROS accumulation can be measured by dichlorofluorescein (DCF), such measurements are confounded by

increases in ROS that occur in response to reoxygenation during cell harvesting (45,81,107,108).

The mechanism of NAC is two-fold in this case: Firstly, it bolsters the cellular concentration of GSH by providing the cysteine necessary for GSH synthesis (109). NAC scavenges $\bullet O_2^-$ in amounts that are undetectable, but GSH is a much more potent $\bullet O_2^-$ scavenger (109,110). Administration of NAC therefore provides $\bullet O_2^-$ scavenging through upregulation of GSH activity. The product of the GSH $\bullet O_2^-$ scavenging reaction is H_2O_2, which subsequently reacts with thiols to form disulfide bridges (109) as shown in the prior elucidation of ATM activation in response to hypoxia (67). It is important to note that any increase H_2O_2 concentration can be purged due to the action of glutathione peroxidase (GPX), an enzyme that requires GSH as a substrate in the reduction of H_2O_2 to H_2O (108). Secondly, both NAC and GSH participate in the thiol-disulfide exchange reaction, which reverses the disulfide bridge formation mentioned above (110,111). The chemical equations for the disulfide bridge-forming reactions are shown in Table 4-2 as equations (4-1) and (4-2), and the thiol-disulfide summary reaction is shown as equation (4-3 (105,110)). The thiol-disulfide exchange reaction mechanism is shown in Figure 1-1.

The administration of TEMPOL, which has cell-protective antioxidant qualities, demonstrated a result that differed from that of NAC (27). TEMPOL was used previously to treat human mammary epithelial cells in an experiment in the Brown lab, at 500 μM concentration, under normoxic (20% O_2) conditions (92). In this example, TEMPOL was shown to suppress ATM activity, as measured by the transcript abundance of the SOD2 gene (Figure 4-1). ATM activation is required for the activation and nuclear translocation

of NF-κB, which transactivates SOD2. TEMPOL was shown to be effective in suppressing ATM activity at 20% O_2 concentration, and this demonstration of TEMPOL potency was the basis of its use in the current experiment.

The mechanism of TEMPOL that acted upon ATM in the current experiment potentially differs from that which was shown previously, due to the differing concentrations of ROS that are present during the two different O_2 concentration exposures. In the previous experiment, basal ATM activity was shown to be suppressed by the action of TEMPOL, which presumably took place through the scavenging of basal $\bullet O_2^-$ and •OH molecules. The chemical equations summarizing the TEMPOL mechanisms of basal ROS scavenging are shown in Table 4-2 as equations (4-4) and (4-7 (27)), and are further illustrated in Figure 1-2 (27,112). It should be noted that the formation of the TEMPOL hydroxylamine by-product (TEM-H) resulting from equation (4-7) is recyclable and regenerates TEMPOL through a cyclic oxygen dependent process (Figure 4-2).

The reactivity of $\bullet O_2^-$ with the thiols at ATM C2991 that would form disulfide bridges is unknown; It has been shown that various thiols present varying rate constants when reacting with $\bullet O_2^-$ (110). However, TEMPOL is a known scavenger of both $\bullet O_2^-$ and •OH, and it is unlikely that the small increase in H_2O_2 resulting from the action of TEMPOL $\bullet O_2^-$ scavenging would cause an increase in ATM activity during normoxic conditions; attributable in part to the activity of catalase and GPX, which reduce H_2O_2 to H_2O. It has been shown that overexpression of catalase or of GPX results in reversal of hypoxia-induced ROS increases, suggesting that the basal action of these two enzymes must be overcome to initiate H_2O_2-mediated signal transduction (71). It is therefore

plausible to hypothesize that TEMPOL acted to suppress basal ATM activity through ROS scavenging-mediated prevention of ATM activation when exposed to 20% O_2 (27,112).

When hypoxia is introduced, the increase in ROS potentially changes the outcome of TEMPOL administration. Higher concentrations of $\bullet O_2^-$ drive a TEMPOL-mediated increase in H_2O_2 (equation 4-4 (27)). Ligand-bound metal ions (L-M^{n+}) bind to H_2O_2, followed by the formation of •OH, which is purged by TEMPOL (Table 4-2, equations 4-5, 4-6, 4-7 (27,112)); however, TEMPOL also acts directly upon ligand-bound metal ions, oxidizing them (equation 4-8 (27)). Oxidation of metal ions prevents the Fenton chemistry of H_2O_2 binding (27). Therefore, TEMPOL scavenges ROS, protects the cell from harmful •OH, but potentially allows an increase in H_2O_2 (27,112-115). This can be seen by observing that equation (4-8) inhibits equation (4-5); this point is shown in Table 4-2 as equation (4-10). It is important to note that the oxidation of metal ions does not prevent the conversion of H_2O_2 to H_2O by catalase or by GPX (27), so any increase in H_2O_2 caused by TEMPOL administration during hypoxia would presumably be due to a hypoxia-driven increase of $\bullet O_2^-$ and subsequent conversion to H_2O_2 by both TEMPOL and SODs, beyond the cell's capacity to purge it. This TEMPOL-driven activity could be contributory to the reason for the increase in CA9 transcript abundance in HMECs as measured by qPCR (Figure 3-8).

A similar effect was shown previously in MCF7 human mammary epithelial carcinoma cells with doses of TEMPOL ranging from 0.1 – 40 mM, with the accumulation of HIF-1α increasing as the TEMPOL dose increased (115). It was also shown that doses of TEMPOL higher than those used in the current experiment ($\geq$ 10

mM) caused decreases in HIF-1α protein (115), suggesting a complex dose-dependent response mechanism. In evidence presented here, it is important to note that VEGF transcript abundance in SKBr3 cells was not significantly increased above hypoxic induction when TEMPOL was added; however, a clear trend was observed that suggests a dose dependent response to TEMPOL. This trend is also evident in the dosage curve shown in Figure 3-4A. It is also important to note that changes in H_2O_2 concentration were not measured during this experimental procedure, and that such measurement would provide a confirmation of the suggested mode of action of TEMPOL.

If the increase in H_2O_2 concentration caused by TEMPOL administration was the reason for the increase in CA9 transcript abundance during hypoxia (Figure 3-8), one would have to suggest that the increase in CA9 must be HIF-1 independent. This is evidenced by the fact that the immunoblot of TEMPOL treated HMEC cells (Figure 3-10) failed to show any detectable HIF-1α accumulation during hypoxia. The fact that the dose response curves (Figures 3-3, 3-4) demonstrate a pattern of increase in CA9 and VEGF transcript abundance with increasing doses of antioxidants (which is a response opposite to that proposed by the current hypothesis), accompanied by a non-linear dose response pattern provokes the question of whether alternate regulatory signaling pathways are affected by decreases in ROS concentration. Figure 4-3 illustrates a proposed scheme of co-regulatory signaling that could be modulated by variable ROS concentrations and by ROS-independent signaling pathways during hypoxia, with cross-talk between pathways potentially explaining the data shown by the dose response curves. Based on the data in Figures 3-3 and 3-4, and based on lack of correlation

between the TEMPOL qPCR data (Figure 3-8) and the TEMPOL immunoblot (Figure 3-10), it is difficult to hypothesize that transcript abundance of the CA9 and VEGF genes is regulated by a single pathway.

As shown in Figure 4-3, MAPK activity resulting in upregulation of the CA9 and VEGF genes can be enhanced by ROS, independent of ATM activation (116). This ROS-dependent enhancement is regulated by the family of MAPK phosphatases (MKPs), which inhibit the activity of MAPK (116). MKPs have been shown to differentially respond to ROS concentration, causing a ROS-driven “balancing” effect that regulates the activity of specific MAPK family members (116). The balance of MKP-mediated inhibition of ROS-driven MAPK activity could explain the non-linear response to gradually increasing doses of antioxidants shown in Figure 3-3 and 3-4. Additionally, prior work has shown that MAPK activity can cause an increase in the transcription of HIF1 target genes such as CA9 and VEGF, requiring only minimal HIF-1 activity, during normoxic intracellular response to low nutrient availability caused by overcrowding of cells (117). Overcrowding has also been shown to cause MAPK-mediated increase in CA9 and VEGF transcription, independent of HIF-1 activity, through the activation of members of the v-ets erythroblastosis virus E26 oncogene homolog (ETS) family of transcription factors (118,119).

The CA9 gene has also been shown to be upregulated by the phosphatidylinositol 3-kinase (PI3K) pathway, independent of increased HIF-1 activity (120). Overcrowding of cells has been shown to initiate PI3K signaling in a manner dependent upon specificity protein 1 (SP1), requiring minimal HIF-1 involvement (120). Regulatory effects caused by overcrowding and/or MAPK regulation could therefore

explain the lack of any decrease in VEGF or CA9 transcript abundance in cells treated with TEMPOL in the absence of HIF-1α stabilization, as shown in Figures 3-8, 3-9, and 3-10 (120). It is important to note that the experiments revealing these MAPK and PI3K-driven effects did not examine the presence of active ATM under their respective experimental conditions (116-119). It is also important to note that since TEMPOL does not participate in thiol-disulfide exchange reactions, its mechanism of deactivation of ATM must stem from its ability to decrease intracellular ROS concentration, which suggests that $\bullet O_2^-$ and/or $\bullet$OH may be required for ATM activation in response to hypoxia (27).

The mechanism by which ATM phosphorylation at S696 of HIF-1α causes its stabilization during hypoxia is unknown. The mechanism of interaction between PHDs and hypoxia-induced ROS, and the magnitude of any modulation of PHD activity from such interaction is also unknown. The results of the current work do not provide data that would specifically elucidate PHD behavior during hypoxia. It is also clear that any attempt to quantify PHD activity by examining the presence of HIF-1α hydroxylation is confounded by the unknown effect(s) that S696 phosphorylation would have upon PHD binding to HIF-1α and/or VHL recognition of HIF-1α. Discovery of sustained PHD activity during hypoxia is of no consequence when accompanied by ATM activation, since ATM activity clearly prevents the degradation of HIF-1α, which is an event downstream of PHD activity. It is important to note that the action of ROS upon PHDs could be treated as a separate mechanism, and investigation of ROS-mediated events involving PHDs could further elucidate hydroxylation of other targets during hypoxia. This suggestion is somewhat confounded by the fact that HIF-1 acts upon a specific

PHD family member (PHD-2) through a negative feedback loop, by upregulating expression of the PHD-2 gene (121).

Evidence from a series of experiments has led to a debate regarding the intracellular source of hypoxia-induced ROS (18,45,122). Experiments conducted prior to the elucidation of non-canonical ATM activation in response to oxidative stress (67) presented an alternative explanation of mitochondrial participation. It was hypothesized that reduced oxidative phosphorylation during hypoxia would make more O_2 available to the PHD active site, neutralizing any suppression of PHD activity caused by low intracellular O_2 (47,122). This “oxygen hypothesis” is less favored, since the “ROS hypothesis” demonstrates the dependence upon ROS for specific pathways (i.e., ATM) that stabilize HIF-1α (17). Additionally, a review of experiments using ρ^0 cells raises a debate regarding the requirement for a functional mitochondrial ETC for stabilization of HIF-1α. Upon examination of the data, it is possible to speculate that the participation of the ETC in hypoxia-induced ROS signaling may be cell type-specific (18,19,44-46,48,58-60). However, as outlined below, results have provided opposing conclusions in the same cell type regarding the implication of the ETC in the response to hypoxia (Table 4-1). These data obscure any characterization of cell-type specific ETC-dependent signaling during hypoxia. Table 4-1 lists the various experiments and their respective cell types, including their implication of the ETC and their respective reference numbers.

An example of how the “oxygen hypothesis” might cause a false interpretation of ρ^0 activity during hypoxia is shown by experimentation examining expression of the Coiled-Coil-Helix-Coiled-Coil-Helix Domain Containing 4 (CHCHD4) protein (123). The

CHCHD4 protein was shown to regulate mitochondrial oxygen consumption, resulting in O_2-dependent HIF-1α stabilization. CHCHD4 regulates protein folding in the mitochondrial intermembrane space, and when CHCHD4 expression was decreased, HIF-1α stabilization also decreased, presumably through decreased mitochondrial respiration (117). The investigators proposed that PHD activity was stimulated due to greater oxygen availability in the cell during hypoxia (117), and this observation was made without any measurement of ATM activity. This data suggests that ρ^0 cells subjected to hypoxia could experience cellular O_2 concentrations sufficient to cause degradation of HIF-1α, or insufficient to cause the degradation of HIF-1α, independent of ATM activity; however, this would require a specific analysis of the O_2 concentrations that were present in cells in each of the debated experiments. Hypothetically, although mitochondrial function may be required to activate ATM in response to hypoxia, it may not be necessary to stabilize HIF-1α in response to hypoxia in all cell types and in all intracellular metabolic statuses.

A second example suggests the possibility that the $\bullet O_2^-$ produced from NOX enzymes is increased and sufficient to cause the change in redox status necessary to activate ATM in response to hypoxia; however, experimental data is limited that conclusively illustrates this possibility (24,124). Paradoxically, it has been shown that while NOX can cause a hypoxia-induced increase in ROS, it was also shown that this event may depend on mitochondrial activity (125).

The two vectors that were constructed to create ρ^0 SKBr3 and HMEC cells as part of the current inquiry were designed to shed more light on the question of ρ^0 cell type specificity and ETC involvement in ATM-dependent signaling. Although the pMSP-

6 vector was successfully sequenced, evidence of transcription was not measurable by reverse-transcriptase PCR after transduction into SKBr3 target cells. This would possibly indicate that the plasmid DNA was integrated into the host genome without the ability to respond to host transcription machinery, or that it was integrated into an unfavorable region of the genome. Future directions for experiments that would determine the nature of the problem with the vector are described below (see “Future Directions”).

The vectors that attempted to employ CRISPR-Cas9 mediated knockout of the nuclear-encoded POLG gene were based on a novel method for creating ρ^0 cells. This method was developed based on the knowledge that human diseases exist that are caused by either nuclear or mitochondria-encoded mutations in the genes that express mitochondrial proteins, rendering the production of mitochondrial proteins insufficient to support mitochondrial function (20). This concept is illustrated in Leigh syndrome, which is caused by the presence of either nuclear or mitochondria-encoded mutations in genes effecting mitochondrial function, with both types of mutation resulting in pathology that ultimately affects the central nervous system and shortens lifespan (126). Although the vectors that were constructed were not successful in causing homozygous knockout of the POLG gene in any of the isolated clones, it is still possible to reattempt the creation of a POLG knockout ρ^0 cell line, possibly with the addition of multiple co-transduced vectors. Plans to construct additional vectors are described in Future Directions below.

Conclusion

The current experimental data demonstrate that antioxidants can modulate the stabilization of HIF-1α during hypoxia, thus causing changes in HIF-1 target gene transcript abundance. Since HIF-1α stabilization has been shown previously to be ATM-dependent in human mammary epithelial carcinoma cell lines, and since antioxidants act through mechanisms that predictably alter intracellular ROS concentrations, it is concluded that the antioxidants NAC and TEMPOL modulate ROS-dependent ATM activation during hypoxia, causing changes in HIF-1 target gene transcript abundance through ATM-dependent stabilization of HIF-1α. To test the hypothesis that ROS specifically produced by the mitochondria are responsible for the ROS-dependent activation of ATM, additional experiments must be carried out. The need for this specific experimentation is predicated by the differential results from previous experimentation in ρ^0 cells that suggest an O_2-dependent mechanism is also present. The precise nature of the modulation of ATM activity resulting from antioxidant-mediated decrease in ROS concentration remains unknown, and shows a differential response to NAC and TEMPOL as measured by changes in CA9 and VEGF transcript abundance. It also remains unknown whether the current experimental conditions were affected by alternate signaling pathways that would alter CA9 and VEGF transcript abundance in a dose-dependent manner.

Future Directions

Continuation of the Current Investigation

Since the current hypothesis states that in response to hypoxia, reactive oxygen species generated by the mitochondria activate ATM, it is naturally obvious that

continued efforts should be made to determine the source of the ROS that were shown to modulate ATM-kinase dependent stabilization of HIF-1α. Although the use of ρ^0 cells as a model for demonstrating mitochondrial ROS generation has failed to provide solid answers, a continued progression of the current experimental methods in HMEC and SKBr3 cells using ρ^0 versions of those cells would be appropriate. Therefore, it is suggested that efforts should be continued to successfully transduce pMSP-6 and/or POLG-CRISPR vectors into HMEC and SKBr3 target cells.

Since both vectors require troubleshooting, the appropriate first steps would be to determine how to resolve the problems that are impeding successful transduction. For the pMSP-6 vector, transfecting Lenti-X cells with pMSP-6 plasmid DNA or with pLV-mitoGFP as a positive GFP control would allow a repeat experiment for troubleshooting purposes. By performing puromycin selection, and then repeating fluorescence microscopy and reverse transcriptase PCR using primers #10 and #11 (Table 3-2), it would be possible to reveal if the previous unsuccessful transduction process was interrupted at the transfection stage or at the transduction stage. It is also possible that successful transfection into Lenti-X cells could create a Lenti-X ρ^0 cell line that could be used to carry out additional hypoxia experiments. Additional technical considerations include the fact that successfully transfected or transduced cells' dependency on uridine and pyruvate is unknown, although it is known that they should eventually become auxotrophic. The possibility exists that daughter cells become auxotrophic immediately upon loss of their mitochondrial function, and therefore require the appropriate level of supplementation to survive the selection process. Conversely, if cells require repeated doublings to sufficiently dilute the mitochondrial copy number in daughter cells, care

must be taken to ensure that characterization of cells would indicate a near-homogenous population of ρ^0 cells, as opposed to a heterogeneous population consisting of subpopulations of various mitochondrial activity. This care must be taken so that interpretation of any future experimental results is not obscured by spurious ETC activity.

The future experiments necessary to characterize cells as ρ^0 would include viability tests to determine uridine auxotrophy and qPCR to detect the presence of mitochondrial DNA. Additionally, DCF assay could be performed to show the production of ROS versus that produced by parent cells. Finally, a fluorescent dye such as MitoTracker (Thermo Fisher) could be used to stain the mitochondria of successfully transduced cells (possibly at an early stage of doubling), to examine co-localization of GFP protein expression with the mitochondria. MitoTracker also fluoresces as a function of mitochondrial membrane potential, and could therefore be used to indicate reduction in cellular respiration activity in ρ^0 cells compared to parent cells.

The POLG-CRISPR knockout method of creating ρ^0 cells could be continued through the design of specific sgRNAs that could be co-transfected to increase the effectiveness and probability of homozygous knockout. This tack may prove to be especially shrewd in cancer cells, since cancer cells have been shown to be aneuploid and could therefore possess extra copies of the POLG gene (127). Additionally, it may prove to be more effective to target exon 3 as opposed to exon 2, and this suggestion could be accommodated using the same process used for the attempt at targeting exon 2. Chromatin arrangements are dynamic and could therefore be more permissive to hybridization with one DNA region versus another. Upon successful identification of

POLG knockout clones, the same characterization of ρ^0 populations could be carried out as described above. With ρ^0 cells in hand it would be logical to perform the hypoxia experiments in an identical fashion as shown above, to compare the results with those gathered in normal cells and cells treated with antioxidants. Based on the current hypothesis, results should indicate that ρ^0 cells fail to stabilize HIF-1α during hypoxia and fail to increase transcript abundance in HIF-1 target genes, and should show qPCR and immunoblot results similar to those seen in cells treated with NAC.

Suggestions for New Investigations

Several possibilities exist for experiments that could provide interesting data in support of the current hypothesis or as characterization of independent cellular activities that are currently not understood. For example, reactions between H_2O_2 and thiols can occur spontaneously or as the result of enzymatic activity (67,110), as seen in the case of GSH and glutathione-S-transferase (GST). It is possible that the disulfide bridge formation at C2991 of ATM is enzymatically catalyzed, at least in part, and therefore it is also possible that the reaction is somehow regulated by one or more intracellular processes. To confirm the participation of the thiol-disulfide exchange mechanism of NAC in the suppression of ATM activity, additional experiments could be designed using alternative reducing agents such as dithiothreitol (110) or β-mercaptoethanol (128). Although these reducing agents also scavenge $\bullet O_2^-$, they do so at different rates, which could provide characterization of the dependency of ATM activity on specific ROS molecules (110,128).

To further refine the experimental methods used in the current work, it would be beneficial to establish control of any cellular overcrowding-induced activation of HIF-1

target gene transcription. It would also be beneficial to establish the cell-type specific nature of any MAPK-driven response to hypoxia that would cause changes in HIF-1 target gene transcript abundance independent of HIF-1α stabilization. The effort to characterize the effect of MAPK signaling upon interpretation of experimental results could also be facilitated by the identification of HIF-1 surrogate markers that respond in a manner solely dependent upon HIF-1α protein accumulation status. Identification of such genes could be accomplished by exposing HIF-1α knockout cell lines to hypoxia.

A crucial component of the mechanism of ATM-dependent stabilization of HIF-1α is the phosphorylation of S696. Since both the function of the phosphorylation and the effect it has upon PHD activity are unknown, additional experiments characterizing PHD activity using amino acid substitutions at position 696 would be revealing (6). Additionally, S696 phosphorylation appears to be a marker of ATM activity specifically in response to hypoxia, and ATM has not been shown to phosphorylate HIF-1α in response to DNA DSBs caused by DSB-inducing reagents such as neocarzinostatin (45). Further experiments that would definitively elucidate S696 phosphorylation as a hypoxia-specific ATM activation marker would help to develop the understanding of stress-specific roles of ATM.

Experiments using alternative antioxidants such as EUK8 could help to substantiate the results from the current work with TEMPOL, since both EUK8 and TEMPOL are SOD mimetics that cause the concentration of H_2O_2 to increase through scavenging $\bullet O_2^-$ (129). To further understand the specific mechanism of ROS-dependent ATM activation, experiments using small-hairpin RNA (shRNA) knockdown

or CRISPR-Cas9-mediated knockout of catalase and/or GPX could demonstrate how H_2O_2 concentration drives signaling in response to hypoxia.

Understanding how the specific function of ATM dimerization and activation in response to varying degrees of oxidative stress and cellular activity may reveal a higher level of characterization of ATM signaling in these cell lines. Additionally, the tapestry of ATM activation in response to oxidative stress could be further elucidated by characterization of how ATM species (monomers versus dimers) distribute in the cell, and how various stressors modulate the ATM-redox signaling axis.

Table 4-1. List of experiments using various ρ^0 cell lines and their resulting implications.

First author	Year	Cell line	Implication	Reference #
Chandel	1998	Hep3B	ETC required	18
Chandel	2000	Hep3B, 293T	ETC required	19
Vaux	2001	143B, A549	ETC not required	46
Srinivas	2001	143B, GM701	ETC not required	48
Schroedl	2002	HT1080, A549	ETC required	59
Enomoto	2002	HeLa	ETC not required	60
Guzy	2005	143B	ETC required	58
Bencocova	2009	A549	ETC not required	45

Table 4-2. Chemical equations for antioxidant mechanisms.

Equation	No.
$R\text{-}S^- + H_2O_2 \rightarrow RS\text{-}OH + H_2O_2.$	(4-1)
$RS\text{-}OH + R\text{-}SH \rightarrow RS\text{-}SR + H_2O$	(4-2)
$2\ R\text{-}SH + R'S\text{–}SR'' \rightarrow R'\text{-}SH + R''\text{-}SH + RS\text{–}SR.$	(4-3)
$TEM + \bullet O_2^- \rightarrow TEM + H_2O_2 + O_2$	(4-4)
$H_2O_2 + L\text{-}M^{n+} \rightarrow L\text{-}M^{n+}\text{-}\ H_2O_2$	(4-5)
$L\text{-}M^{n+}\text{-}\ H_2O_2 \rightarrow L\text{-}M^{n+} + OH^- + \bullet OH$	(4-6)
$TEM + \bullet OH + NADH \rightarrow TEM\text{-}H + NAD^+$	(4-7)
$TEM + L\text{-}M^{n+} + H^+ \rightarrow TEM\text{-}H + L\text{-}M^{(n+1)+}$	(4-8)
$TEM \rightleftharpoons TEM\text{-}H$	(4-9)
(4-8) ┤ (4-5)	(4-10)

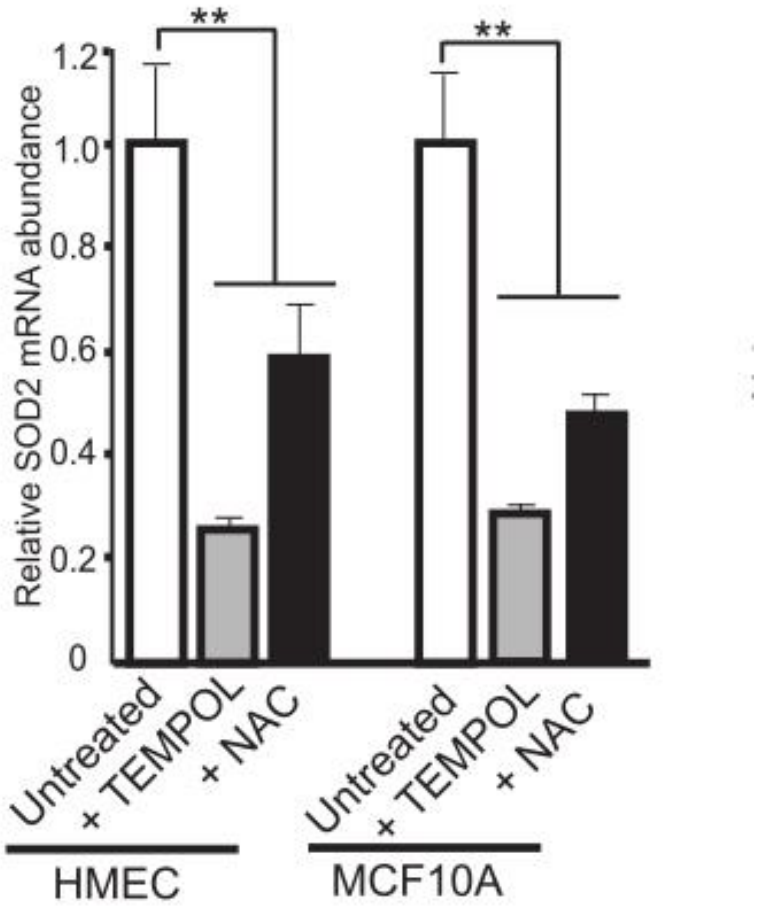

Figure 4-1. Mean relative transcript abundance of the SOD2 gene in HMEC and MCF10A cells, following treatment with either 500 μM TEMPOL or 10 mM NAC for 18 hours, at atmospheric oxygen concentration (20% O_2). Relative transcript abundance was measured by qPCR using the $2^{-\Delta\Delta CT}$ method and normalized to the mean transcript abundance value for untreated cells for n = 3 experiments. Unpaired *t*-tests were performed to determine the differences between the means, and equal variance was assumed in all conditions. **, $p<0.01$.

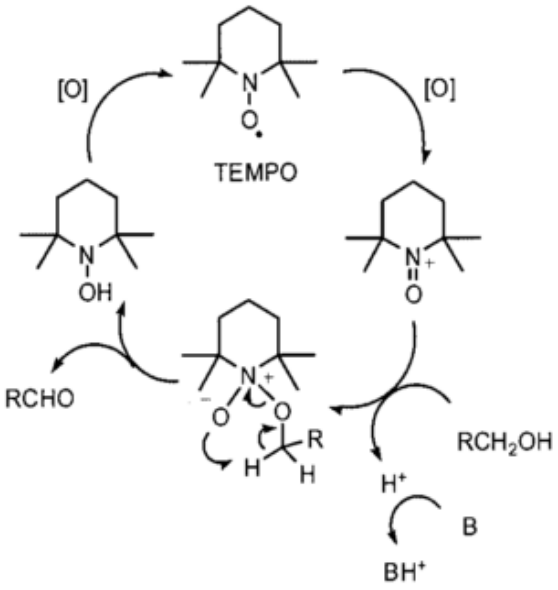

Figure 4-2. Proposed mechanism for TEMPOL regeneration, based upon the parent compound TEMPO, showing the reformation of TEMPO from its hydroxylamine by-product.

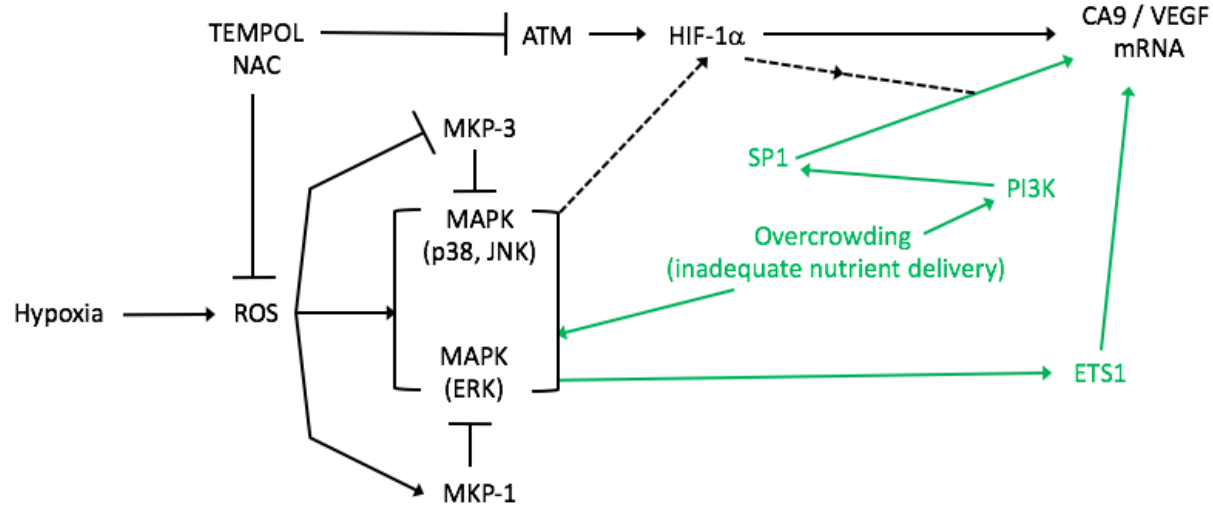

Figure 4-3. Regulatory cross-talk between Hypoxia-induced ROS signaling, MAPK signaling, and ROS-independent signaling resulting in changes in CA9 and VEGF transcript abundance. Dashed lines indicate a requirement for minimal HIF-1 activity. Events independent of HIF-1 activity are indicated in green.

LIST OF REFERENCES

1. Health, United States, 2015: With special feature on racial and ethnic health disparities (2015). Retrieved from https://www.cdc.gov/nchs/hus/index.htm

2. Cancer facts and figures 2017. (2017). Retrieved from https://www.cancer.org/research/cancer-facts-statistics/all-cancer-facts-figures/cancer-facts-figures-2017.html

3. Keith, B., and Simon, M. C. (2007) Hypoxia-inducible factors, stem cells, and cancer. *Cell* **129**, 465-47

4. McKeown, S. R. (2014) Defining normoxia, physoxia and hypoxia in tumours - implications for treatment response. *British Journal of Radiology* **87**, 1-12

5. Dükel, M., Streitfeld, W. S., Tang, T. C. C., Backman, L. R. F., Ai, L., May, W. S., and Brown, K. D. (2016) The breast cancer tumor suppressor TRIM29 is expressed via ATM-dependent signaling in response to hypoxia. *Journal of Biological Chemistry* **291**, 21541-21552

6. Cam, H., Easton, J. B., High, A., and Houghton, P. J. (2010) mTORC1 signaling under hypoxic conditions is controlled by atm-dependent phosphorylation of HIF-1α. *Molecular Cell* **40**, 509-520

7. Finley, L. W. S., Carracedo, A., Lee, J., Souza, A., Egia, A., Zhang, J., Teruya-Feldstein, J., Moreira, P. I., Cardoso, S. M., Clish, C. B., Pandolfi, P. P., and Haigis, M. C. (2011) SIRT3 opposes reprogramming of cancer cell metabolism through HIF-1a destabilization. *Cancer Cell* **19**, 416-428

8. Thomlinson, R. H., and Gray, L. H. (1955) The histological structure of some human lung cancers and the possible implications for radiotherapy. *British Journal of Cancer* **9**, 539-549

9. Tochhawng, L., Deng, S., Pervaiz, S., and Yap, C. T. (2013) Redox regulation of cancer cell migration and invasion. *Mitochondrion* **13**, 246-253

10. Ma, J., Zhang, Q., Chen, S., Fang, B., Yang, Q., Chen, C., Miele, L., Sarkar, F. H., Xia, J., and Wang, Z. (2013) Mitochondrial dysfunction promotes breast cancer cell migration and invasion through HIF1-a accumulation via increased production of reactive oxygen species. *PLoS ONE* **8,** 1-10

11. Gatenby, R. A., Kessler, H. B., Rosenblum, J. S., Coia, L. R., Moldofsky, P. J., Hartz, W. H., and Broder, G. J. (1988) Oxygen distribution in squamous cell carcinoma metastases and its relationship to outcome of radiation therapy. *International Journal of Radiation Oncology, Biology, Physics* **14**, 831-838

12. Wijeratne, S. S. K., Cuppett, S.L., Schlegel, V. (2005) Hydrogen peroxide induced oxidative stress damage and antioxidant enzyme response in caco-2 human colon cells. *Journal of Agricultural and Food Chemistry* **53**, 8768-8774

13. Singh, K. K., Ayyasamy, V., Owens, K. M., Koul, M. S., and Vujcic, M. (2009) Mutations in mitochondrial DNA polymerase-gamma promote breast tumorigenesis. *J. Hum. Genet.* **54**, 516-524

14. Kovac, S., Angelova, P. R., Holmström, K. M., Zhang, Y., Dinkova-Kostova, A. T., and Abramov, A. Y. (2015) Nrf2 regulates ROS production by mitochondria and NADPH oxidase. *Biochimica et Biophysica Acta - General Subjects* **1850**, 794-801

15. Teicher, B. A. (1994) Hypoxia and drug resistance. *Cancer and Metastasis Reviews* **13**, 139-168

16. Chen, J., Ding, Z., Peng, Y., Pan, F., Li, J., Zou, L., Zhang, Y., and Liang, H. (2014) HIF-1α inhibition reverses multidrug resistance in colon cancer cells via downregulation of MDR1/P-Glycoprotein. *PLoS ONE* **9**, 1-9

17. Hagen, T. (2012) Oxygen versus reactive oxygen in the regulation of HIF-1α: the balance tips. *Biochemistry Research International* **2012**, 1-5

18. Chandel, N. S., Maltepe, E., Goldwasser, E., Mathieu, C. E., Simon, M. C., and Schumacker, P. T. (1998) Mitochondrial reactive oxygen species trigger hypoxia-induced transcription. *Cell Biology* **95**, 11715-11720

19. Chandel, N. S., McClintock, D. S., Feliciano, C. E., Wood, T. M., Melendez, J. A., Rodriguez, A. M., and Schumacker, P. T. (2000) Reactive oxygen species generated at mitochondrial Complex III stabilize hypoxia-inducible factor-1α during hypoxia: A mechanism of O2 sensing. *Journal of Biological Chemistry* **275**, 25130-25138

20. Brunelle, J. K., Bell, E. L., Quesada, N. M., Vercauteren, K., Tiranti, V., Zeviani, M., Scarpulla, R. C., and Chandel, N. S. (2005) Oxygen sensing requires mitochondrial ROS but not oxidative phosphorylation. *Cell Metabolism* **1**, 409-414

21. Semenza, G. L. (1996) Transcriptional regulation by hypoxia-inducible factor 1: molecular mechanisms of oxygen homeostasis. *Trends in Cardiovascular Medicine* **6**, 151-157

22. Semenza, G. L. (1999) Perspectives on oxygen sensing. *Cell* **98**, 281-284

23. Jiang, B. H., Semenza, G. L., Bauer, C., and Marti, H. H. (1996) Hypoxia-inducible factor 1 levels vary exponentially over a physiologically relevant range of O2 tension. *The American Journal of Physiology* **271**, C1172-C1180

24. Tafani, M., Sansone, L., Limana, F., Arcangeli, T., De Santis, E., Polese, M., Fini, M., and Russo, M. A. (2016) The interplay of reactive oxygen species, hypoxia, inflammation, and sirtuins in cancer initiation and progression. *Oxidative Medicine and Cellular Longevity* **2016**, 1-18

25. Zhao, K., Huang, Z., Lu, H., Zhou, J., and Wei, T. (2010) Induction of inducible nitric oxide synthase increases the production of reactive oxygen species in RAW264.7 macrophages. *Bioscience Reports* **30**, 233-241

26. Morgan, M. J., and Liu, Z. (2011) Crosstalk of reactive oxygen species and NF-κB signaling. *Cell Research* **21**, 103-115

27. Mohsen, M., Pinson, A., Zhang, R., and Samuni, A. (1995) Do nitroxides protect cardiomyocytes from hydrogen peroxide or superoxide? *Molecular and Cellular Biochemistry* **145**, 103-110

28. Ziech, D., Franco, R., Pappa, A., and Panayiotidis, M. I. (2011) Reactive oxygen species (ROS) - induced genetic and epigenetic alterations in human carcinogenesis. *Mutation Research/Fundamental and Molecular Mechanisms of Mutagenesis* **711**, 167-173

29. Sabharwal, S. S., and Schumacker, P. T. (2014) Mitochondrial ROS in cancer: initiators, amplifiers or an Achilles' heel? *Nature Reviews Cancer* **14**, 709-721

30. Kauppinen, A., Suuronen, T., Ojala, J., Kaarniranta, K., and Salminen, A. (2013) Antagonistic crosstalk between NF-κB and SIRT1 in the regulation of inflammation and metabolic disorders. *Cellular Signalling* **25**, 1939-1948

31. Zhou, L. Z. H., Johnson, A. P., and Rando, T. A. (2001) NFκB and AP-1 mediate transcriptional responses to oxidative stress in skeletal muscle cells. *Free Radical Biology and Medicine* **31**, 1405-1416

32. D'Ignazio, L., Batie, M., and Rocha, S. (2017) Hypoxia and inflammation in cancer, focus on HIF and NF-κB. *Biomedicines* **2017**, 1-23

33. Pham, C. G., Bubici, C., Zazzeroni, F., Papa, S., Jones, J., Alvarez, K., Jayawardena, S., De Smaele, E., Cong, R., Beaumont, C., Torti, F. M., Torti, S. V., and Franzoso, G. (2004) Ferritin heavy chain upregulation by NF-kappaB inhibits TNFα-induced apoptosis by suppressing reactive oxygen species. *Cell* **119**, 529-542

34. Pelicano, H. L., W; Zhou, Y;. (2010) Mitochondrial dysfunction and reactive oxygen species imbalance promote breast cancer cell motility through a CXCL14-mediated mechanism. **69**, 2375-2383

35. Sullivan, L., and Chandel, N. (2014) Mitochondrial reactive oxygen species and cancer. *Cancer & Metabolism* **2**, 1-12

36. Bae, Y. S., Kang, S. W., Seo, M. S., Baines, I. C., Tekle, E., Chock, P. B., and Rhee, S. G. (1997) Epidermal growth factor (EGF)-induced generation of hydrogen peroxide. *Journal of Biological Chemistry* **272**, 217-221

37. Kim, S. Y., Kim, T.-B., Moon, K.-a., Kim, T. J., Shin, D., Cho, Y. S., Moon, H.-B., and Lee, K.-Y. (2008) Regulation of pro-inflammatory responses by lipoxygenases via intracellular reactive oxygen species in vitro and in vivo. *Experimental and Molecular Medicine* **40**, 461-476

38. Tobar, N., Guerrero, J., Smith, P. C., and Martínez, J. (2010) NOX4-dependent ROS production by stromal mammary cells modulates epithelial MCF-7 cell migration. *British journal of cancer* **103**, 1040-1047

39. von Lohneysen, K., Noack, D., Wood, M. R., Friedman, J. S., and Knaus, U. G. (2010) Structural insights into Nox4 and Nox2: motifs involved in function and cellular localization. *Molecular and Cellular Biology* **30**, 961-975

40. Bedard, K., and Krause, K.-H. (2007) The NOX family of ROS-generating NADPH oxidases: physiology and pathophysiology. *Physiological reviews* **87**, 245-313

41. Zeeshan, H., Lee, G., Kim, H.-R., and Chae, H.-J. (2016) Endoplasmic reticulum stress and associated ROS. *International Journal of Molecular Sciences* **17**, 327-346

42. Murphy, M. P. (2009) How mitochondria produce reactive oxygen species. *The Biochemical journal* **417**, 1-13

43. Andreyev, A. Y., Kushnareva, Y. E., and Starkov, A. A. (2005) Mitochondrial metabolism of reactive oxygen species. *Biochemistry. Biokhimiya* **70**, 200-214

44. Sanjuán-Pla, A., Cervera, A. M., Apostolova, N., Garcia-Bou, R., Víctor, V. M., Murphy, M. P., and McCreath, K. J. (2005) A targeted antioxidant reveals the importance of mitochondrial reactive oxygen species in the hypoxic signaling of HIF-1α. *FEBS Letters* **579**, 2669-2674

45. Bencokova, Z., Kaufmann, M. R., Pires, I. M., Lecane, P. S., Giaccia, A. J., and Hammond, E. M. (2009) ATM activation and signaling under hypoxic conditions. *Molecular and Cellular Biology* **29**, 526-537

46. Vaux, E. C., Metzen, E., Yeates, K. M., and Ratcliffe, P. J. (2001) Regulation of hypoxia-inducible factor is preserved in the absence of a functioning mitochondrial respiratory chain. *Regulation* **98**, 296-302

47. Chua, Y. L., Dufour, E., Dassa, E. P., Rustin, P., Jacobs, H. T., Taylor, C. T., and Hagen, T. (2010) Stabilization of hypoxia-inducible factor-1α protein in hypoxia occurs independently of mitochondrial reactive oxygen species production. *Journal of Biological Chemistry* **285**, 31277-31284

48. Srinivas, V., Leshchinsky, I., Sang, N., King, M. P., Minchenko, A., and Caro, J. (2001) Oxygen sensing and HIF-1 activation does Not require an active mitochondrial respiratory chain electron-transfer pathway. *Journal of Biological Chemistry* **276**, 21995-21998

49. Han, D., Antunes, F., Canali, R., Rettori, D., and Cadenas, E. (2003) Voltage-dependent anion channels control the release of the superoxide anion from mitochondria to cytosol. *Journal of Biological Chemistry* **278**, 5557-5563

50. Ratcliffe, P. J. (2007) HIF-1 and HIF-2: Working alone or together in hypoxia? *Journal of Clinical Investigation* **117**, 862-865

51. Drevytska, T., Gavenauskas, B., Drozdovska, S., Nosar, V., Dosenko, V., and Mankovska, I. (2012) HIF-3α mRNA expression changes in different tissues and their role in adaptation to intermittent hypoxia and physical exercise. *Pathophysiology* **19**, 205-214

52. Semenza, G. L. (2010) Defining the role of hypoxia-inducible factor 1 in cancer biology and therapeutics. *Oncogene* **29**, 625-634

53. Hogenesch, J. B., Chan, W. K., Jackiw, V. H., Brown, R. C., Gu, Y. Z., Pray-Grant, M., Perdew, G. H., and Bradfield, C. A. (1997) Characterization of a subset of the basic-helix-loop-helix-PAS superfamily that interacts with components of the dioxin signaling pathway. *Journal of Biological Chemistry* **272**, 8581-8593

54. BelAiba, R. S., Djordjevic, T., Bonello, S., Flügel, D., Hess, J., Kietzmann, T., and Görlach, A. (2004) Redox-sensitive regulation of the HIF pathway under non-hypoxic conditions in pulmonary artery smooth muscle cells. *Biological Chemistry* **385**, 249-257

55. Raval, R. R., Lau, K. W., Tran, M. G. B., Sowter, H. M., Mandriota, S. J., Li, J.-L., Pugh, C. W., Maxwell, P. H., Harris, A. L., and Ratcliffe, P. J. (2005) Contrasting properties of hypoxia-inducible factor 1 (HIF-1) and HIF-2 in von Hippel-Lindau-associated renal cell carcinoma. *Molecular and cellular biology* **25**, 5675-5686

56. Semenza, G. L. (2012) Hypoxia-inducible factors in physiology and medicine. *Cell* **148**, 399-408

57. Benita, Y., Kikuchi, H., Smith, A. D., Zhang, M. Q., Chung, D. C., and Xavier, R. J. (2009) An integrative genomics approach identifies hypoxia inducible factor-1 (HIF-1)-target genes that form the core response to hypoxia. *Nucleic Acids Research* **37**, 4587-4602

58. Guzy, R. D., Hoyos, B., Robin, E., Chen, H., Liu, L., Mansfield, K. D., Simon, M. C., Hammerling, U., and Schumacker, P. T. (2005) Mitochondrial complex III is required for hypoxia-induced ROS production and cellular oxygen sensing. *Cell Metabolism* **1**, 401-408

59. Schroedl, C., Clintock, D. S. M. C., Budinger, G. R. S., Chandel, N. S., Mcclintock, D. S., and Scott, G. R. (2002) Hypoxic but not anoxic stabilization of HIF-1a requires mitochondrial reactive oxygen species. *Am. J. Physiol. Lung Cell. Mol. Physiol.* **283**, 922-931

60. Enomoto, N., Koshikawa, N., Gassmann, M., Hayashi, J. I., and Takenaga, K. (2002) Hypoxic induction of hypoxia-inducible factor-1α and oxygen-regulated gene expression in mitochondrial DNA-depleted HeLa cells. *Biochemical and Biophysical Research Communications* **297**, 346-352

61. Pan, Y., Mansfield, K. D., Bertozzi, C. C., Rudenko, V., Chan, D. A., Giaccia, A. J., and Simon, M. C. (2007) Multiple factors affecting cellular redox status and energy metabolism modulate hypoxia-inducible factor prolyl hydroxylase activity In vivo and In vitro. *Molecular and Cellular Biology* **27**, 912-925

62. Hamanaka, R. B., and Chandel, N. S. (2009) Mitochondrial reactive oxygen species regulate hypoxic signaling. *Current Opinion in Cell Biology* **21**, 894-899

63. Qutub, A. A., and Popel, A. S. (2008) Reactive oxygen species regulate hypoxia-inducible factor 1 differentially in cancer and ischemia. *Molecular and Cellular Biology* **28**, 5106-5119

64. Ditch, S., and Paull, T. T. (2012) The ATM protein kinase and cellular redox signaling: beyond the DNA damage response. *Trends in Biochemical Sciences* **37**, 15-22

65. Guo, Z., Deshpande, R., and Paull, T. T. (2010) ATM activation in the presence of oxidative stress. *Cell Cycle* **9**, 4805-4811

66. Cortez, D., Wang, Y., Qin, J., and Elledge, S. (1999) Requirement of ATM-dependent phosphorylation of Brcal in the DNA damage response to double-strand breaks. *Science* **286**, 1162-1166

67. Guo, Z., Kozlov, S., Lavin, M. F., Person, M. D., and Paull, T. T. (2010) ATM activation by oxidative stress. *Science (New York, N.Y.)* **330**, 517-521

68. Olcina, M. M., Grand, R. J., and Hammond, E. M. (2014) ATM activation in hypoxia - causes and consequences. *Molecular & Cellular Oncology* **1**, 1-8

69. Cam, H., and Houghton, P. J. (2011) Regulation of mammalian target of rapamycin complex 1 (mTORC1) by hypoxia: causes and consequences. *Targeted Oncology* **6**, 95-102

70. Guzy, R. D., Sharma, B., Bell, E., Chandel, N. S., and Schumacker, P. T. (2008) Loss of the SdhB, but not the SdhA, subunit of complex II triggers reactive oxygen species-dependent hypoxia-inducible factor activation and tumorigenesis. *Molecular and cellular biology* **28**, 718-731

71. Wang, Q.-S., Zheng, Y.-M., Dong, L., Ho, Y.-S., Guo, Z., and Wang, Y.-X. (2007) Role of mitochondrial reactive oxygen species in hypoxia-dependent increase in intracellular calcium in pulmonary artery myocytes. *Free Radical Biology and Medicine* **42**, 642-653

72. Badalà, F., Nouri-Mahdavi, K., and Raoof, D. A. (2012) HIF1A induces expression of the WASF3 metastasis associated gene under hypoxic conditions. *International Journal of Cancer* **131**, E905-E915

73. Garayoa, M., Martínez, A., Lee, S., Pio, R., An, W. G., Neckers, L., Trepel, J., Montuenga, L. M., Ryan, H., Johnson, R., Gassmann, M., and Cuttitta, F. (2000) Hypoxia-inducible factor-1 (HIF-1) up-regulates adrenomedullin expression in human tumor cell lines during oxygen deprivation: a possible promotion mechanism of carcinogenesis. *Molecular Endocrinology* **14**, 848-862

74. Mitchell, J. B., Samuni, J. A., Krishna, M. C., DeGraff, W. G., Ahn, M. S., Samuni, U., and Russo, A. (1990) Biologically active metal-Independent superoxide dismutase mimics. *Biochemistry* **29**, 2802-2807

75. Reliene, R. F., Sheila M; Chesselet, Marie-Françoise;, and Schiestl, R. H. (2008) Effects of antioxidants on cancer prevention and neuromotor performance in ATM deficient mice. *Food Chem. Toxicol.* **46**, 1371-1377

76. Sun, S.-Y. (2010) N-acetylcysteine, reactive oxygen species and beyond. *Cancer Biology & Therapy* **9**, 109-110

77. Głębska, J., Skolimowski, J., Kudzin, Z., Gwoździński, K., Grzelak, A., and Bartosz, G. (2003) Pro-oxidative activity of nitroxides in their reactions with glutathione. *Free Radical Biology and Medicine* **35**, 310-316

78. Sceneay, J., Liu, M. C. P., Chen, A., Wong, C. S. F., Bowtell, D. D. L., and Möller, A. (2013) The antioxidant N-acetylcysteine prevents HIF-1 stabilization under hypoxia in vitro but does not affect tumorigenesis in multiple breast cancer models in vivo. *PLoS ONE* **8**, 1-15

79. Trnka, J., Blaikie, F. H., Logan, A., Smith, R. a. J., and Murphy, M. P. (2009) Antioxidant properties of MitoTEMPOL and its hydroxylamine. *Free Radical Research* **43**, 4-12

80. Wilcox, C. S. (2010) Effects of tempol and redox-cycling nitroxides in models of oxidative stress. *Pharmacology & Therapeutics* **126**, 119-145

81. Yamada, J., Yoshimura, S., Yamakawa, H., Sawada, M., Nakagawa, M., Hara, S., Kaku, Y., Iwama, T., Naganawa, T., Banno, Y., Nakashima, S., and Sakai, N. (2003) Cell permeable ROS scavengers, tiron and tempol, rescue PC12 cell death caused by pyrogallol or hypoxia/reoxygenation. *Neuroscience Research* **45**, 1-8

82. Kukat, A., Kukat, C., Brocher, J., Schäfer, I., Krohne, G., Trounce, I. a., Villani, G., and Seibel, P. (2008) Generation of ρ0 cells utilizing a mitochondrially targeted restriction endonuclease and comparative analyses. *Nucleic Acids Research* **36**, 1-10

83. Jo, A., Ham, S., Lee, G. H., Lee, Y., Kim, S., Lee, Y., Shin, J., and Lee, Y. (2015) Efficient mitochondrial genome editing by CRISPR / Cas9. *Biomed Research International* **2015**, 1-10

84. Schubert, S., Heller, S., Löffler, B., Schäfer, I., Seibel, M., Villani, G., and Seibel, P. (2015) Generation of rho zero cells: visualization and quantification of the mtDNA depletion process. *International Journal of Molecular Sciences* **16**, 9850-9865

85. King, M. P., and Attardi, G. (1996) Isolation of human cell lines lacking mitochondrial DNA. *Methods in enzymology* **264**, 304-313

86. Hashiguchi, K., and Zhang-Akiyama, Q. (2009) Establishment of human cell lines lacking mitochondrial DNA. *Mitochondrial DNA Methods and Protocols* **554**, 383-391

87. Fang, J., Uchiumi, T., Yagi, M., Matsumoto, S., Amamoto, R., Takazaki, S., Yamaza, H., Nonaka, K., and Kang, D. (2013) Dihydro-orotate dehydrogenase is physically associated with the respiratory complex and its loss leads to mitochondrial dysfunction. *Bioscience Reports* **33**, 217-227

88. Livak, K. J., and Schmittgen, T. D. (2001) Analysis of relative gene expression data using real-time quantitative PCR and the 2^(delta-delta-CT) method. *Methods* **25**, 402-408

89. Ouiddir, A., Planes, C., Fernandes, I., VanHesse, A., and Clerici, C. (1999) Hypoxia upregulates activity and expression of the glucose transporter GLUT1 in alveolar epithelial cells. *Am. J. Respir. Cell Mol. Biol.* **21**, 710-718

90. Papandreou, I., Cairns, R. A., Fontana, L., Lim, A. L., and Denko, N. C. (2006) HIF-1 mediates adaptation to hypoxia by actively downregulating mitochondrial oxygen consumption. *Cell Metabolism* **3**, 187-197

91. Alpay, M., Backman, L. R. F., Cheng, X., Dukel, M., Kim, W.-J., Ai, L., and Brown, K. D. (2015) Oxidative stress shapes breast cancer phenotype through chronic activation of ATM-dependent signaling. *Breast Cancer Research and Treatment* **151**, 75-87

92. Dyer, L. M., Ai, L., Kepple, J., Xu, J., Kim, W., Stanton, V., Reinhard, M. K., Backman, L. R. F., Streitfeld, W.S., Tang, M., Treiber, N., Scharffetter-Kochanek, K., Mckinnon, P. J., and Brown, K. D. ATM is required for SOD2 expression and homeostasis within the lactating mammary gland (*in revision*). 1-28

93. Newman, A. K., Rubin, R. A., Kim, S.-H., and Modrich, P. (1981) DNA sequences of structural genes for EcoRI restriction and modification enzymes. **256**, 2131-2139

94. Relative quantitation of gene expression experimental design and analysis. (2004). In Applied Biosystems, a guide to performing relative quantitation of gene expression using real-time quantitative PCR. Retrieved from https://tools.thermofisher.com/content/sfs/manuals/cms_042380.pdf

95. Lin, C. S., Wang, Y. C., Huang, J. L., Hung, C. C., and Chen, J. Y. F. (2012) Autophagy and reactive oxygen species modulate cytotoxicity induced by suppression of ATM kinase activity in head and neck cancer cells. *Oral Oncology* **48**, 1152-1158

96. Li, Y., and Yang, D.-Q. (2010) The ATM inhibitor KU-55933 suppresses cell proliferation and induces apoptosis by blocking AKT in cancer cells with overactivated AKT. *Molecular Cancer Therapeutics* **9**, 113-125

97. Boveris A. (1977) Mitochondrial production of superoxide radical and hydrogen peroxide. In Tissue Hypoxia and ischemia, New York: Plenum, p. 67–82

98. Clanton, T. L. (2007) Hypoxia-induced reactive oxygen species formation in skeletal muscle. *J. Appl. Physiol.* **102**, 2379-2388

99. Mehta, J. P., Campian, J. L., Guardiola, J., Cabrera, J. A., Weir, E. K., and Eaton, J. W. (2008) Generation of oxidants by hypoxic human pulmonary and coronary smooth-muscle cells. *Chest* **133**, 1410–1414

100. Hoffman, D. L., and Brookes, P. S. (2009) Oxygen sensitivity of mitochondrial reactive oxygen species generation depends on metabolic conditions. *Journal of Biological Chemistry* **284**, 16236-16245

101. Hoffman, D. L., Salter, J. D., and Brookes, P. S. (2006) Response of mitochondrial reactive oxygen species generation to steady-state oxygen tension: implications for hypoxic cell signaling. *AJP: Heart and Circulatory Physiology* **292**, H101-H108

102. Alexander, A., Cai, S., Kim, J., Nanez, A., Sahin, M., MacLean, K. H., Inoki, K., Guan, K.-L., Shen, J., Person, M. D., Kusewitt, D., Mills, G. B., Kastan, M. B., and Walker, C. L. (2010) ATM signals to TSC2 in the cytoplasm to regulate mTORC1 in response to ROS. *PNAS* **107**, 4153-4158

103. Li, M., Fang, X., Baker, D. J., Guo, L., Gao, X., Wei, Z., Han, S., van Deursen, J. M., and Zhang, P. (2010) The ATM – p53 pathway suppresses aneuploidy-induced tumorigenesis. *PNAS* **107**, 14188-14193

104. Grosjean-Raillard, J., Tailler, M., Adès, L., Perfettini, J.-L., Fabre, C., Braun, T., De Botton, S., Fenaux, P., and Kroemer, G. (2009) ATM mediates constitutive NF-κB activation in high-risk myelodysplastic syndrome and acute myeloid leukemia. *Oncogene* **28**, 1099-1109

105. Hanschmann, E., Godoy, J. R., Berndt, C., Hudemann, C., and Lillig, C. H. (2013) Thioredoxins, glutaredoxins, and peroxiredoxins—molecular mechanisms and health significance: from cofactors to antioxidants to redox signaling. *Antioxidants & Redox Signaling* **19**, 1539-1605

106. Kondoh, M., Ohga, N., Akiyama, K., Hida, Y., Maishi, N., Towfik, A. M., Inoue, N., Shindoh, M., and Hida, K. (2013) Hypoxia-induced reactive oxygen species cause chromosomal abnormalities in endothelial cells in the tumor microenvironment. *PLoS ONE* **8**, 1-14

107. Freiberg, R. A., Hammond, E. M., Dorie, M. J., Welford, S. M., and Giaccia, A. J. (2006) DNA damage during reoxygenation elicits a CHK2-dependent checkpoint response. *Molecular and Cellular Biology* **26**, 1598-1609

108. Hammond, E. M., Dorie, M. J., and Giaccia, A. J. (2003) ATR/ATM targets are phosphorylated by ATR in response to hypoxia and ATM in response to reoxygenation. *Journal of Biological Chemistry* **278**, 12207-12213

109. Rushworth, G. F., and Megson, I. L. (2014) Existing and potential therapeutic uses for N-acetylcysteine: The need for conversion to intracellular glutathione for antioxidant benefits. *Pharmacology and Therapeutics* **141**, 150-159

110. Winterbourn, C. C., and Metodiewa, D. (1999) Reactivity of biologically important thiol compounds with superoxide and hydrogen peroxide. *Free Radical Biology and Medicine* **27**, 322-328

111. Deponte, M. (2013) Glutathione catalysis and the reaction mechanisms of glutathione-dependent enzymes. *Biochimica et Biophysica Acta - General Subjects* **1830**, 3217-3266

112. Kudo, W., Yamato, M., Yamada, K., Kinoshita, Y., Shiba, T., Watanabe, T., and Utsumi, H. (2008) Formation of TEMPOL-hydroxylamine during reaction between TEMPOL and hydroxyl radical: HPLC/ECD study. *Free Radical Research* **42**, 505-512

113. Chen, Y., Pearlman, A., Luo, Z., and Wilcox, C. S. (2007) Hydrogen peroxide mediates a transient vasorelaxation with tempol during oxidative stress. *American Journal of Physiology. Heart and Circulatory Physiology* **293**, H2085-H2092

114. Chen, Y., Cowley, A. W., and Zou, A. (2003) Increased H_2O_2 counteracts the vasodilator and natriuretic effects of superoxide dismutation by tempol in renal medulla. *American Journal of Physiology. Regulatory, Integrative and Comparative Physiology* **285**, R827-833

115. Kaewpila, S., Venkataraman, S., Buettner, G., and Oberly, L. (2008) Manganese superoxide dismutase modulates hypoxia inducible factor-1 alpha induction via superoxide. *Cancer Res.* **68**, 2781-2788

116. Son, Y., Cheong, Y., Kim, N., Chung, H., Kang, D. G., and Pae, H. (2011) Mitogen-activated protein kinases and reactive oxygen species: How can ROS activate MAPK pathways? *Journal of Signal Transduction* **2011**, 1-6

117. Kopacek, J., Barathova, M., Dequiedt, F., Sepelakova, J., Kettmann, R., Pastorek, J., and Pastorekova, S. (2005) MAPK pathway contributes to density and hypoxia-induced expression of the tumor-associated carbonic anhydrase IX. **1729**, 41-49

118. Taylor, M. A., Wappett, M., Delpuech, O., Brown, H., and Chresta, C. M. (2016) Enhanced MAPK signaling drives ETS1-mediated induction of miR-29b leading to downregulation of TET1 and changes in epigenetic modifications in a subset of lung SCC. *Nature Publishing Group* **35**, 4345-4357

119. Salnikow, K., Aprelikova, O., Ivanov, S., Tackett, S., Kaczmarek, M., Karaczyn, A., Yee, H., and Kasprzak, K. S. (2008) Regulation of hypoxia-inducible genes by ETS1 transcription factor. **29**, 1493-1499

120. Kaluz, S., Kaluzova, M., Chrastina, A., Olive, P. L., Pastorekova, S., Lerman, M. I., and Stanbridge, E. J. (2002) Lowered oxygen tension induces expression of the hypoxia marker MN/carbonic anhydrase IX in the absence of hypoxia-inducible factor-1α stabilization: a role for phosphatidylinositol 3'-kinase. *Cancer Research* **62**, 4469-4477

121. Ziello, J. E., Jovin, I. S., and Huang, Y. (2007) Hypoxia-inducible factor (HIF)-1 regulatory pathway and its potential for therapeutic intervention in malignancy and ischemia. *Yale Journal of Biology and Medicine* **80**, 51-60

122. Movafagh, S., Crook, S., and Vo, K. (2015) Regulation of hypoxia-inducible factor-1α by reactive oxygen species: new developments in an old debate. *Journal of Cellular Biochemistry* **116**, 696-703

123. Yang, J., Staples, O., Thomas, L. W., Briston, T., Robson, M., Poon, E., Simões, M. L., El-Emir, E., Buffa, F. M., Ahmed, A., Annear, N. P., Shukla, D., Pedley, B. R., Maxwell, P. H., Harris, A. L., and Ashcroft, M. (2012) Human CHCHD4 mitochondrial proteins regulate cellular oxygen consumption rate and metabolism and provide a critical role in hypoxia signaling and tumor progression. *Journal of Clinical Investigation* **122**, 600-611

124. Hsieh, C. H., Shyu, W. C., Chiang, C. Y., Kuo, J. W., Shen, W. C., and Liu, R. S. (2011) NADPH oxidase subunit 4-mediated reactive oxygen species contribute to cycling hypoxia-promoted tumor progression in glioblastoma multiforme. *PLoS ONE* **6**, 1-10

125. Rathore, R., Zheng, Y. M., Niu, C. F., Liu, Q. H., Korde, A., Ho, Y. S., and Wang, Y. X. (2008) Hypoxia activates NADPH oxidase to increase $[ROS]_i$ and $[Ca^{2+}]_i$ through the mitochondrial ROS-PKCε signaling axis in pulmonary artery smooth muscle cells. *Free Radical Biology and Medicine* **45**, 1223-1231

126. Baertling, F., Rodenburg, R. J., Schaper, J., Smeitink, J. A., Koopman, W. J. H., Mayatepek, E., Morava, E., and Distelmaier, F. (2014) A guide to diagnosis and treatment of Leigh syndrome. *Journal of Neurology, Neurosurgery & Psychiatry* **85**, 257-265

127. Giam, M., and Rancati, G. (2015) Aneuploidy and chromosomal instability in cancer: a jackpot to chaos. *Cell Division* **10**, 1-12

128. Petrov, L., Atanassova, M., and Alexandrova, A. (2012) Comparative study of the antioxidant activity of some thiol-containing substances. *Open Medicine* **7**, 269-273

129. Sharpe, M., Ollosson, R., Stewart, V., and Clark, J. (2002) Oxidation of nitric oxide by oxomanganese–salen complexes: a new mechanism for cellular protection by superoxide dismutase/catalase mimetics. *Biochem. J* **366**, 97-107

BIOGRAPHICAL SKETCH

William Streitfeld graduated from high school in Harbor City, California in 1988. After brief studies in electronics, and after many years of academic absence, he succeeded in earning a Bachelor of Arts in Sports and Recreation Management from Ashford University in 2012. After discovering an interest in fitness and health, he continued his studies by earning a Master of Science in Exercise Science and Health Promotion from California University of Pennsylvania in 2013. While working as a fitness professional, his interest in allied health professions and health sciences compelled him to continue studying, and he spent another 18 months at the University of North Florida as a post-baccalaureate student, immersing himself in basic science and biology. After developing a keen interest in cancer research, he enrolled in the Biochemistry and Molecular Biology master's degree program at the College of Medicine at the University of Florida, to earn a second master of science degree. William aspires to complete his education by earning a doctoral degree, and will be attending the Medical University of South Carolina in 2017, in pursuit of his goal.